DOE/ID/13514

High-Efficiency, High-Capacity, Low-No_x Aluminum Melting Using Oxygen-Enhanced Combustion

Final Report – 10/01/1997 – 03/31/2000

M. D. D'Agostini

May 2000

Work Performed Under Contract No. DE-FC07-97ID13514

For
U.S. Department of Energy
Assistant Secretary for
Energy Efficiency and Renewable Energy
Washington, DC

By
Air Products and Chemicals, Inc.
Allentown, PA

DOE/ID/13514

HIGH-EFFICIENCY, HIGH-CAPACITY, LOW-NO_X ALUMINUM MELTING USING OXYGEN-ENHANCED COMBUSTION

FINAL REPORT
10/01/1997 – 03/31/2000

M. D. D'Agostini

May 2000

Work Performed Under Contract No. DE-FC07-97ID13514

Prepared for the
U.S. Department of Energy
Assistant Secretary for
Energy Efficiency and Renewable Energy
Washington, DC

Prepared by
Air Products and Chemicals, Inc.
Allentown, PA

DISCLAIMER

DOE/ID/13514

HIGH-EFFICIENCY, HIGH-CAPACITY, LOW-NO_X ALUMINUM MELTING USING OXYGEN-ENHANCED COMBUSTION

FINAL REPORT

FOR THE

U.S. DEPARTMENT OF ENERGY
COOPERATIVE AGREEMENT NO. DE-FC07-97ID13514

MARK D. D'AGOSTINI
AIR PRODUCTS AND CHEMICALS, INC.
ALLENTOWN, PA

MAY 2000

HIGH-EFFICIENCY, HIGH-CAPACITY, LOW-NO_X ALUMINUM MELTING USING OXYGEN-ENHANCED COMBUSTION

FINAL REPORT

FOR THE

U.S. DEPARTMENT OF ENERGY
COOPERATIVE AGREEMENT NO. DE-FC07-97ID13514

MARK D. D'AGOSTINI
AIR PRODUCTS AND CHEMICALS, INC.
ALLENTOWN, PA

MAY 2000

Abstract

This report describes the development and application of a novel oxygen enhanced combustion system with an integrated vacuum swing adsorption (VSA) oxygen supply providing efficient, low NOx melting in secondary aluminum furnaces. The mainstay of the combustion system is a novel air-oxy-natural gas burner that achieves high productivity and energy efficiency with low NOx emissions through advanced mixing concepts and the use of separate high- and low-purity oxidizer streams. The overall oxygen concentration in the two oxidizer streams is 35 to 50 volume percent, by design. Integration of the oxygen supply with the combustion system was accomplished primarily by incorporating an oxygen storage vessel at the outlet of the VSA. The vessel uses adsorption technology to significantly increase storage capacity beyond that of an empty tank of the same size. Oxygen is delivered to the sieve tank during periods in which VSA output exceeds furnace demand, then extracted from the vessel, as needed, to meet furnace peak oxygen requirements. A secondary means of integrating the oxygen supply into the combustion system was designing the burner to make use of the low-purity VSA waste stream as a tool for additional NOx reduction. The technology was installed on a reverberatory, secondary aluminum melting plant at the Wabash Aluminum Alloys' Syracuse, N.Y. plant, where it is currently in operation.

Field testing gave evidence that the new burner technology meets the stringent NOx emissions target of 0.323 lb NO_2/ton aluminum, thus complying with regulations promulgated by Southern California's South Coast Air Quality Management District (SCAQMD). Test results also indicated that the burner technology exceeded fuel efficiency and melting capacity goals. These were, respectively, to reduce specific fuel consumption below the 1600 Btu/lb level achieved with pre-development air-oxy-fuel (AOF) technology, and to increase furnace melting capacity by 30 percent over that previously attained with air-fuel combustion. Economic modeling showed that the novel AOF combustion technology provides a substantial increase in furnace profitability relative to air-fuel operation. Model results also suggest favorable economics for the air-oxy-fuel technology relative to a full oxy-fuel conversion of the furnace.

Tests were also conducted at the host facility to determine operating characteristics of the sieve-assisted oxygen storage vessel. Results indicated that the sieve-filled vessel has oxygen storage capacity in excess of 2.5 times that of an equal-sized empty tank operating over the same pressure range. Further, use of the vessel reduced the required consumption of a backup liquid oxygen supply by 33 percent during a controlled field trial spanning several days of operation. However, calculations suggest that economics do not favor the use of this oxygen storage technology at the current sieve price level.

Section 1
Introduction

Overview

The use of high-purity oxygen has proven to be an effective means of enhancing combustion processes in many industrial heating, melting and incinerating applications [1]. Typical benefits of oxygen enrichment include higher productivity, greater energy efficiency and reduced pollutant emissions. Productivity is increased due to higher flame temperatures (Figure 1-1) that are capable of more rapid heating and melting. Thermal efficiency increases since the removal of nitrogen through oxygen enrichment means more complete utilization of available energy (Figure 1-2). This energy savings translates into reduced CO_2 emissions per unit of product. Moreover, particulate emissions are lowered due to the lower volume flow of exhaust gas in oxygen-enriched systems (Figure 1-3).

Air Products has played a leading role in the integration of oxygen enrichment into secondary aluminum melting furnaces. The commercialized EZ-Fire™ burner technology, used in both rotary and reverberatory furnaces, has demonstrated sustainable productivity improvements of 20 percent and fuel savings in excess of 30 percent compared to air-fuel operation. With annual secondary aluminum production rates approaching 4 MM tons/year in the U.S. (1995 figures), the potential therefore exists for significant energy, economic and environmental benefits. Domestic aluminum producers have nevertheless been reluctant to implement oxygen-enhanced combustion (OEC) systems. This is due, in part, to concern over the potential for furnace damage and reduced product yield [2]. However, the major reasons are related to NOx (i.e., oxides of nitrogen) emissions and the added cost of the oxygen supply. Most burner technologies that utilize low levels of oxygen enrichment (35 to 50 percent oxygen by volume) are plagued with high NOx emissions. Those that can deliver low NOx are more costly to operate since they typically require nearly 100 percent oxygen enrichment. Moreover, even at low enrichment levels, the cost of a liquid oxygen supply, or even an on-site O_2 VSA that is not optimally integrated with furnace operation, can be higher than acceptable for many aluminum producers. These limitations point to the need for an improved burner technology and lower cost oxygen supply for secondary aluminum melting.

Project Concept

In accordance with the needs noted above, there are two main aspects to this project. The first is the design and construction of a burner technology capable of delivering low NOx emissions, high capacity (i.e., productivity) and energy efficiency, at low levels of oxygen enrichment and lower than typical oxygen purity. The second is the development of a proprietary oxygen storage technology that will permit sizing of an on-site VSA based on average, rather than peak, oxygen demand. Although the concept is primarily targeted for secondary aluminum producers, it should nevertheless be suitable for other industrial applications, including copper smelting, glass melting and steel production. Additional details for both of the technology concepts are provided in the following paragraphs.

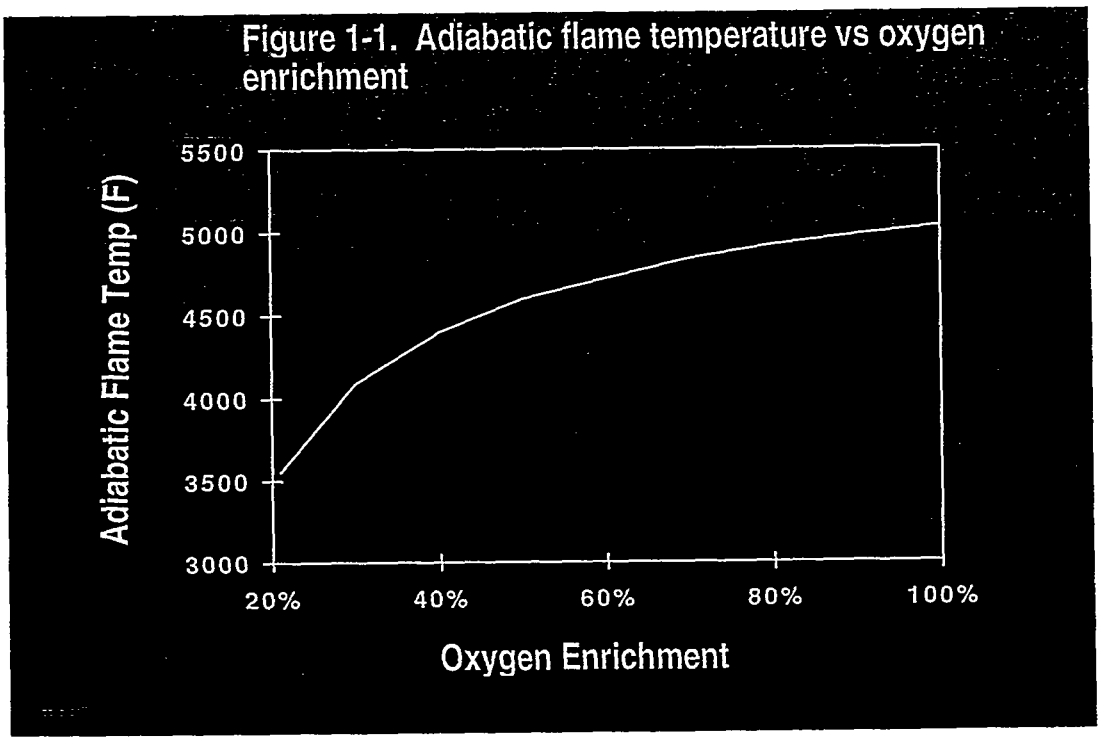
Figure 1-1. Adiabatic flame temperature vs oxygen enrichment
Adiabatic Flame Temp (F)
5500
5000
4500
4000
3500
3000
20%
40%
60%
80%
100%
Oxygen Enrichment

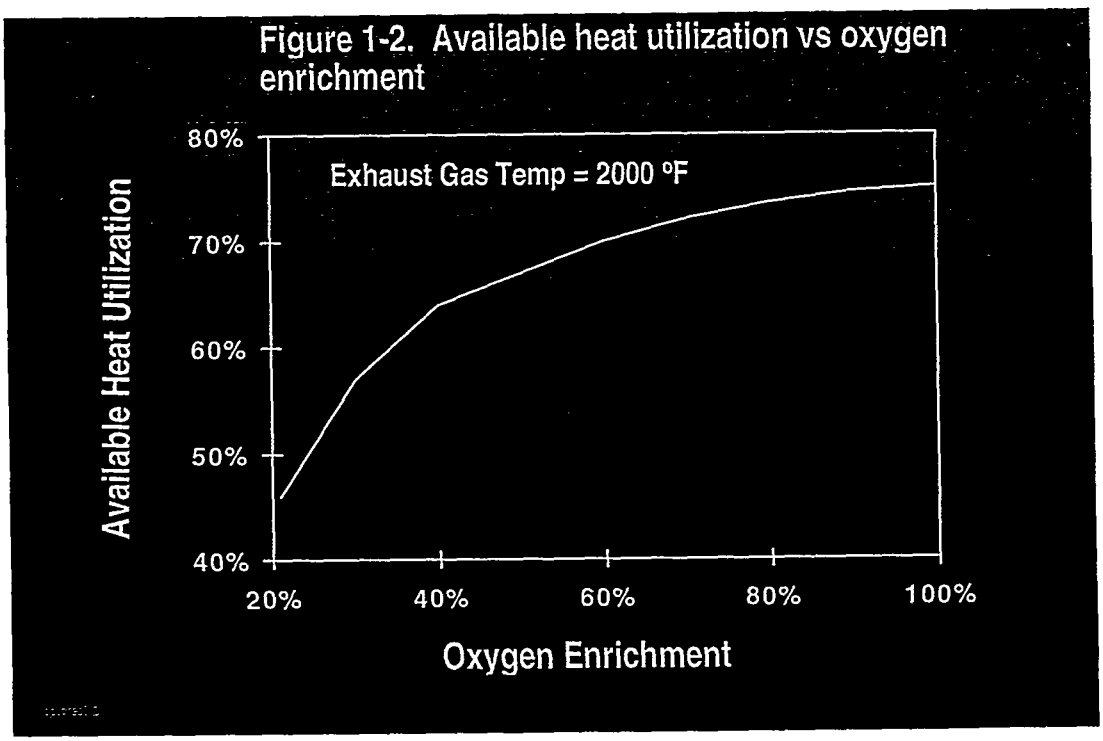
Figure 1-2. Available heat utilization vs oxygen enrichment
Available Heat Utilization
80%
70%
60%
50%
40%
Exhaust Gas Temp = 2000 °F
20%
40%
60%
80%
100%
Oxygen Enrichment

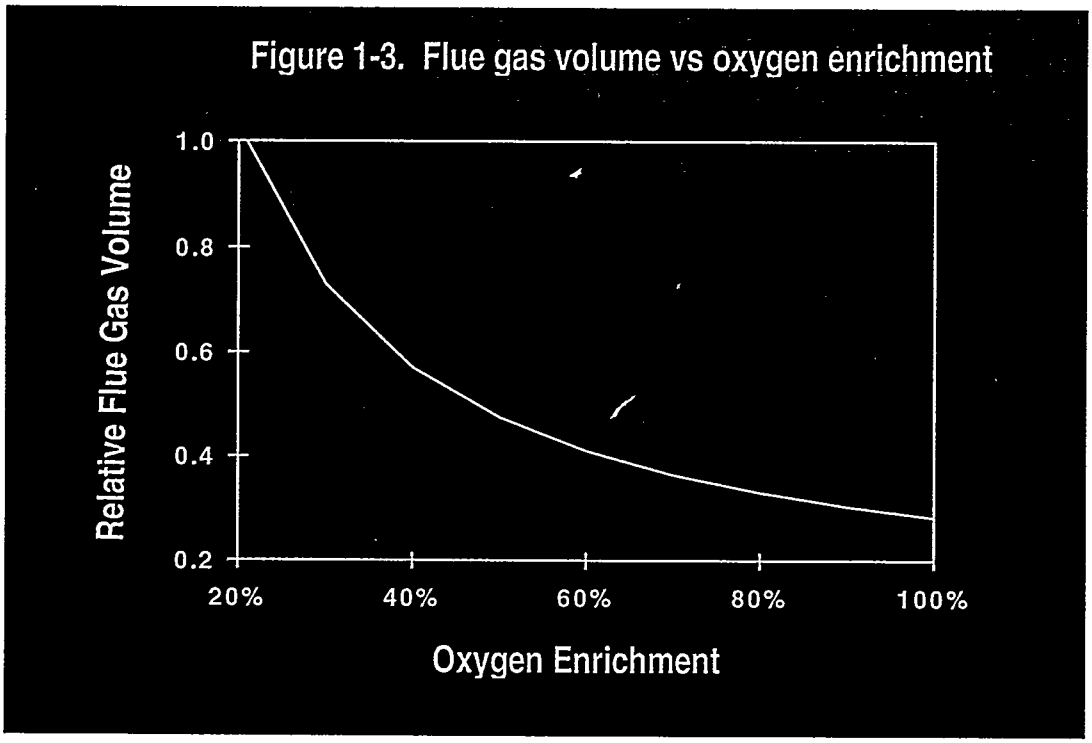
Figure 1-3. Flue gas volume vs oxygen enrichment
Relative Flue Gas Volume
1.0
0.8
0.6
0.4
0.2
20%
40%
60%
80%
100%
Oxygen Enrichment

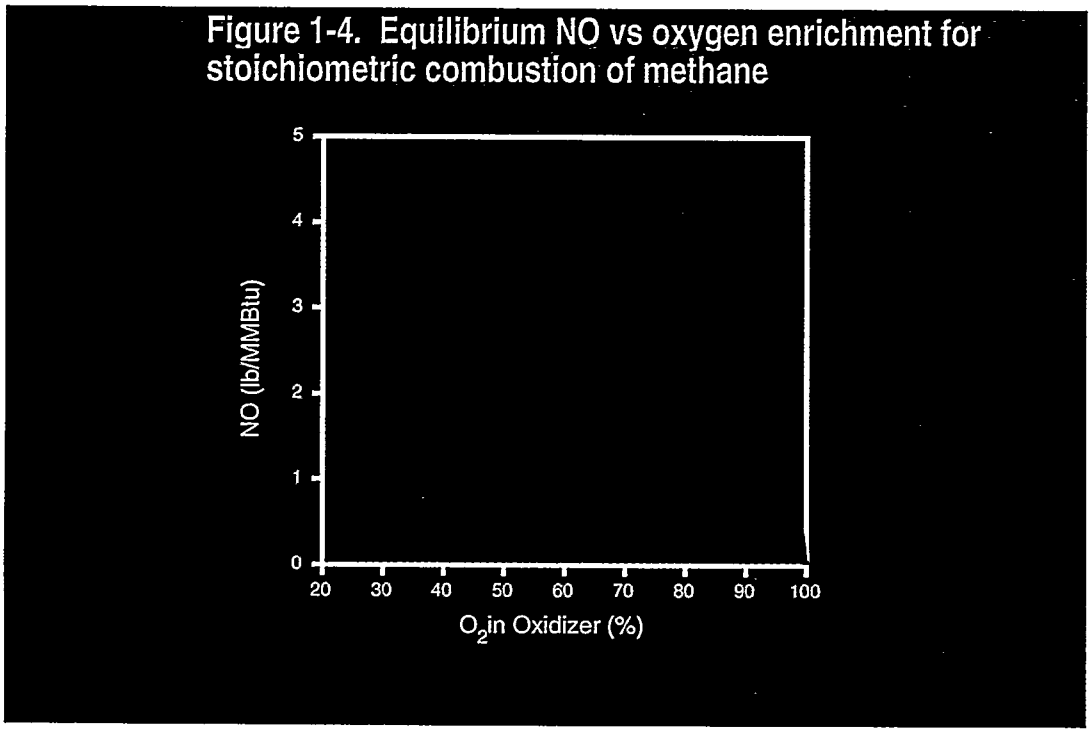
Figure 1-4. Equilibrium NO vs oxygen enrichment for stoichiometric combustion of methane
NO (lb/MMBtu)
5
4
3
2
1
0
20
30
40
50
60
70
80
90
100
O_2 in Oxidizer (%)

High-Capacity, High-Efficiency, Low-NOx Combustion System

Despite the many benefits inherent in OEC, high NOx emissions have traditionally posed a challenge over the intermediate range of oxygen enrichment due to dramatically increased flame temperatures and the high availability of both nitrogen and oxygen molecules. Figure 1-4 shows the equilibrium NO level plateaus (NO is the principal NOx compound) at or around 50 percent enrichment, which is near the point of optimal economics for many industrial applications. NOx is eventually reduced on the high-enrichment side due to the absence of available nitrogen, while on the low-enrichment side the reduction is due to both the lower oxygen concentration and lower flame temperature. The burner technology developed in this project uses two concepts, oxidizer control and advanced mixing, to reduce NOx emissions in the intermediate oxygen enrichment range.

Oxidizer Control. The principle of oxidizer control is illustrated in Figure 1-5, which is a graph of equilibrium NO versus oxygen enrichment and burner stoichiometry. (Burner stoichiometry, as defined here, is the molar ratio of oxygen to natural gas molecules. A value of 2.0 corresponds to the theoretical minimum amount required for complete combustion.) Assume an optimal operating point of between 35 and 50 percent oxygen enrichment and a burner stoichiometry of 2.0. The equilibrium value of NO at this point is approximately 4.0 lb/MMBTU. However, the shape of these curves suggests that the NOx level at this operating point can be substantially lowered by using a two-stage combustion process making separate use of a high- and low-purity oxidizer (see Figure 1-6). The first, or primary, combustion stage employs a high-purity oxidizer operating at fuel-rich conditions (stoich less than 2.0), while a secondary combustion stage utilizes a low-purity oxidizer to consume the remaining fuel. The total number of oxygen and nitrogen molecules present in these two oxidizer streams is equal to that contained in a single "mixed" stream at the original operating point.

There are two additional observations concerning this figure. First, the variation of NO with oxygen enrichment in the fuel-rich primary combustion zone is relatively weak, in the range of 75 to 95 percent. Typical O_2 purity produced by a commercial VSA is in the range of 90 percent. However, operating costs can be reduced by operating the VSA at lower product purity levels. The figure suggests that this can be accomplished with relatively small impact on NOx emissions. The second observation concerns the relatively sharp reduction of NO with purity in the secondary combustion zone, suggesting that secondary oxidizers with oxygen concentrations lower than that of air can further contribute to lowering NOx emissions. The exhaust stream from a VSA, normally vented, has an O_2 purity of 10 to 15 percent, and is therefore ideal for this application. The burner technology developed in this project will be capable of utilizing relatively low-purity primary and secondary oxidizer streams to assist in reducing NOx emissions and the cost of on-site oxygen production.

Advanced Mixing. Success of the oxidizer control concept in lowering NOx emissions depends upon effective mixing of fuel and oxidizer streams to control flame temperature and chemical kinetics. Excessive peak flame temperatures must be avoided in order to maintain low NOx levels. This is accomplished in the new burner design by maximizing the recirculation of furnace gases into the flame, enhancing radiation heat transfer and optimizing flame length. Control of chemical kinetics is needed to ensure adequate isolation between the primary and

Figure 1-5. Equilibrium NO vs oxygen enrichment and stoichiometry illustrating oxidizer control concept

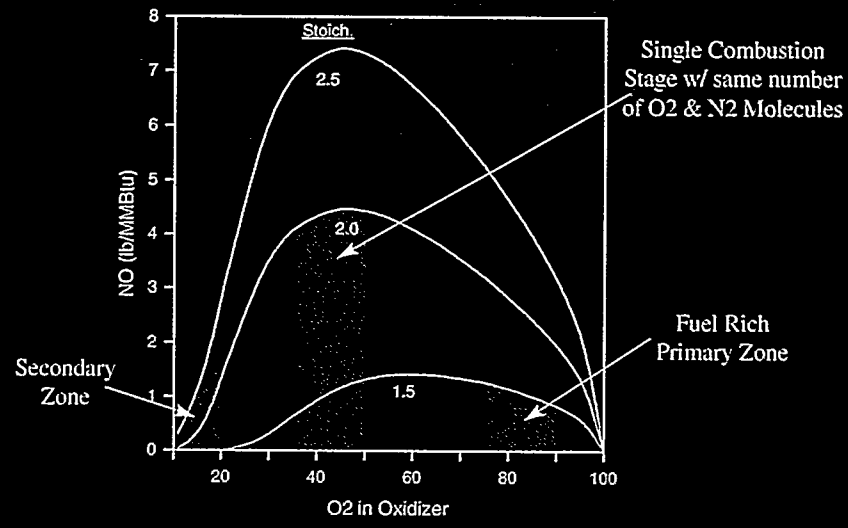

Figure 1-6. Illustration of two-stage combustion process

secondary combustion zones. These ends were attained through proper design of fuel and oxidizer passage sizes, shapes and locations, and were verified through both laboratory and field experimentation.

Integrated O_2 VSA with Sieve-Assisted Storage

Generation of gaseous oxygen using Vacuum Swing Adsorption (VSA) technology provides a low-cost alternative to cryogenic liquid oxygen (LOX) supply. Although the oxygen product is at a lower purity than that for a cryogenic liquid supply, this is typically not an overriding issue in OEC applications. The relatively small size of the VSA plant is ideal for locating oxygen generation at the customer site. However, to obtain the maximum cost reduction, an "integrated" on-site oxygen VSA, i.e., one whose design accounts for end-use characteristics, is essential.

An aluminum melting facility will typically run several furnaces, each operating a batch cycle with periods of high and low fire corresponding, respectively, to furnace charging/melting of scrap and holding/tapping of the finished product. This gives rise to an unsteady oxygen demand, with periodic peaks and valleys, as idealized in Figure 1-7. Conventional design of an on-site VSA calls for sizing based on the peak expected demand; the excess product is then vented during off-peak periods. The unique approach followed in this project was to size the VSA based on the average, rather than peak, demand, and store excess oxygen, generated during periods of low demand, in a tank that uses a proprietary adsorption (i.e., sieve) technology. This stored oxygen is then drawn from the tank during periods of peak demand through the use of a programmable logic controller (PLC) and software logic that link the oxygen supply with furnace demand. Thus, capital and operating costs are reduced, and more complete utilization is made of the generated oxygen relative to the conventional approach.

However, the system integration envisioned in this project extends beyond just matching oxygen supply characteristics with furnace oxygen demand. A further aspect of the integration is between oxygen supply and burner design to produce a low-cost, low-NOx system. Hence, this project intended to show the feasibility of using the low-purity VSA vent stream as a secondary oxidizer and operating the VSA with lower than typical product purity without incurring an increase in NOx emissions.

Project Objectives

The primary objective of this project is to reduce NOx emissions of secondary aluminum melting operations, while improving productivity and energy efficiency. The target for NOx is the Southern California (SCAQMD) regulatory limit of 0.323 lb NO_2/ton aluminum, while the performance target is a 30 percent increase in production (i.e., melt rate) over air-fuel combustion technology. A secondary objective is to reduce the overall cost of melting below that of conventional oxygen-enhanced combustion systems through a combination of improved combustion performance and optimal integration of the oxygen supply. The target enrichment range for the technology is 35 to 50 volume percent oxygen in the oxidizer.

Project Organization and Host Site

This project was funded through a 50/50 cost-share between Air Products and the Department of Energy's Office of Industrial Technologies. The DOE technical manager was John Yankeelov.

Figure 1-7. Oxygen demand varies with time at a secondary aluminum melting facility

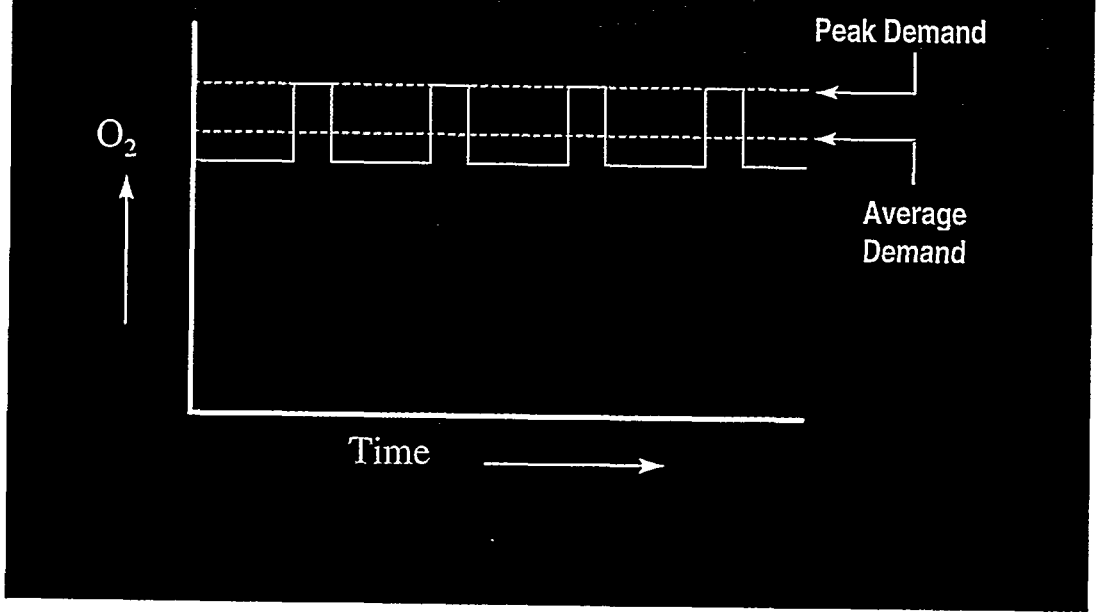

Project management and contract administration were handled by Air Products. The three primary subcontractors were Brigham Young University, which was responsible for official furnace emissions measurements; Argonne National Laboratories, which developed a virtual reality computer simulation of the furnace operation; and Wabash Aluminum Alloys, which hosted the technology at its East Syracuse, N.Y. plant. This plant consists of four reverberatory, secondary aluminum melting furnaces. It should be noted that at the start of the project, the host site was owned by Phillip Services Corporation.

The project duration was approximately two years, with a total contract value of $1.6 MM.

Project Tasks

The six major tasks and subtasks for this project are listed below:

1. *Application and Process Development*

   Base Data Collection. Collect data for existing operation at host site to gain understanding of technical and economic issues.

   CFD Modeling. Simulate the combustion process, fluid mechanics and heat transfer within the combustion space to aid in the development and evaluation of the proposed burner technology.

   Virtual Reality Simulation. Use results generated from CFD modeling as input to a three-dimensional virtual reality simulation of the melting furnace in order to gain a better physical understanding of conditions within the combustion space.

   Laboratory Testing. Test new burner concepts in Air Products' state-of-the-art combustion lab to aid in product development and evaluation.

   Industry Advisory Group. Meet periodically with experts from the aluminum industry to receive feedback on progress and guidance for continuing work.

2. *Economic and Process Evaluation*

   Base Case Evaluation. Use the information collected in Task 1 to evaluate performance, emissions and economics of the existing process.

   New Concept Costs. Determine capital and operating costs of new concepts for oxygen supply and combustion systems.

3. *Design and Construction*

   Combustion System Design. Key elements of the combustion system design include burner flow passages, burner block and ranges of required oxidizer and fuel flow rates.

   Oxygen Supply System Design. This includes an oxygen VSA with sieve-assisted storage tank and piping.

   Flow Control System Design. The flow control system consists primarily of the piping components (valves, gauges, flow elements), electrical control panel, safety monitoring system and automatic feedback loop to maintain the proper flow rates of oxidizer and fuel to each burner.

   Field Installation. This subtask consists of installing all hardware associated with the combustion, oxygen supply and flow control systems at the host facility. Use of the VSA

vent stream as a secondary combustion oxidizer was simulated during field trials, but not included as part of the field installation.

4. *Integrated System Testing*

   Collect performance and emissions data during controlled field tests of the combustion system to determine energy efficiency, melting capacity and emissions. Collect operating data during controlled field tests of the oxygen supply system to determine the effectiveness of the sieve-assisted storage tank.

5. *Process Environmental and Economic Assessment*

   Quantify the advantages and/or disadvantages of the newly developed technology by comparing results from the baseline evaluation with those from the integrated systems testing.

6. *Management and Reporting*

Outline of Report

The main body of this report consists of six sections: Following Section 1, the Introduction, Section 2 describes the host furnace and the development, testing and technical evaluation of the combustion system. CFD modeling results and the virtual reality simulation of the reverberatory aluminum melting furnace are covered in Section 3. Section 4 describes the integrated oxygen supply system, as well as performance evaluation of the sieve storage tank. Economic models for both the aluminum melting furnace and the oxygen supply system are presented in Section 5. Results of the process economic analyses are also presented in this section. Finally, a summary and conclusions are provided in Section 6.

Section 2
Combustion System Development, Performance and Emissions

Introduction

This section of the report describes the performance and emissions characteristics of the combustion technology developed under this project. Particular emphasis is placed on the attainment of objectives with respect to NOx emission, energy efficiency and furnace productivity. Since these objectives are based, in part, on improvements to performance and emissions levels attained with the air-fuel and air-oxy-fuel combustion technologies previously used at the host site, baseline data for these prior technologies are presented first. Features of the new burner design are then described, and performance and emissions data are presented and compared against the pre-development technologies. Finally, an assessment is made as to the degree of success in achieving project goals.

Secondary Aluminum Melting in a Side-Well Reverberatory Furnace

The host furnace for implementing the new air-oxy-fuel burner technology is furnace #8 of Wabash Aluminum Alloys' Syracuse, N.Y. plant. The furnace, depicted in Figure 2-1, is a side-well reverberatory design utilizing four burners. The melting process is initiated by the transfer of thermal energy from the products of natural gas combustion to molten aluminum circulating within the combustion space. Combustion products are exhausted through the stack, while liquid metal flows from the combustion space into the pump well through a submerged arch in the furnace back wall. The circulating pump (within the pump well) propels the liquid into the adjacent charge well, where melting occurs by direct contact of hot flowing metal with the aluminum scrap charge. Molten aluminum flows back into the combustion space via a second submerged arch at the charge well exit.

Definition of Burner Technologies

Prior to 1993, Wabash furnace #8 utilized North American Series 6821 air-fuel burners, which are henceforth referred to as the original air-fuel (AF) technology. The conversion from air-fuel to oxygen-enriched air-fuel operation took place in 1993 with the installation of Air Products' EZ-Fire® burner technology. These burners were designed to fit within the existing North American burner shell and thus permitted rapid conversion (within minutes) to oxygen-enhanced operation without significant disruption to furnace operation. This technology, which was in use at the start of the project, is referred to herein as the pre-development air-oxy-fuel (AOF) burner technology. The low NOx burner technology developed under this project, and now in operation at Wabash furnace #8, is Air Products' EZ-FireLN® burner, designated herein as the post-development AOF burner technology.

Baseline Performance of Original Air-Fuel Burner Technology

Baseline furnace productivity and specific energy usage data pertaining to air-fuel operation on Wabash furnace #8 were provided by the host facility at the start of the project. These data are summarized in Table 2-1. No baseline NOx data were available for the original air-fuel burner technology. However, NOx data were collected for the pre-development AOF burner technology operating in the air-fuel mode, and are presented later in this section.

AIR PRODUCTS

Figure 2-1. Depiction of secondary aluminum melting in side-well reverberatory furnace

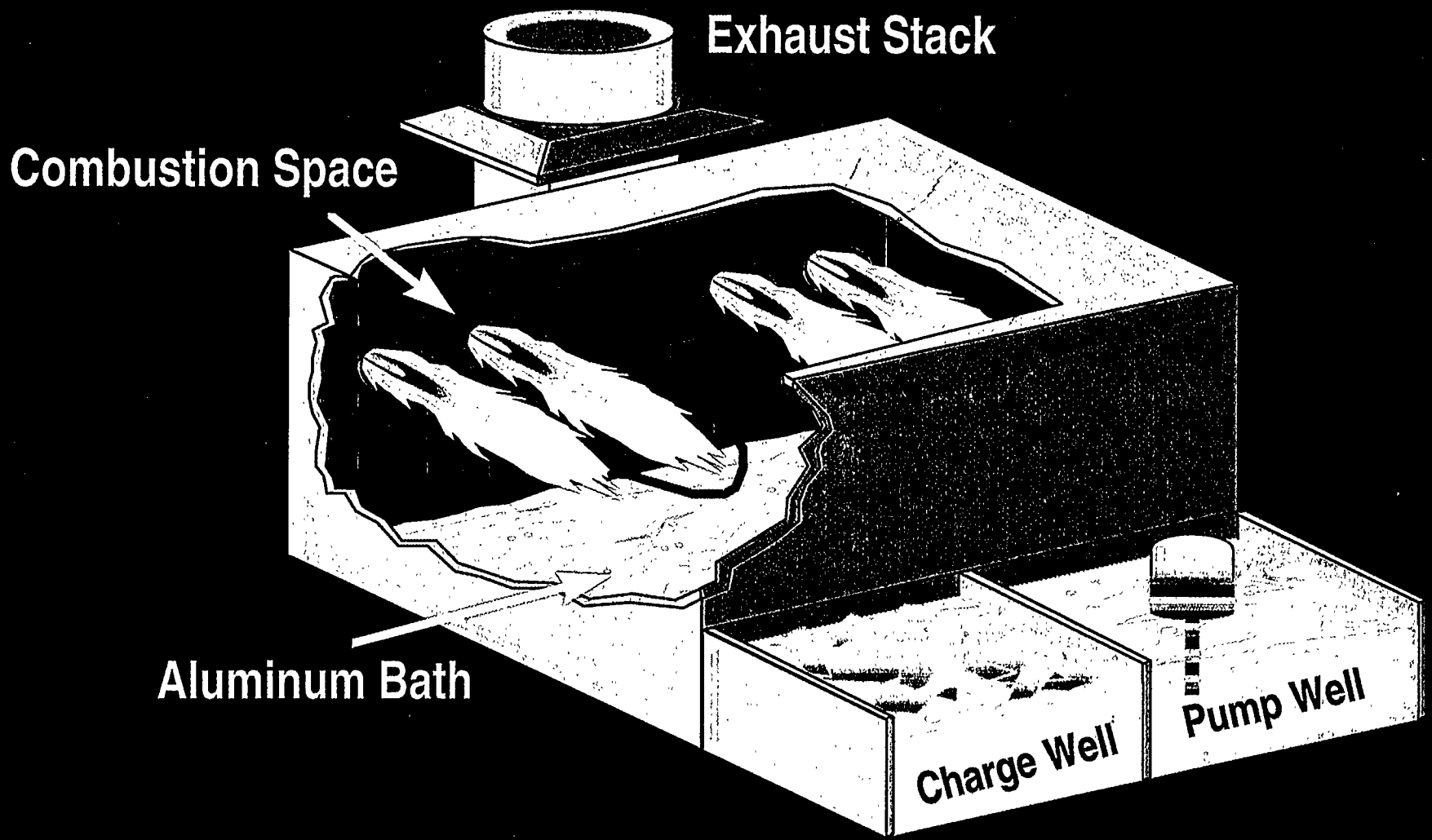

Table 2-1
Original Air-Fuel Performance Data for Wabash Furnace #8

Date	Burner Technology	Furnace Productivity (lb Al/day)	Specific Energy Usage (Btu/lb Al Produced)
1993	Original Air-Fuel	156,000	2395

Description of Pre-Development Air-Oxy-Fuel Burner Technology
A front view of the pre-development AOF burner technology is presented in Figure 2-2. The burner face consists of a central natural gas passage surrounded by a concentric oxygen passage and an outer concentric fuel passage. Combustion air is introduced through a series of eight pipes distributed around the outer periphery of the burner. The principle of this burner design was to produce an inner, fuel-rich, oxy-fuel flame to enhance thermal radiation and reduce NOx emissions (relative to pre-mixing of air and oxygen) and an outer, fuel-lean air-fuel flame to ensure complete combustion. The matrix between the air passages and the concentric fuel and oxygen passages was filled with a refractory casting to provide mechanical and thermal protection to the burner metal.

Baseline Data for the Pre-Development AOF Burner Technology
Baseline performance and emissions data for the pre-development AOF burner technology were collected at the start of the project. Furnace productivity and specific energy usage data representing several weeks of normal operation are summarized in Table 2-2. The original AF performance data are also included for comparison purposes. These data indicate that the pre-development AOF burners provided an improvement relative to the original AF technology—a 25.6 percent production increase and a 33.3 percent reduction in specific energy utilization.

Table 2-2
Pre-Development AOF Burner Performance Data

Date	Burner Technology	Furnace Productivity (lb Al/day)	Specific Energy Usage (Btu/lb Al Produced)
1993	Original Air-Fuel	156,000	2395
1997	Pre-Development AOF	196,000	1598

Faculty from the Mechanical Engineering Department at Brigham Young University were sub-contracted to characterize the baseline emissions for the pre-development AOF burner technology. Measurements were made in the exhaust stack of furnace #8 under both air-fuel and air-oxy-fuel operating conditions. Limited measurements were also made in the combustion space of furnace #8 and the exhaust stacks of the other three furnaces at the host facility. All high-purity oxygen for these tests was supplied from liquid oxygen (LOX) tanks, at essentially 100 percent purity.

A complete description of test results is included in Appendix 1, while a summary of key findings is provided within this section.

Figure 2-2. Front View of Pre-Development Air-Oxy-Fuel Burner

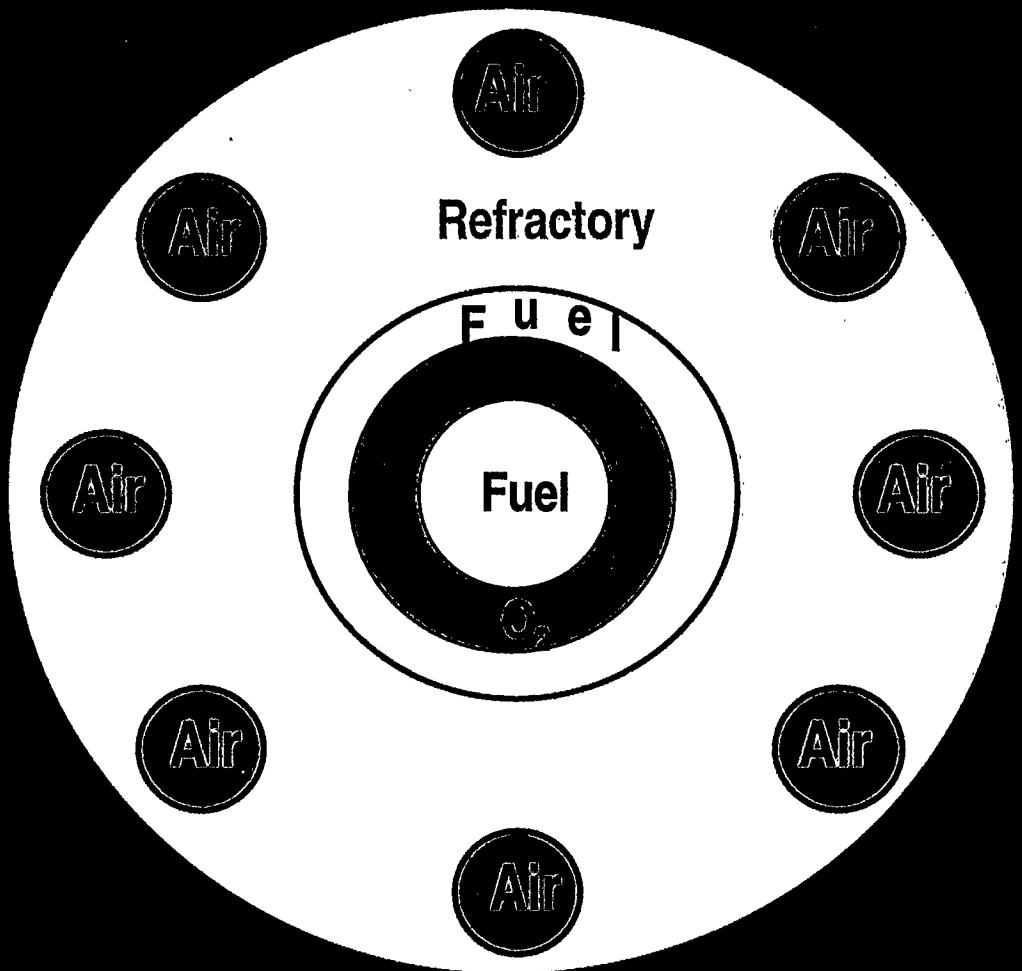

Baseline Test Results

Multi-point traverses of gas temperature and species concentrations were made in the exhaust stack of furnace #8 for five test conditions encompassing typical air-fuel and air-oxy-fuel burner operating conditions. Results are summarized in Table 2-3. The terms stoich and oxygen enrichment used in this table and elsewhere are defined as:

> **Stoich** = moles O_2 /mole natural gas
> A stoich of 2.0 is the theoretical minimum value required for complete combustion of methane.
>
> **O_2 enrichment** = moles O_2 in oxidizer (i.e., high-purity oxygen + air)/[mole O_2 + N_2]
> An O_2 enrichment level of 20.9 percent pertains to pure air, while an enrichment of 100 percent pertains to pure oxygen.

Results show the disparity in NOx levels between the air-fuel and air-oxy-fuel operating modes with this burner technology. Air-oxy-fuel operation at between 35-36 percent oxygen enrichment generated NOx levels between 0.8 to 2.3 lb NO_2/MMBTU, while air-fuel NOx levels were an order of magnitude lower, varying from 0.06 to 0.09 lb NO_2/MMBTU. It should be mentioned that these air-fuel NOx levels are consistent with those measured on furnace #9, which uses North American air-fuel burners. Data also highlight the sensitivity of NOx and CO emissions to stoich. Comparison of air-oxy-fuel tests 1, 3 and 4 show that NOx decreased from 2.29 to 0.81 lb NO_2/MMBTU as stoich decreased from 2.22 to 2.01, while CO concurrently increased from 5 to over 10,000 ppmv. It is also interesting to note that, at a nominal firing rate of 15,000 scfh natural gas, there is little difference in stack temperature between air-oxy-fuel (test #1) and air-fuel (test #5) operation. Since the total exhaust flow rate is significantly higher for air-fuel operation, this confirms the higher thermal efficiency inherent in air-oxy-fuel combustion.

Table 2-3
Pre-Development Burner Emissions Data at Wabash Furnace #8

Test #	Fuel Flow	Stoich	O_2 Enrich	Stack Nox	Stack CO	Stack Gas Temp
	scfh		%	lb NO_2 /MMBTU	ppmv dry	deg F
1	15,000	2.22	36.0	2.29	5	2153
2	4400	3.68	20.9	0.090	3	1558
3	16,970	2.01	35.3	0.81	10,820	2132
4	16,970	2.10	35.5	1.00	7700	2281
5	14,900	2.45	20.9	0.062	13	2118

Post-Development, Low NOx, Air-Oxy-Fuel Burner Technology

The primary objective of the burner technology developed under this program was to maintain or increase the melting capacity and energy efficiency of the "first generation" air-oxy-fuel burner,

while achieving a substantial reduction in NOx emissions. Technology development was aided by the collective burner design expertise of Air Products' Global Applications Development Team, the state-of-the art Combustion Laboratory at Air Products' World Headquarters in Allentown, Pa. and CFD modeling efforts. The final burner design emerged after fabrication and testing of several prototype burners.

Burner Design and Operation

A front view of the final low-NOx burner design, presented in Figure 2-3, shows a center fuel passage surrounded by a high-purity oxygen annulus, two butterfly-shaped, low-purity oxidizer (i.e., air or waste gas from the VSA) flow passages, and two high-purity oxygen "lances" outside the burner face. This new burner design reduces NOx, relative to the pre-development AOF burner technology, through controlled mixing of fuel and oxidizer streams. This occurs principally through heavy staging (i.e., delayed introduction) of oxidants and by the recirculation of partially combusted furnace gases into the flame. Staging of oxidants helps to lower NOx emissions by reducing the availability of oxygen in the high-temperature region of the flame, and also produces a relatively long, luminous (i.e., highly radiating) flame, providing efficient heat transfer to the load. Recirculation of furnace gases into the burner flame lowers peak flame temperatures and oxygen concentrations, further lowering NOx emissions. The effectiveness of gas recirculation in this burner is enhanced by the butterfly-shaped, low-purity oxidizer passages. These passages create open spaces immediately above and below the oxygen annulus, thereby allowing deep penetration of the recirculated gases into the core oxy-fuel flame.

The burner was designed to operate in both the air-oxy-fuel and air-fuel operating modes, since this is consistent with the cyclic energy input and productivity demands for the charging and tapping cycles of furnace operation. The target oxygen enrichment range for this application was between 35 and 50 percent. The burners were field tested for extended operating periods at both ends of this enrichment range.

Emissions Data for Post-Development Low-NOx Burner Technology

Emissions data presented within this section illustrate the effects of oxidizer purity, burner design and operating conditions on NOx and CO emissions for the post-development burner technology. Emissions levels achieved with the post-development technology are then compared to those of the pre-development technology, as well as to the SCAQMD regulatory limits.

Effect of Oxidizer Purity on NOx Emissions

The post-development burner technology uses two oxidizer streams, the primary, or high-purity, oxidizer surrounding the fuel jet, and the secondary, or low-purity, oxidizer flowing through the butterfly-shaped passages. Primary oxidizer purity will vary depending on whether oxygen is supplied from an O_2 VSA or from liquid oxygen (LOX) tanks. Typical O_2 VSA oxygen purity ranges from 90-93 percent, although lower purity results from operation at higher than design flow rates. Oxygen supplied from LOX tanks is essentially 100 percent pure. Secondary purity can vary from approximately 12 percent oxygen in the VSA vent stream to 21 percent oxygen in pure air.

Figure 2-3. Front View of Post-Development AOF Burner Technology

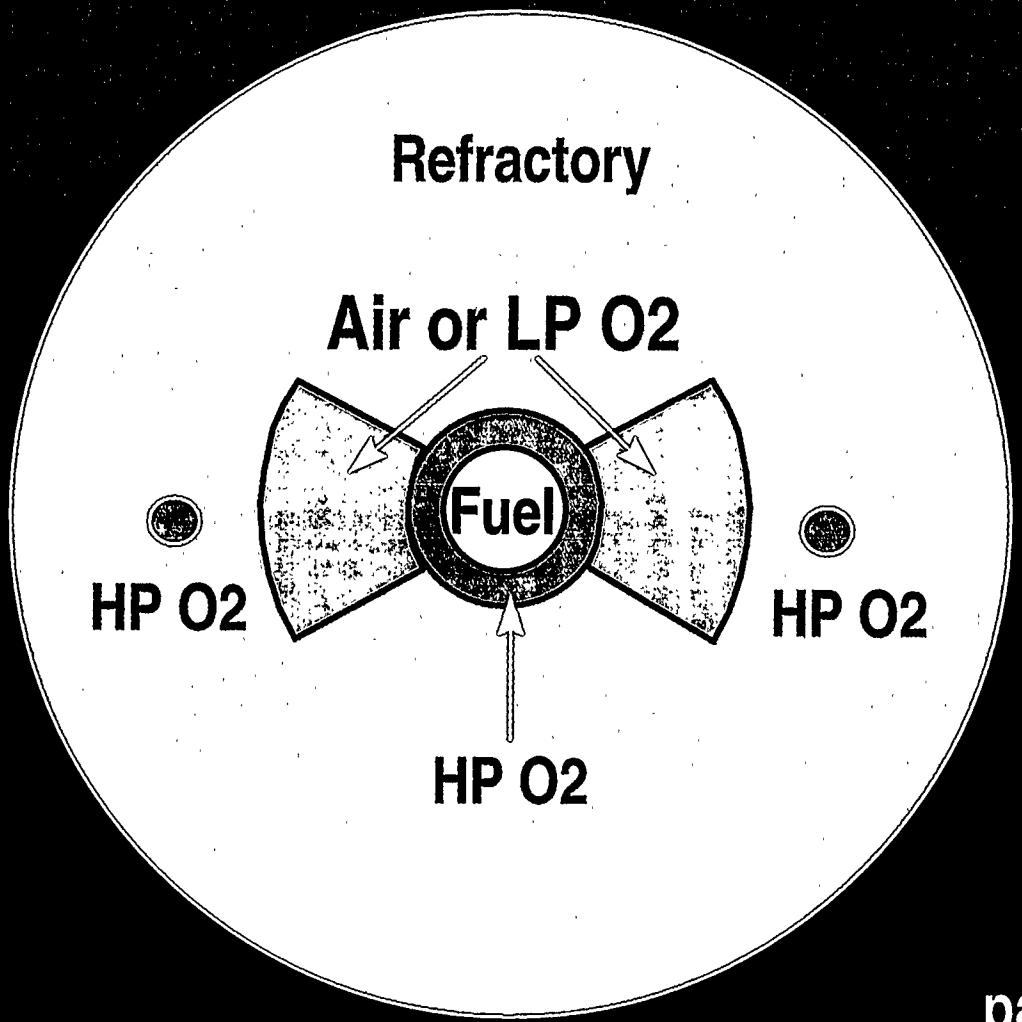

patent allowed

Field tests were conducted at Wabash furnace #8 prior to the installation of the on-site O_2 VSA to determine the influence of the oxidizer purity of both streams on NOx emissions. Variations in primary oxidizer purity were achieved by blending oxygen from LOX tanks with essentially 100 percent pure nitrogen from liquid nitrogen (LIN) tanks. Secondary oxidizer purity was varied by controlled mixing of nitrogen with air.

Effect of Primary O_2 Purity on NOx Emissions. Figure 2-4 shows NOx as a function of primary O_2 purity. NOx drops sharply as O_2 purity increases from 90 to100 percent due to the reduction in available nitrogen in the immediate vicinity of the high-temperature flame. For example, the NOx reduction between 90 and 100 percent oxygen purity is roughly 30 percent (~1.7 to 1.2 lb NO_2/MMBTU). Since typical O_2 VSA oxygen purity is in the range of 91-93 percent, this mode of oxygen supply will generate higher NOx emissions than those from a liquid oxygen supply. However, the NOx variation between a purity of 78 and 90 percent is small, suggesting that operating the VSA in a "low-purity" mode would not result in substantially higher NOx compared to more traditional VSA operation.

Effect of Secondary O_2 Purity on NOx Emissions. Secondary oxidizer oxygen concentrations were varied between 17 and 20.9 percent during field testing at the host furnace. Lower concentrations were not attained due to limitations on flow controls for nitrogen blending. Results are summarized in Figures 2-5 (primary oxidizer purity equal to 100 percent) and 2-6 (primary oxidizer purity equal to 80 percent) as plots of NOx versus oxygen enrichment for different secondary O_2 purity levels. At a given oxygen enrichment level and primary oxidizer purity, the lower purity secondary oxidizer yielded NOx levels that were at or below those corresponding to the use of air as the secondary oxidizer. However, it is evident from the graphs that scatter in the data was relatively large compared to differences in NOx between the higher and lower secondary oxidizer purity levels. Nevertheless, these results indicate the potential for lowering NOx through the use of a low-purity VSA vent stream integrated with the new AOF burner technology.

Effect of Burner Operating Conditions on NOx and CO Emissions

Aside from overall firing rate, which is dictated by furnace demand, the post-development, low-NOx burner technology has three adjustable parameters: oxygen split between the annulus and the lances, oxygen enrichment level, and burner stoichiometry. These variables were systematically evaluated during field trials at Wabash furnace #8. The effect of lance O_2 flow on NOx is illustrated in Figure 2-7. The data indicate a minimum in NOx emissions occurring with roughly a 50/50 split in O_2 flow between the lances and inner annulus. With all of the oxygen going to the inner annulus (zero lance flow), NOx increases (relative to the minimum NOx condition) because of higher flame temperatures and the greater availability of oxygen in the high-temperature region. The cause for the increase in NOx at the other extreme (100 percent lance flow) is uncertain. However, it is known that the void between the natural gas and air streams created by removing oxygen from the inner annulus acts as a "bluff body," producing vortices that increase the rate of mixing between these streams. Moreover, it is probable that, in the absence of stabilizing oxygen, the high momentum of the natural gas and air streams caused the flame to separate (i.e., lift) away from the nozzle tip. This phenomenon is also known to

Figure 2-4. NOx vs Primary Oxidizer Purity at Wabash Furnace #8. Secondary Oxidizer is Air. Burner Stoich ~ 1.7, O2 Enrichment ~ 40%

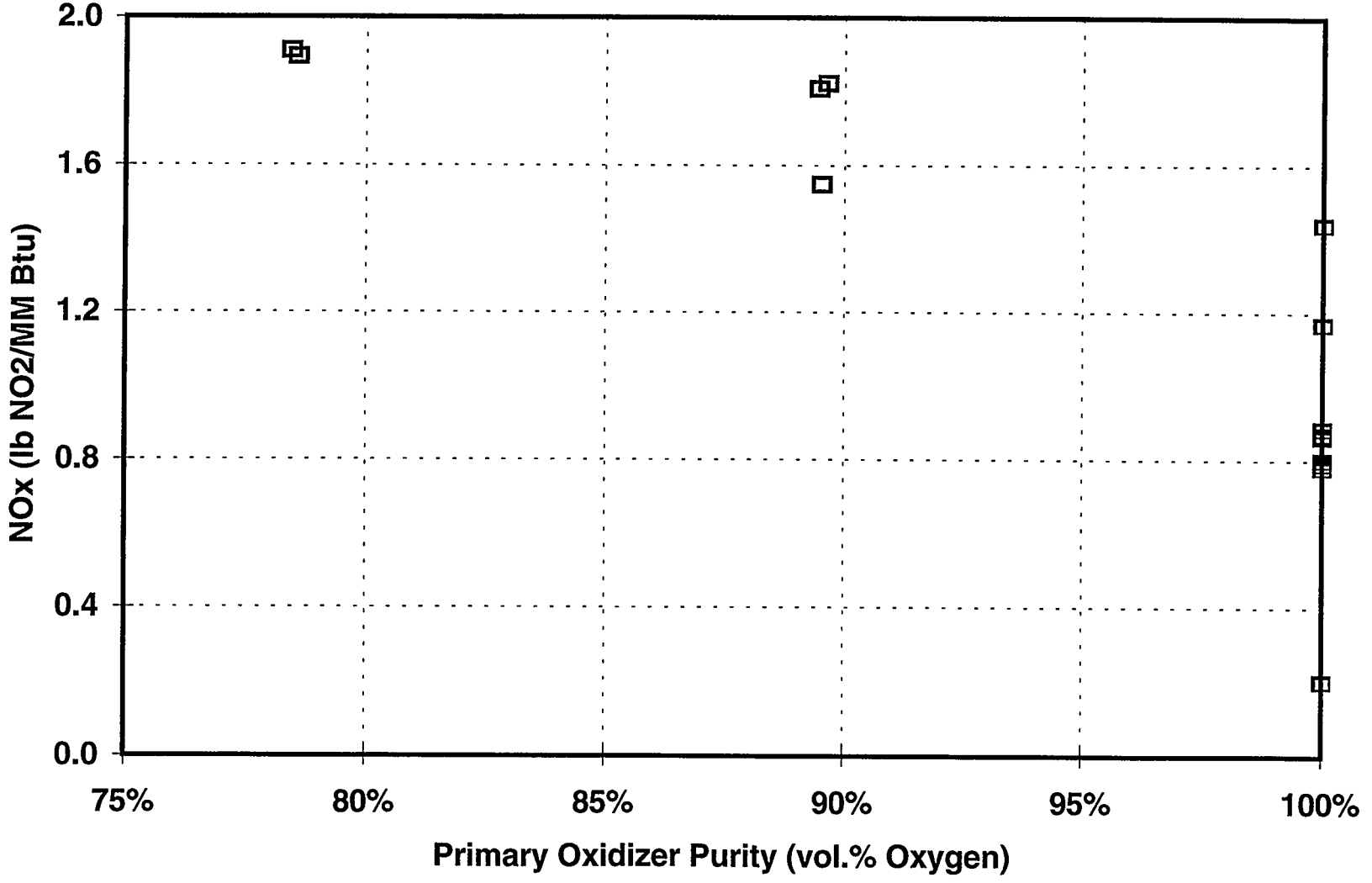

Figure 2-5. NOx vs Enrichment and Secondary Oxidizer Purity at Wabash Furnace #8; Burner Stoich ~ 1.7; Primary O2 Purity = 100%

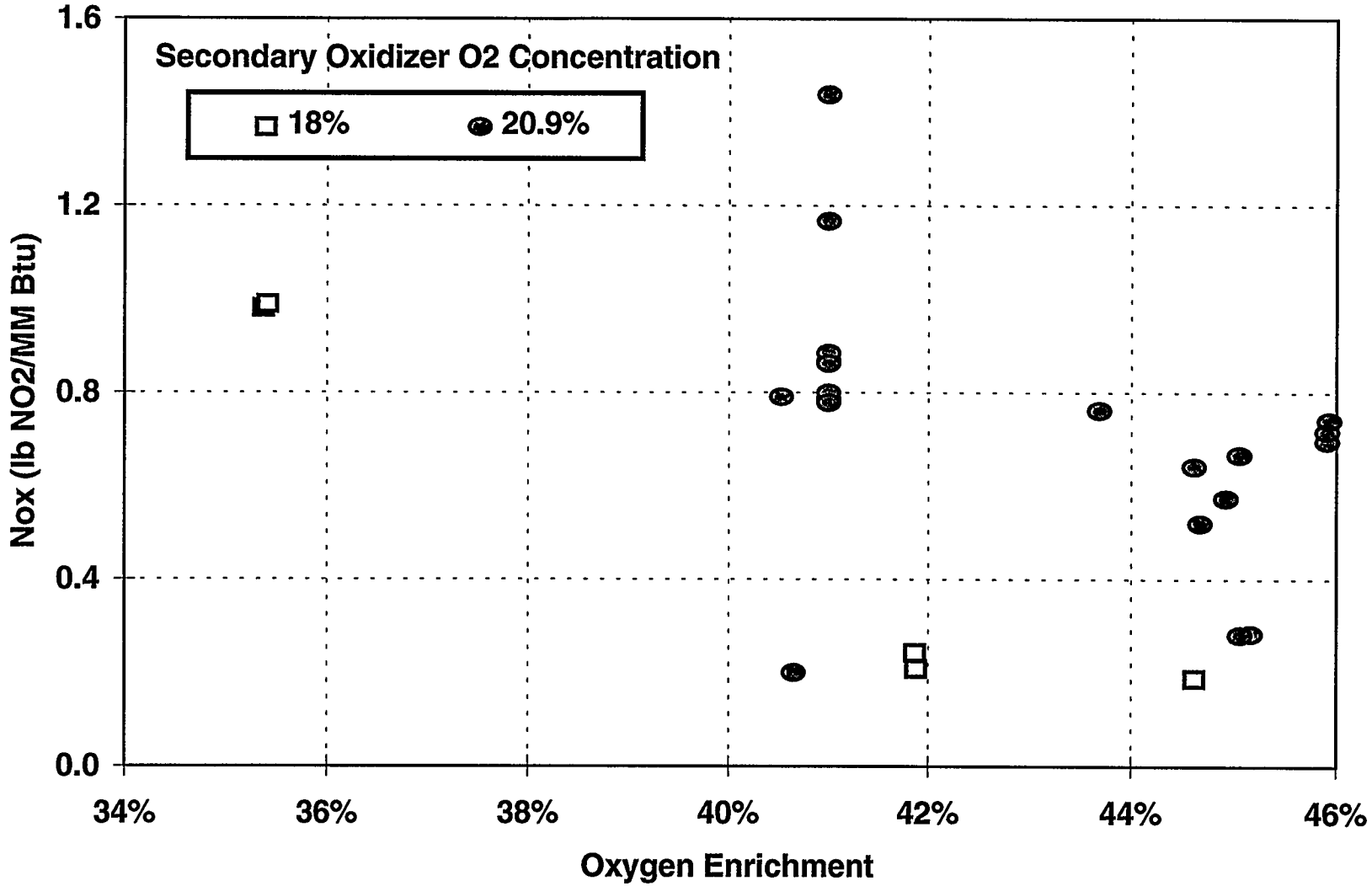

Figure 2-6. NOx vs Enrichment and Secondary Oxidizer Purity at Wabash Furnace #8; Burner Stoich ~ 1.7; Primary O2 Purity = 80%

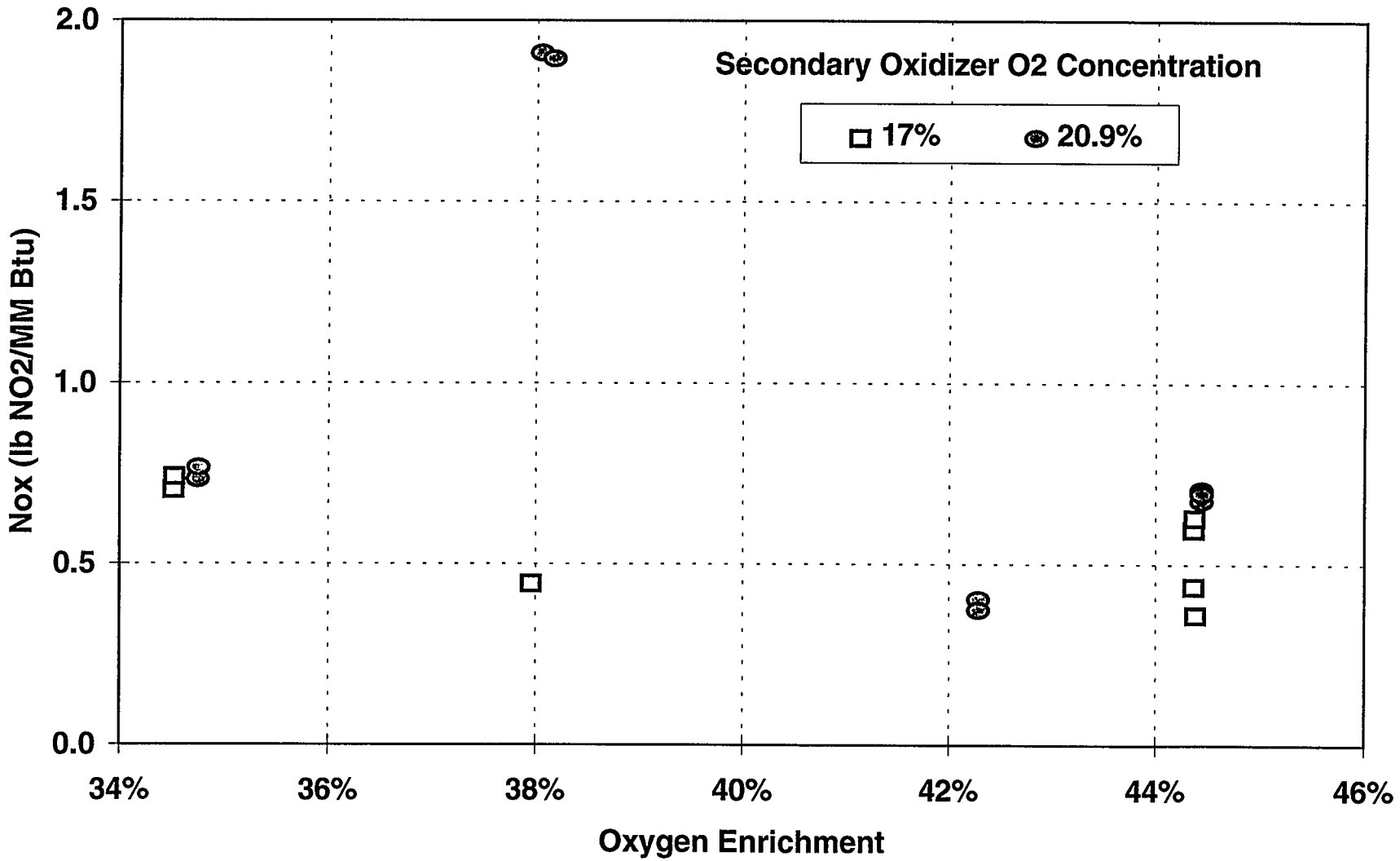

Figure 2-7. NOx vs Oxygen Lance Flow at Wabash Furnace #8; Burner Stoich ~ 1.7; Primary O2 Purity = 100%; Secondary Oxidizer is air; O2 Enrichment = 41%

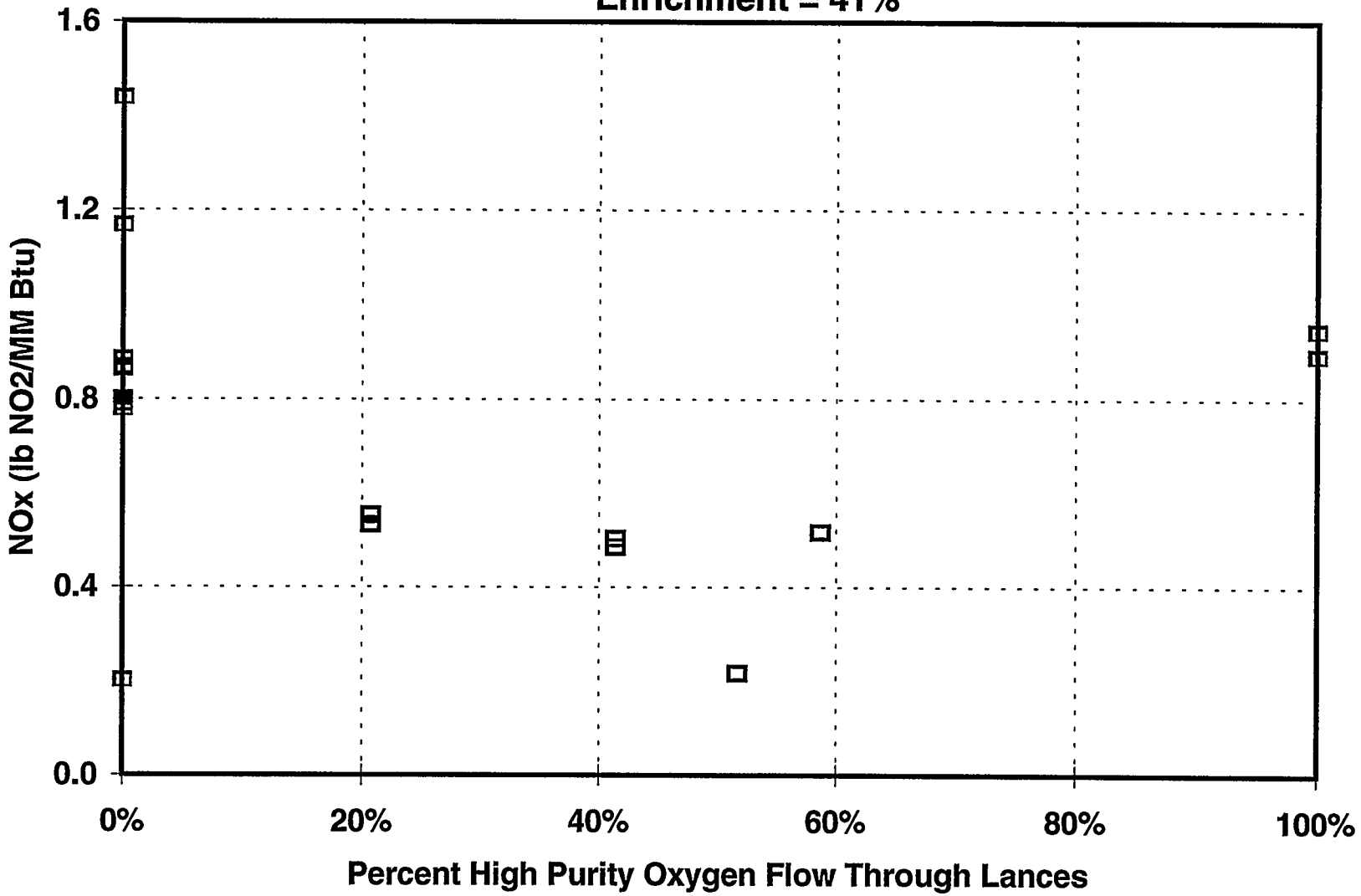

enhance mixing rates [3]. It is believed that this increase in mixing rate was responsible for the increase in NOx.

The effects of burner stoichiometry and oxygen enrichment on NOx and CO were measured by BYU during a set of field tests at Wabash furnace #8 in January 1999. These data are considered to be the "official" emissions levels for the post-development burner technology. Figure 2-8 shows the effects of stoichiometry and oxygen enrichment on stack NOx emissions. While NOx increases with both parameters, it is more sensitive to enrichment than stoichiometry over the range of conditions tested. For example, at stoich of 2.1, there is nearly a fourfold increase in NOx (0.1 to nearly 0.4 lb NO_2/MMBTU) as oxygen enrichment is increased from 32 to 40 percent. However, at an enrichment level of approximately 39 percent, the increase in NOx is less than a factor of two, from 0.18 lb NO_2/MMBTU at stoich = 1.94 to 0.33 lb NO_2/MMBTU at stoich = 2.2.

Stack CO emissions from the same data set are provided in Figure 2-9. In contrast to the NOx trends shown in the preceding figure, CO increases with decreasing enrichment and stoich. Moreover, the changes in CO with enrichment are much more drastic than those for NOx. This is illustrated by the data at stoich equal to 2.0. CO is essentially zero at 39 percent enrichment, but climbs in an exponential fashion to greater than 12,000 ppm as enrichment drops to 33 percent. Key data from this test series are provided in Table 2-4. A more detailed summary is presented in Appendix 2.

Since independent control of burner firing rate was not possible in the field, systematic testing of the effect of firing rate on NOx emissions was conducted in the Air Products Combustion lab. Results, summarized in Figure 2-10, show that NOx is relatively insensitive to firing rate over the range from 2.0 to 5.0 MMBTU/hr (per burner).

Influence of Burner Design on NOx Emissions

The unique shape of the secondary oxidizer passage was cited as an important factor in producing a low-NOx burner design. Laboratory tests were conducted to determine the effect of passage shape on NOx emissions. A burner prototype was designed with removable inserts, allowing for variation of the secondary oxidizer passage cross-section between a full annulus and a butterfly shape (see Figure 2-11). Test results, summarized in Figure 2-12, showed that NOx emissions were approximately 50 percent lower over a wide range of oxygen enrichment levels for the burner with the butterfly-shaped passage. Experimental results such as these were used as the basis for incorporating this feature into the post-development burner design.

Having established the importance of the butterfly-shaped secondary oxidizer passage in reducing NOx, there were nevertheless several iterations in burner design prior to installation of the final post-development technology in Wabash furnace #8. One intermediate design, which was installed into a reverberatory aluminum melting furnace in Southern California, was found to yield higher NOx emissions than the final design installed at Wabash. Figure 2-13 provides a comparison of the two burner designs.

Fig. 2-8 NOx vs Enrichment and Stoich at Wabash Furnace #8; 50% Oxygen Flow to Lances; 90% Oxygen Purity

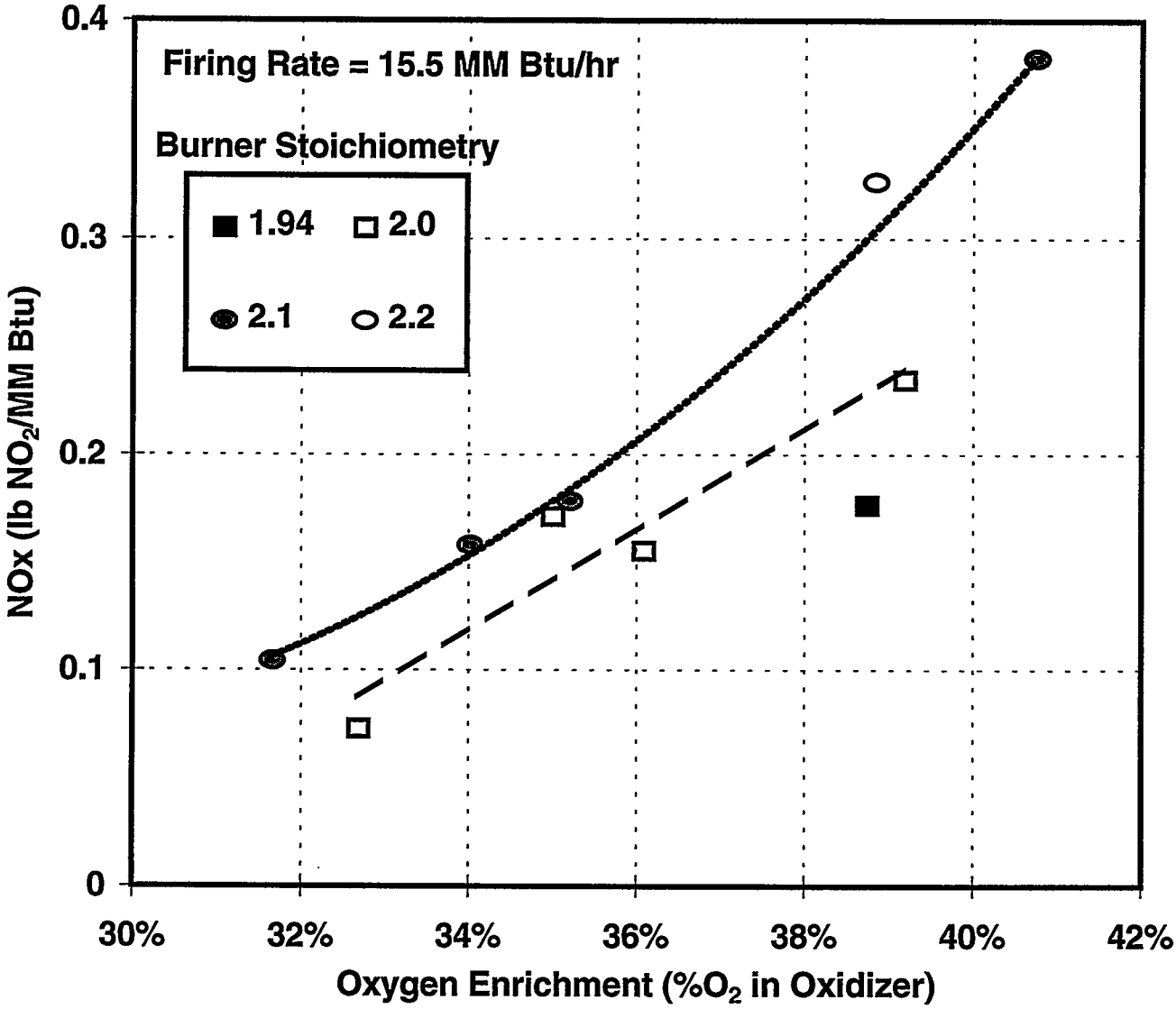

Fig. 2-9 CO vs Enrichment and Stoich at Wabash Furnace #8; 50% Oxygen Flow to Lances; 90% Oxygen Purity

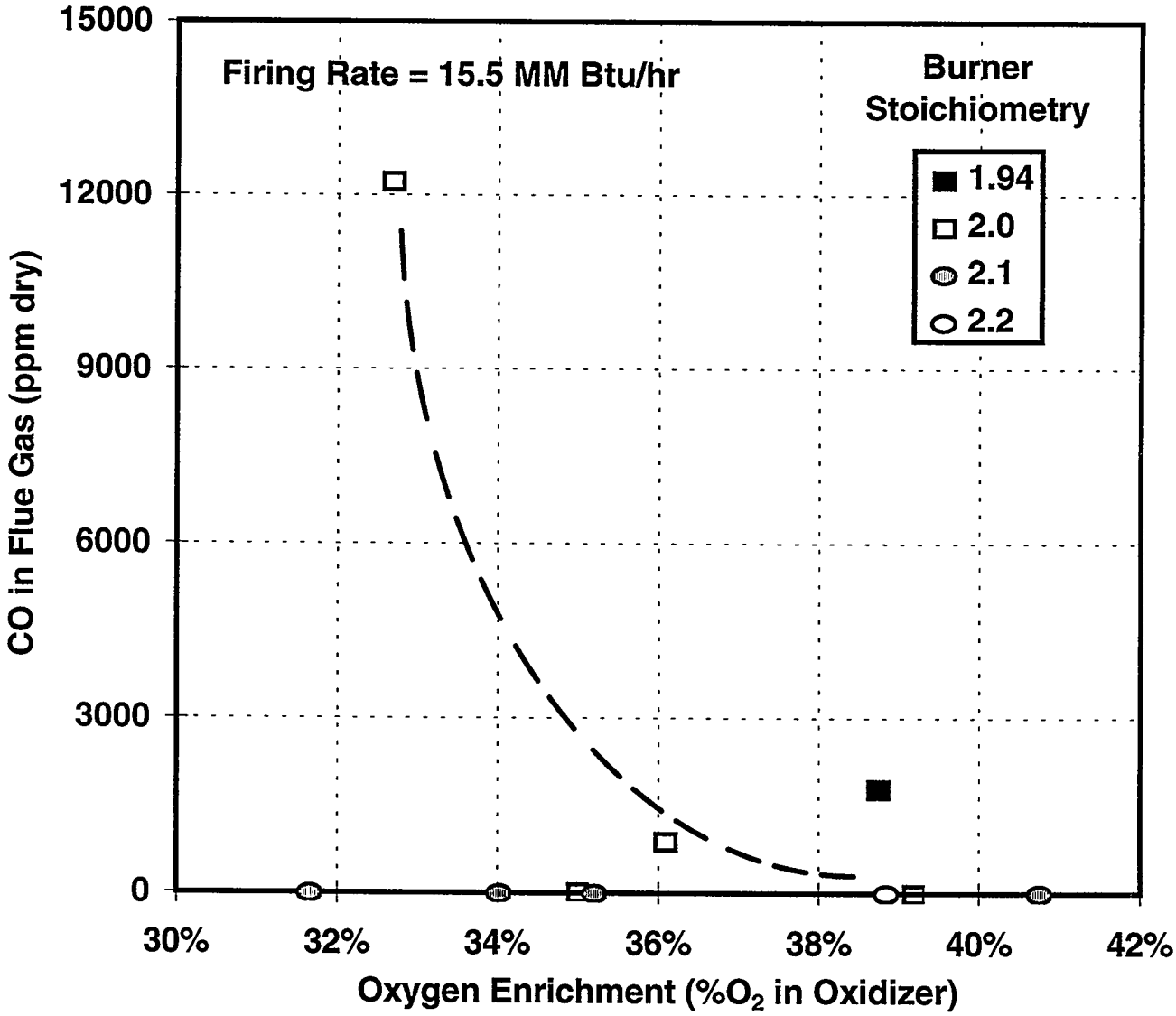

Figure 2-10. Laboratory Data Showing the Effect of Burner Firing Rate on NOx: Oxygen Enrichment = 35%; Primary O2 Purity = 90%; Secondary O2 Purity = 21%

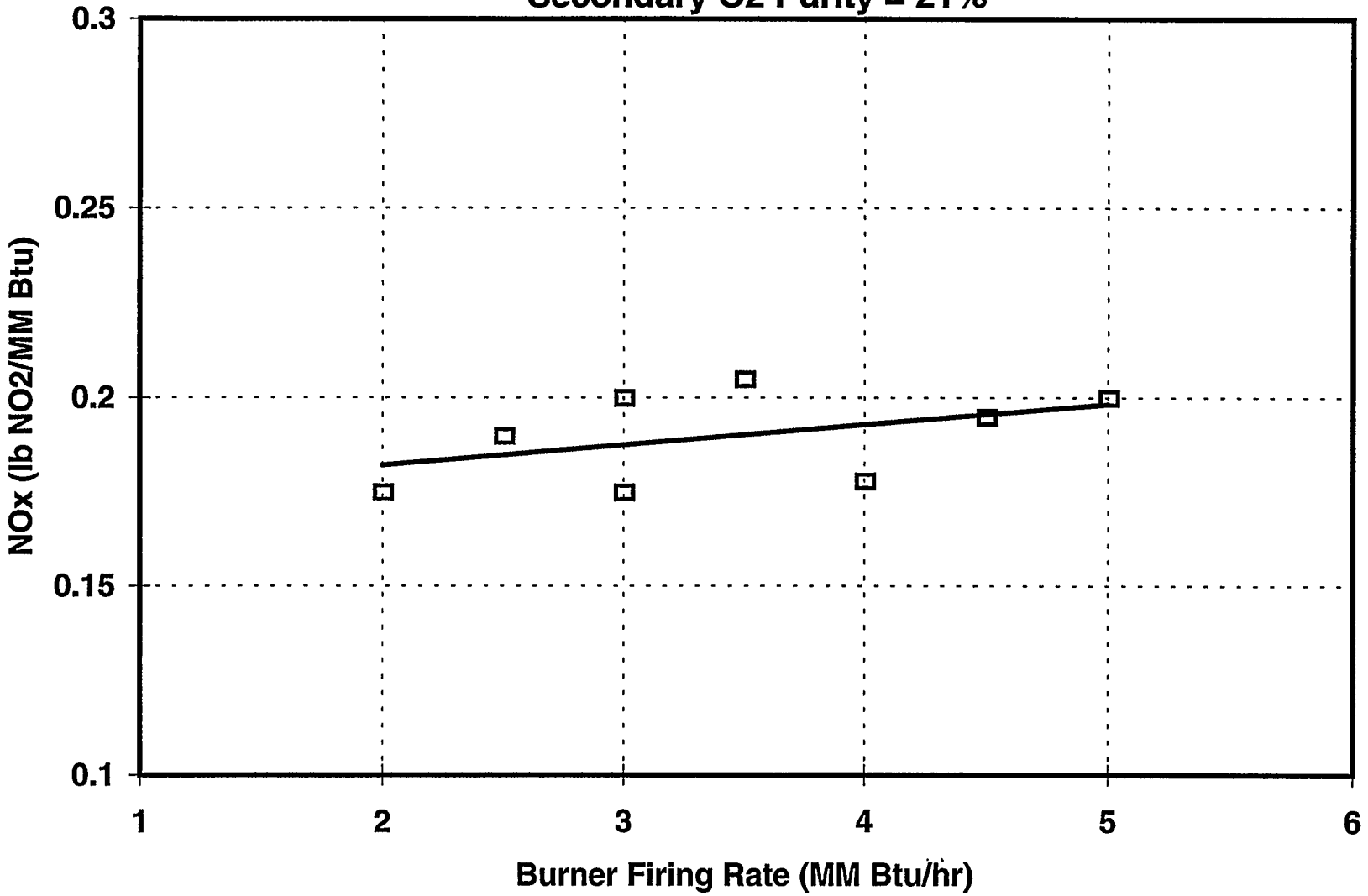

Figure 2-11. Laboratory Burner Prototypes with Annular and Butterfly-shaped Secondary Oxidizer Passages

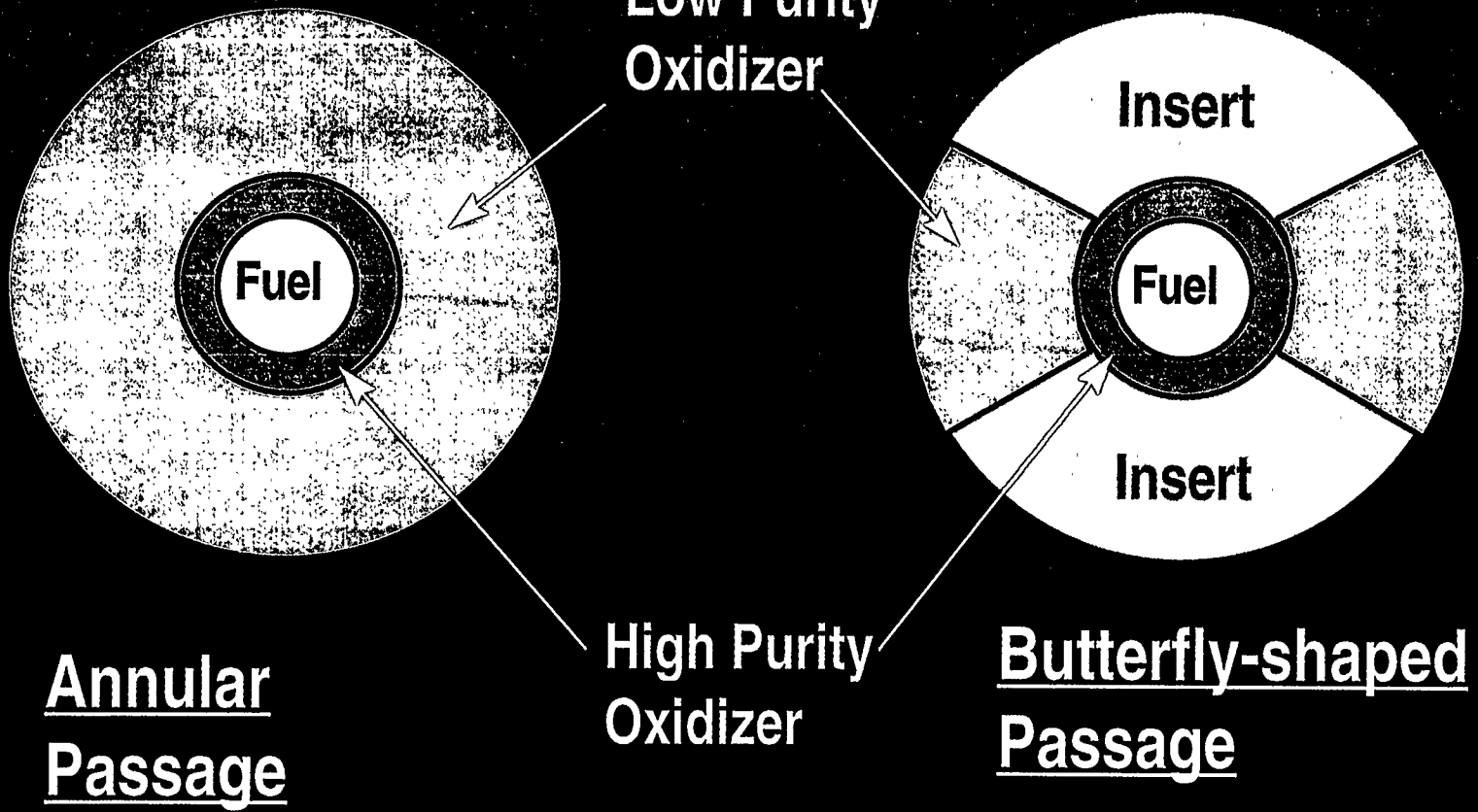

Figure 2-12. NOx Emissions for Laboratory Burners with Butterfly-shaped and Annular Secondary Oxidizer Flow Passages; Primary O2 Purity = 90%; Secondary O2 Purity = 21%; Firing Rate = 3 MM Btu/hr

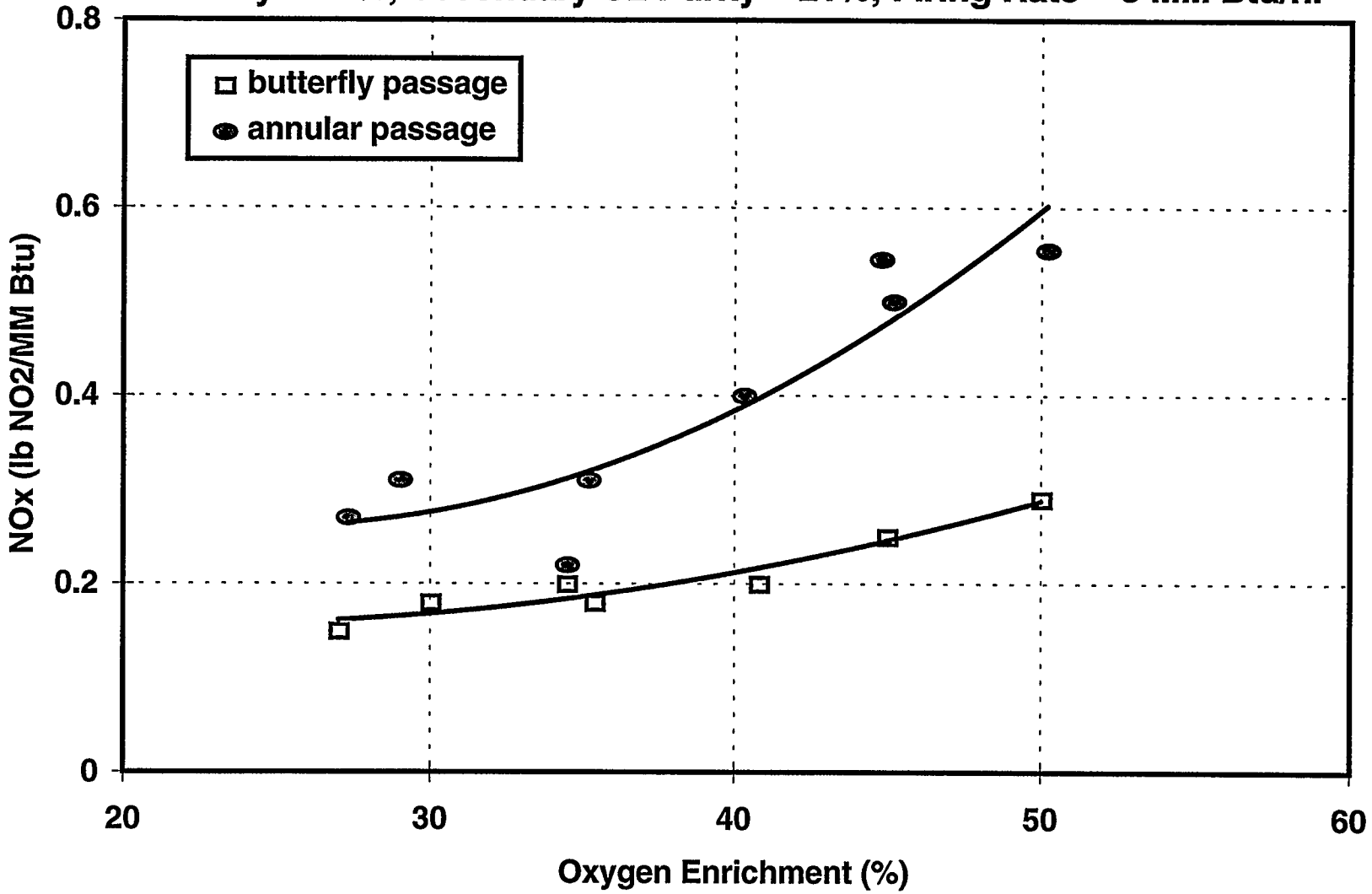

Figure 2-13. Comparison of Burner Designs at Wabash and Southern California Furnace

AIR PRODUCTS

Wabash Furnace #8

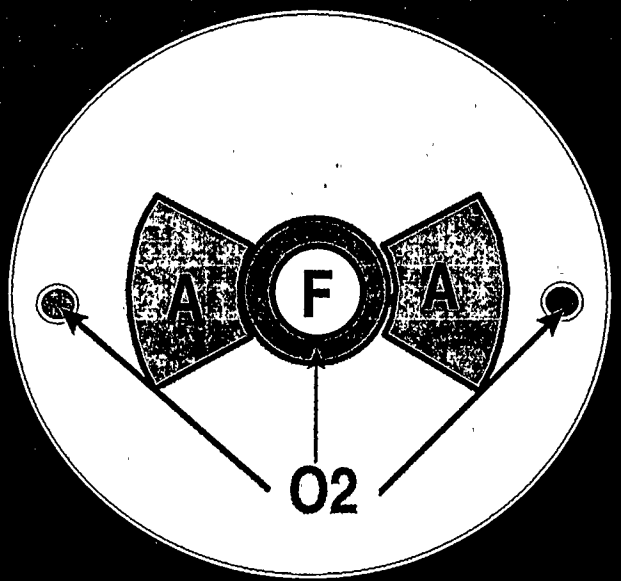

Southern California Site

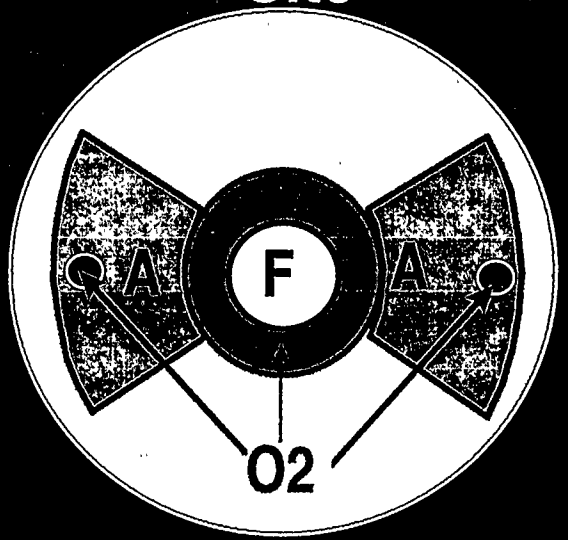

Table 2-4
Summary of Post-Development Burner Emissions Data at Wabash Furnace #8

Test #	Fuel Flow	Stoich	O_2 Enrich	Stack NOx	Stack CO	Stack Gas Temp
	scfh		%	lb NO_2 /MMBTU	ppmv dry	deg F
1	15,513	2.22	39	0.327	0	1963
2	15,532	2.09	34	0.159	0	1918
3	15,529	2.10	32	0.105	0	1961
4	15,533	1.98	33	0.073	12,250	2053
5	15,518	2.11	41	0.383	0	1939
6	15,545	2.10	35	0.179	0	1983
7	15,536	2.02	36	0.156	892	2037
8	15,551	2.01	39	0.235	0	1957
9	15,548	1.94	39	0.177	1800	2056
10	15,552	2.00	35	0.172	21	1983

* Primary oxidizer purity was 100 percent for test 1 and approximately 90 percent for tests 2-10.

Although the fundamental design features are present in both burners, there are differences in the specific application of these features. For example, the flow passages are larger in the burner at the Southern California site. Thus, at given operating flow rates, the gas velocities are lower in this burner. This translates into less recirculation of furnace gases and, consequently, less dilution of the high-temperature flame. Moreover, the air passage angle is wider in the Southern California burner. Access of the recirculated gases to the core oxy-fuel flame is therefore restricted. Note also the relative positioning of the oxygen lances. While they are located outside the air passage for the Wabash burner, limitations in available space required their placement to be inside the air passage for the Southern California burner. This amounted to reduced staging in the latter case and, hence, higher NOx emissions. No significant differences were found in either fuel nitrogen content or furnace temperature. A comparison of these factors, and the NOx emissions for the two burners, is provided in Table 2-5. At conditions of similar furnace firing rate, burner stoichiometry and enrichment, the NOx level for the Southern California burner was twice that of the Wabash burner. It should also be noted that the Southern California site used a high-purity liquid oxygen supply. Results presented in Figure 2-4 strongly suggest that the NOx levels at the Southern California site would therefore have been even higher with the lower purity VSA oxygen supply used at Wabash, thus further emphasizing the strong effect of burner design on NOx.

Table 2-5
Summary of Burner Design and NOx Emissions Comparison
Oxygen Enrichment = 35%; Stoich = 2.0; Furnace Firing Rate = 15 MMBTU/hr

	Wabash Burner	Southern California Burner
O_2 Lance Location	Outside Air Passages	Within Air Passages
Burner Design Velocity (air and natural gas)	100 ft/sec	40 ft/sec
Air Passage Angle	60 degrees	95 degrees
Fuel Nitrogen	1-2 %	1-2 %
NOx	0.16 lb NO_2/MMBTU	0.32 lb NO_2/MMBTU

Comparison of Pre- and Post-Development Burner NOx and CO Emissions
Comparison of the official pre- and post-development emissions data in Tables 2-3 and 2-4, respectively, indicates that a substantial NOx reduction was achieved with the post-development burner technology. The magnitude of this reduction is highlighted in Table 2-6, which presents pre- and post-development NOx and CO emissions data for comparable burner operating conditions. The table shows that a NOx reduction of greater than 80 percent was achieved with the new design at stoich equal to 2.0 and 2.1 and oxygen enrichment between 35 and 36 percent. The NOx reduction for stoich equal to 2.2 was 86 percent, despite the fact that oxygen enrichment was higher for the post-development test (39 percent) than for the pre-development test (36 percent). The relative NOx reduction would therefore have been greater if these data were at equal enrichment levels. NOx reduction achieved by the post-development burner would have been even higher if NOx levels were adjusted for the difference in oxygen purity between the two data sets (pre-development ~ 100 percent; post- development ~ 90 percent).

Pre- and post-development CO emissions, also presented in Table 2-6, show a sharp reduction in CO emissions with the post-development burner technology. These results indicate that, in addition to lower NOx emissions, combustion efficiency was also improved. More information concerning burner thermal performance is provided later in this section.

Table 2-6
Pre- versus Post-Development Burner NOx and CO Emissions

		Stoich = 2.0		Stoich = 2.1		Stoich = 2.2	
		Pre	**Post**	**Pre**	**Post**	**Pre**	**Post**
Enrich	%	35.3	35.3	35.5	35.5	36.0	39.0
NOx	lb NO_2/ MMBTU	0.81	0.15	1.00	0.18	2.29	0.327
CO	ppmv dry	10,820	457 (see note)	7700	0	5	0

Note: This number represents an average of CO levels for data points 7 and 10 from Table 2-4.

Comparison of Post-Retrofit NOx and CO Emissions with SCAQMD Regulatory Limits
An additional objective of the burner development effort with respect to emissions was to achieve compliance with regulations promulgated by the SCAQMD in Southern California. These regulations call for a maximum NOx production of 0.323 lb NO_2/ton aluminum, with CO emissions not exceeding 2000 ppmv. The units in which NOx limits are stated, [lb NO_2/ton aluminum], establish a link between burner NOx production [lb NO_2/MMBTU] and furnace specific energy usage [Btu/lb aluminum]. That is:

$$\text{lb } NO_2\text{/ton aluminum} = 2 \times 10^{-3} [\text{ lb } NO_2\text{/MMBTU }] * [\text{ Btu/lb aluminum }] \qquad (1)$$

Furnace specific energy usage achieved at Wabash furnace #8 with the post-development burner technology operating with between 34 and 38 percent oxygen enrichment was in the range from 1000 to 1600 Btu/lb aluminum (these data are discussed in more detail later in this section). Figure 2-14 shows the relationship of NOx in lb NO_2/ton aluminum to NOx in lb NO_2/MMBTU for the lower and upper limits of this specific energy utilization range. Analysis of this graph shows that stack NOx levels in the range of 0.10 - 0.16 lb NO_2/MMBTU, or less, are needed at Wabash furnace #8 to achieve compliance with the SCAQMD regulations. Examination of the data in Table 2-4 shows that three of the ten post-development test points (#s 2, 3 and 7) simultaneously satisfy both the NOx and CO criteria.

Thermal Performance Data for Post-Development Burner Technology
Thermal performance of the post-development burner technology was evaluated at Wabash furnace #8 in terms of furnace-specific energy usage, aluminum melt rate and stack exit gas temperatures. Representative long-term performance trends, utilized for evaluation of the original air-fuel pre-development AOF technologies, could not be obtained for the post-development technology due to reduced production demand and the lack of a dedicated casting line for furnace #8. Data on specific energy usage and melt rate were therefore obtained during 27 distinct periods of scrap charging into the furnace. The normal mixture of scrap, including both heavy and light metal components, was employed during these tests. Oxygen enrichment levels ranged from 34 to38 percent, while furnace firing rate varied, typically between 13 and 15 MMBTU/hr, as a result of the furnace control algorithm, which automatically modulates firing rate based on roof temperature.

Test results are summarized in Figure 2-15 as a plot of specific energy usage versus scrap charge rate. Data shown in this figure have been corrected for the difference between starting and ending melt (i.e., bath) temperature, thereby accounting for variations in thermal energy storage within the bath. The average correction to the raw energy usage data was +12 percent. Data show a trend of decrease in specific energy usage (increase in efficiency) with increasing charge rate, dropping from approximately 1600 Btu/lb at a melt rate of 9000 lb/hr to 1000 Btu/lb at 18,000 lb/hr. Several effects are contributing to this trend. First, increasing the charge rate accelerates the reduction in bath temperature, producing a greater driving force for heat transfer from the refractory and hot combustion gases to the melt. The magnitude of this effect is illustrated in Figure 2-16, which gives a comparison of the rate of change in roof minus bath temperature for a relatively high and low charge rate. Within roughly the same time period from

Figure 2-14. Conversion of NOx from lb NO2/MMBtu to lb NO2/ton Aluminum

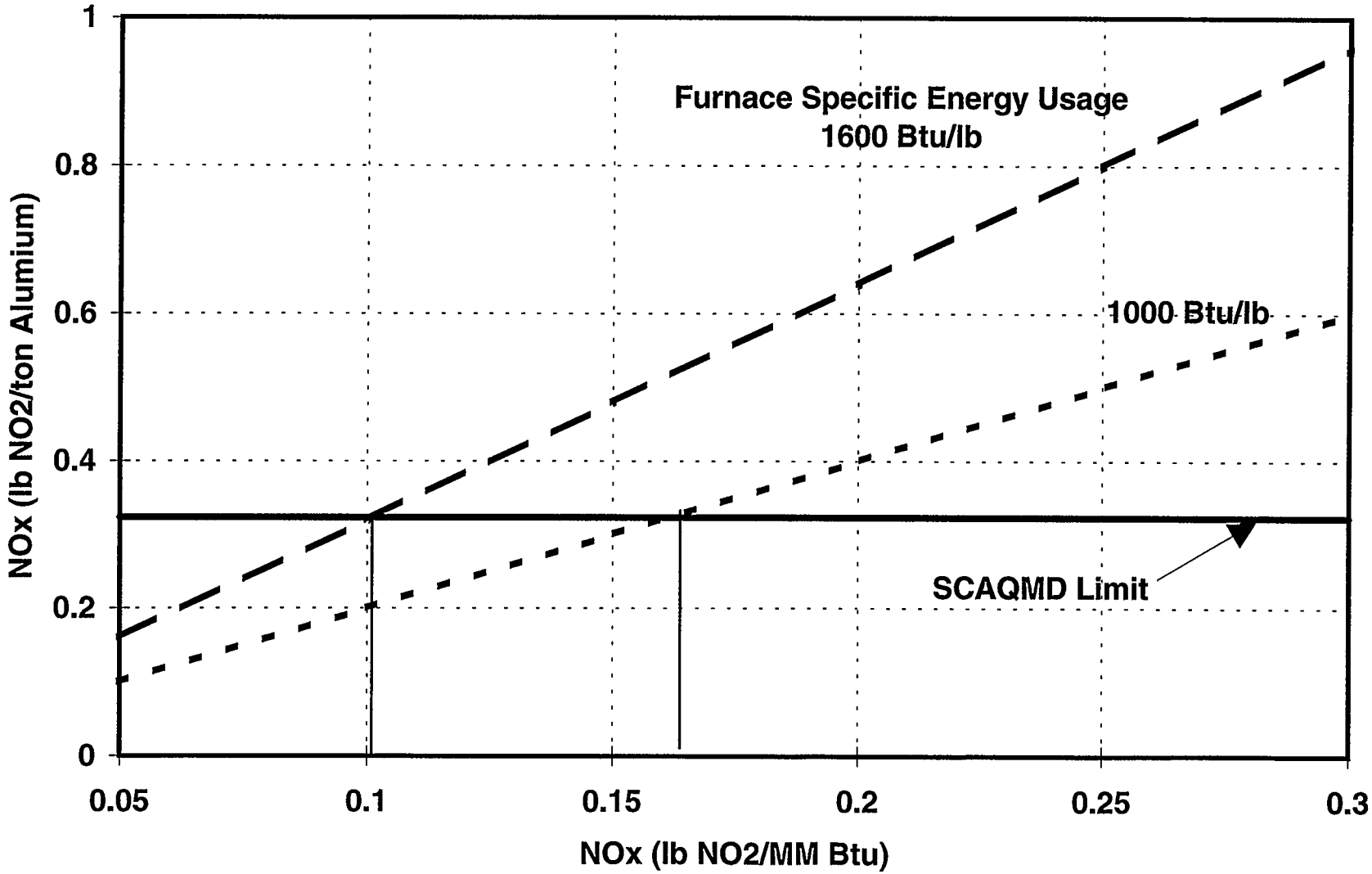

Figure 2-15. Furnace Melting Efficiency vs Scrap Charge Rate
Wabash Furnace #8: 34 - 38 % Oxygen Enrichment

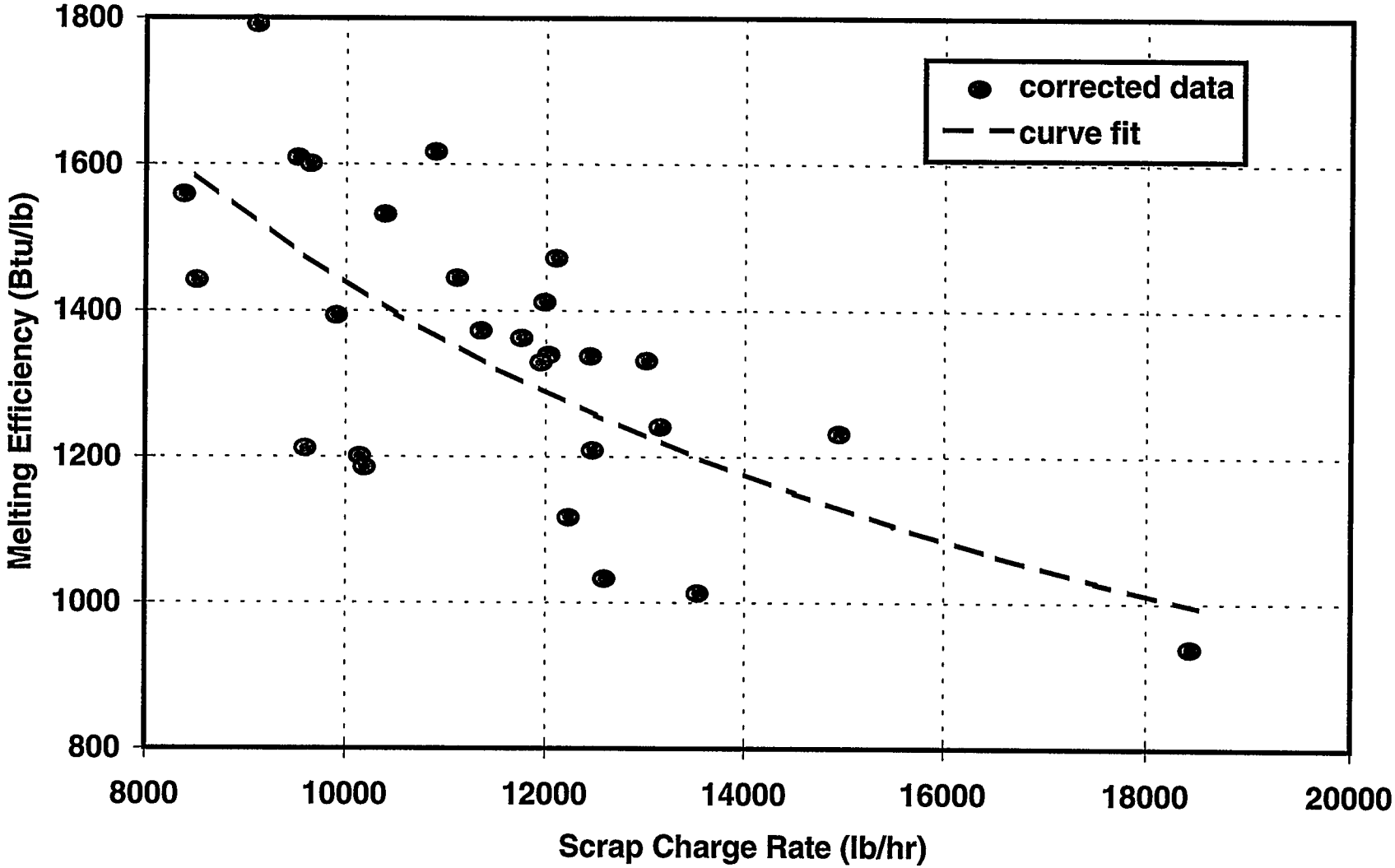

Figure 2-16. Effect of Charge Rate on Difference Between Roof and Bath Temperature: Wabash Furnace #8

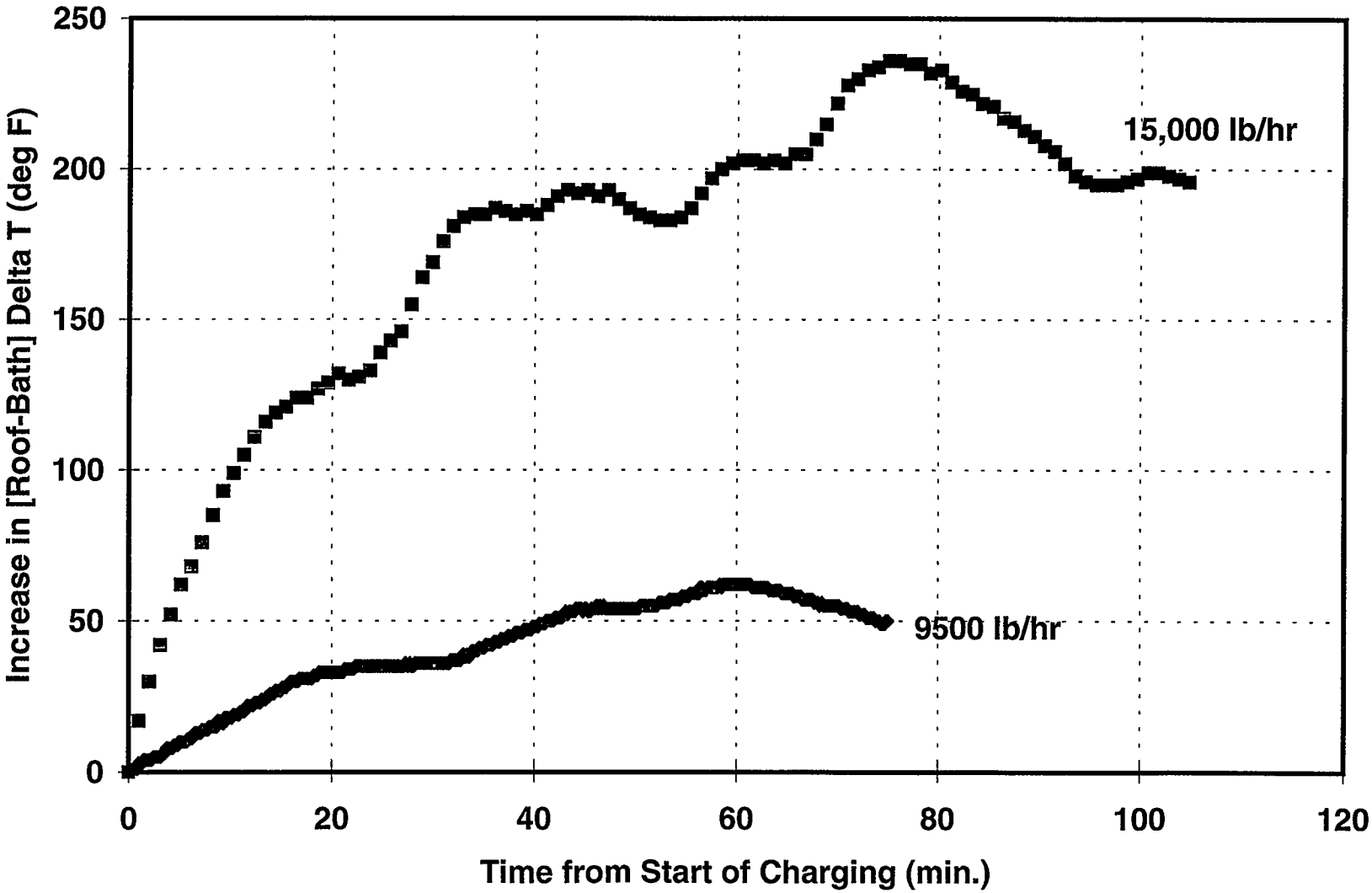

the start of charging, the high charge rate (15,000 lb/hr) case shows an increase of approximately 240°F, compared to an increase of only 60°F for the low charge rate (9500 lb/hr) case. An additional factor in the improved efficiency is that the rate of heat transfer between the circulating melt and the charge increases with increasing charge rate, since more surface area (i.e., scrap) is present at any given time. Finally, variation in the overall time required to melt a given mass of aluminum must be taken into account. As the rate of heat loss from furnace to ambient is essentially constant, the shorter melt time associated with higher charge rates translates into a lower total ambient energy loss per unit of melted aluminum.

Aside from illustrating the high efficiency and productivity levels achievable with the new burner technology, these data also point out the strong dependence of overall furnace performance on process efficiency. That is, although test data indicate the burners are capable of conservative melt rates of 13,000 - 14,000 lb/hr, operators must be capable of keeping up with this pace; otherwise overall furnace efficiency will suffer.

It should also be pointed out that the effect of oxygen enrichment level on furnace efficiency was insignificant over the range of conditions tested (34 to 38 percent).

Comparison of Pre- and Post-Development Burner Thermal Performance

The baseline furnace productivity and specific energy usage data for the original air-fuel and pre-development air-oxy-fuel burner technologies were based on average performance levels derived from several weeks or more of operation encompassing both high-fire charging and low-fire holding/tapping periods. Thermal performance data presented for the post-development AOF burner technology, by contrast, were obtained exclusively during the furnace melting cycle. These latter data must therefore be adjusted to account for both phases of the operation if a valid comparison of pre- and post-development performance is to be carried out.

Specific energy usage for the full cycle (charge plus hold) is calculated from furnace operating parameters via the following equation:

$$\varepsilon_{FC} = \varepsilon_{Charge} + 10^6 \, [(FR \times Time)_{Hold}]/M_{Alum} \qquad (2)$$

where

ε_{FC} = furnace full cycle specific energy usage [Btu/lb]

ε_{Charge} = specific energy usage for charging cycle [Btu/lb]

FR_{Hold} = furnace firing rate during holding cycle [MMBTU/hr]

$Time_{Hold}$ = duration of holding cycle [hours]

M_{alum} = mass of aluminum charged per cycle [lbs].

Specific energy usage was calculated from the charge rate using a curve-fit of the data shown in Figure 2-15. The equation for the curve-fit is:

$$\varepsilon_{Charge} = 3.61 \times 10^5 \, [CR]^{-0.6} \qquad (3)$$

where CR is the scrap charge rate in lb/hr.

The aluminum melt rate, MR, in lbs/day is calculated from:

$$MR = 24 \times M_{Alum} / Time_{Cycle} \quad (4)$$

where the total cycle time, $Time_{Cycle}$, in hours, is calculated from:

$$Time_{Cycle} = Time_{Hold} + M_{Alum} / CR \quad (5)$$

Having derived this calculation procedure, the melt cycle data of Figure 2-15 were adjusted to represent full cycle performance. The following constants were used for the analysis, based on typical operation at Wabash furnace #8:

$Time_{Hold}$ = 2.5 hours
FR_{Hold} = 5 MMBTU/hr
M_{alum} = 70,000 lbs

Results for full cycle specific energy usage and daily aluminum melt rate versus charge rate are presented in Figures 2-17 and 2-18, respectively. Superimposed on these figures is the baseline specific energy usage and melt rate levels for the pre-development AOF burner technology, previously presented in Table 2-2. The comparison in Figure 2-17 shows that, provided charge rates are maintained above 10,200 lb/hr, an overall reduction in specific energy usage will be achieved with the new burner technology relative to the 1598 Btu/lb attained with the pre-development technology. With respect to melt rates, the comparison in Figure 2-18 indicates that charge rates with the new burner technology need to be maintained above 11,500 lb/hr to improve on the pre-development melt rate of 196,000. However, the project goal was to increase air-fuel productivity by 30 percent, which puts the actual target at approximately 203,000 lb/day; this target is therefore also superimposed on Figure 2-18. With this higher target as the basis, a charge rate of 12,000 lb/hr is needed with the new burner technology. As the data of Figure 2-15 proved the capability of the new burner technology to exceed these charge rates, it is clear that the performance goals of the burner technology have been attained.

Additional evidence in support of improved thermal performance for the new burner technology comes from stack temperature data. A comparison of the stack temperatures measured during pre- and post-development tests (see Tables 2-3 and 2-4, respectively) shows a significant reduction in stack gas temperature with the post-development burner technology. A summary of this comparison, presented in Table 2-7, shows that the average post-development stack temperature was approximately 150°F lower than the pre-development level, even though the post-development data were obtained at a higher furnace firing rate. This indicates more efficient utilization of thermal energy with the post-development burner technology, which can be attributed to a longer, more luminous flame providing enhanced heat transfer to the aluminum bath.

Figure 2-17. Projected Full Cycle Energy Usage vs Charge Rate Wabash Furnace #8: Post-Development AOF Burners

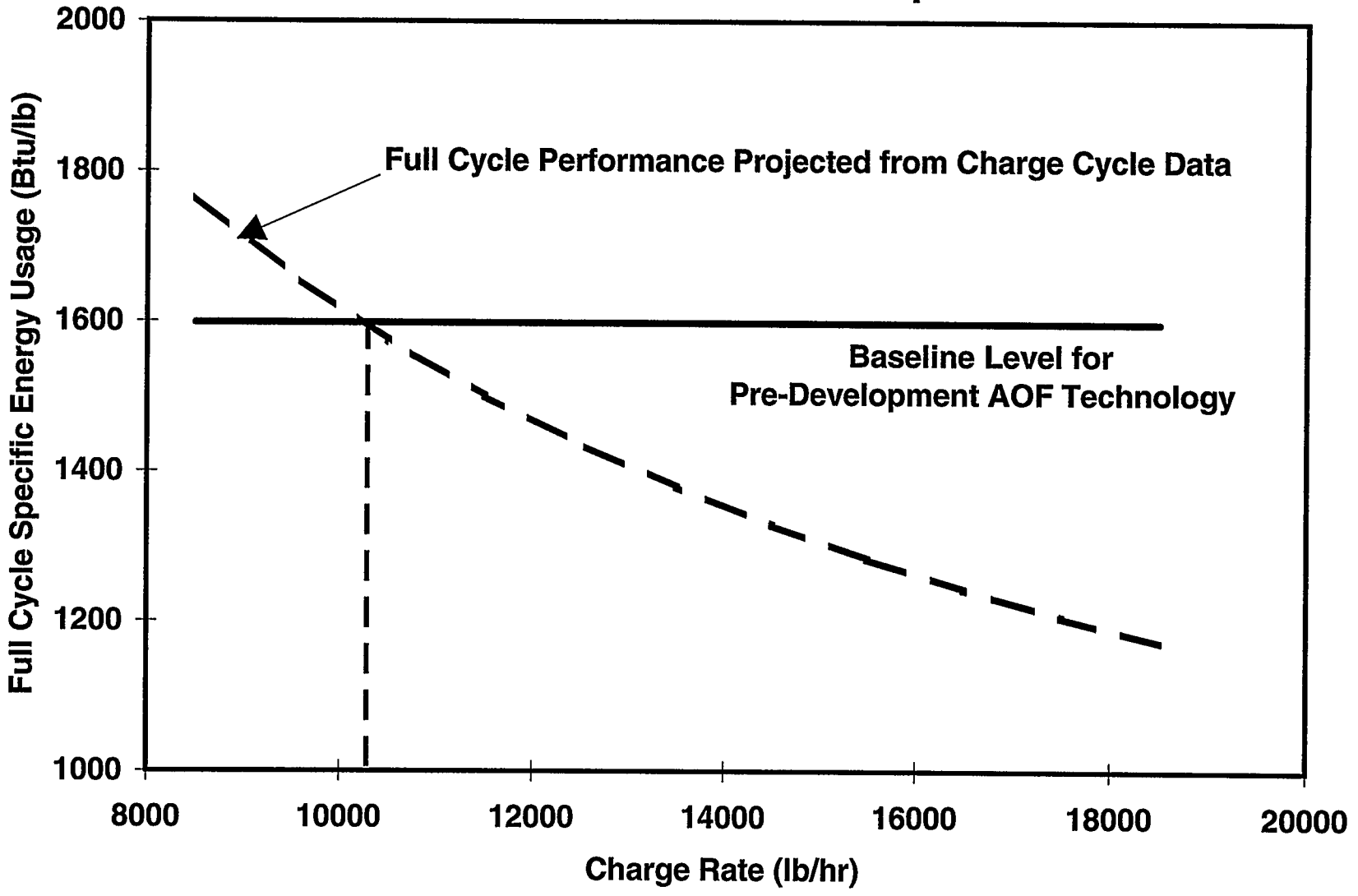

Figure 2-18. Projected Daily Melt Rate vs Charge Rate
Wabash Furnace #8: Post-Development AOF Burners

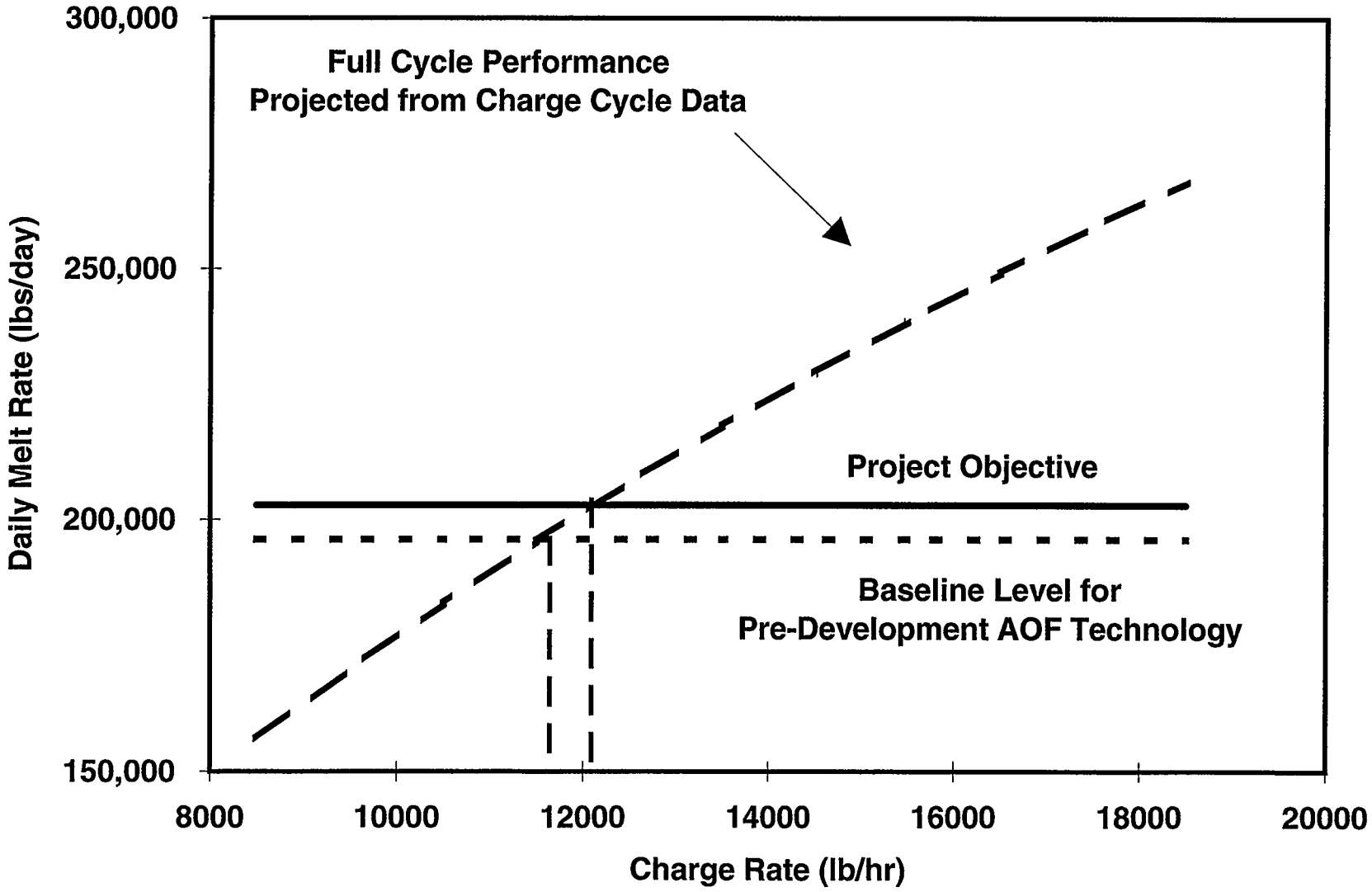

Table 2-7
Comparison of Pre- and Post-Development Stack Temperature Data

Technology	Firing Rate	Average Stack Temperature
	MMBTU/hr	°F
Pre-Development AOF	15.0	2136
Post-Development AOF	15.5	1985

Summary of Combustion System Development and Performance
Utilizing a combination of heavy oxidizer staging and enhanced gas recirculation, the novel air-oxy-fuel burner technology installed at Wabash furnace #8 successfully lowered NOx emissions by more than 80 percent relative to the pre-development AOF technology, while simultaneously lowering stack CO emissions. Further, provided the furnace is operated at or near the maximum efficiency proven for the post-development technology, NOx (and CO) levels achieved at Wabash furnace #8 will satisfy the stringent SCAQMD emissions regulations of 0.323 lb NO_2/MMBTU. Test results also showed the potential for achieving the NOx targets using a combination of low-purity VSA oxygen and the VSA waste stream as the primary and secondary oxidizers, respectively, in the post-development burner technology.

Data on furnace specific energy usage, melt rate and stack gas temperature showed that the thermal performance of the new AOF burner technology exceeded that of the pre-development AOF technology for efficiency and production. The technology also showed the potential to exceed the targeted 30 percent production increase relative to the original air-fuel technology, provided that the speed of plant operations keeps pace with burner melting capability.

Section 3
Computer Modeling of Wabash Aluminum Alloys Furnace #8

Introduction

The primary objective of computer modeling in this project was to highlight and quantify differences in furnace operating characteristics among air-fuel, air-oxy-fuel and oxy-fuel combustion technologies. This goal was achieved through a combination of Computational Fluid Dynamics (CFD) modeling and simulations within a three-dimensional "virtual reality" environment residing at Argonne National Laboratories in Chicago, Ill. The so-called "CAVE" (Cave Automated Virtual Environment) utilized numerical results from the CFD simulations to create an environment within which attributes of the flow, temperature and concentration fields in the furnace could be studied and understood in greater detail than through conventional means of visualization. A summary of the CFD modeling results is provided within this section while, due to presentation limitations, only the general features and capabilities of the virtual reality simulator are described.

CFD Modeling of Wabash Furnace #8

A CFD model of the Wabash #8 furnace was developed using the commercially available FLUENT code. Utilizing a computational grid consisting of 90,000 cells and convection boundary conditions at the refractory walls and gas/melt interface, the model simultaneously solves equations describing the 3-dimensional turbulent reacting flow of gases in the combustion space and the laminar flow of liquid within the molten aluminum bath. Model output includes the velocity, temperature and gas concentration (CO, CO_2, O_2) field within the gas space, as well as the temperature and velocity field within the circulating aluminum bath. The CFD model was used to compare the characteristics of furnace operation using the following three combustion technologies:

1. Air-fuel combustion (AF)
2. Air-oxy-fuel combustion (AOF) at 35% total oxygen enrichment
3. Oxy-fuel combustion (OF)

The model calculations described in this report are for steady-state operation with a firing rate of 14 MMBTU/hr (3.5 MMBTU/hr through each of four burners) and a charge rate of 12,000 lb/hr. The rate of liquid metal circulation, as controlled by the circulation pump, was assumed to be 8800 lb/minute. Results illustrating the differing characteristics among air-fuel, oxy-fuel and air-oxy-fuel meltings of aluminum in the Wabash #8 reverb furnace are highlighted in the remainder of this section.

CFD Model Results

Furnace Temperatures

Computational results indicate that flame and refractory temperatures are highest for OF firing and lowest for AF firing, with AOF temperatures in-between. The peak flame temperature, average refractory temperature and oxygen concentration above the melt (significance discussed later in this section) calculated for the three cases are summarized in Table 3-1.

Table 3-1
Summary of CFD Model Calculation Results

Technology	Peak Flame Temperature (°F)	Avg. Refractory Temperature (°F)	O_2 Conc. in gas space above melt (vol %)
AF	2650	1700	1.5
AOF	4000	2960	1.4
OF	4500	3410	2.0

The table shows that calculated air-oxy-fuel peak flame and average refractory temperatures are much closer to oxy-fuel temperatures than to air-fuel temperatures. This implies that most of the increase in aluminum melt rate derived from oxygen-enhanced combustion can be achieved with air-oxy-fuel firing at relatively low levels of oxygen enrichment.

Maximum service temperature of the refractory is a key maintenance and reliability issue in the retrofit of OEC technology into an existing air-fuel furnace. The service limit for many high-quality refractory materials used in aluminum melting furnaces is approximately 3000°F. The average temperatures predicted by the model were 3410°F for OF firing and 2960°F for AOF firing. These results therefore suggest that the oxy-fuel firing rate would have to be lowered, relative to the AOF firing rate, in order to avoid refractory damage. This will reduce the melting rate that can be achieved using this technology. (Note: The model prediction for refractory temperature during AOF operation was approximately 500°F higher than measurements made by BYU at Wabash furnace #8 under similar conditions. This discrepancy is largely due to high rates of furnace air-infiltration not accounted for in the CFD model.)

The average air-fuel refractory temperature of 1700°F is significantly lower than typical roof temperatures (~2000-2100°F) achieved during the melt cycle at Wabash furnace #8. Model calculations indicate that the rate of heat transfer to the melt, at 14 MMBTU/hr, is not sufficient to keep up with the charging rate of 12,000 lb/hr. It would therefore be necessary to increase the AF firing rate in order to achieve the desired melting rate. This would of course yield a higher refractory temperature than reported in Table 3-1 for this technology.

Oxygen Concentration near Surface of Melt

Economic model results for the reverb furnace proved that furnace yield is one of the principal economic parameters in secondary aluminum melting. Yield is maximized by minimizing the formation of aluminum oxides (dross). Dross formation increases with increasing temperature and oxygen concentration at the melt surface. It is therefore crucial, from a financial standpoint, to maintain as low a concentration of oxygen above the melt as possible. The CFD modeling results summarized in Table 3-1 predict the oxygen concentration directly above the melt to be lower with AOF technology (~1.4 vol %) than with either oxy-fuel (2.0 vol %) or air-fuel (1.5 vol %) technology. The explanation for this is that oxygen concentration above the melt depends principally on the rate of oxygen consumption (i.e., chemical reaction) and the amount of dilution. While OF technology provides the highest rates of consumption and AF technology the greatest dilution, AOF technology produces the most favorable combination of the two with

respect to minimizing oxygen concentration. Considering the significantly higher gas temperatures with oxy-fuel relative to air-oxy-fuel combustion, these predictions strongly suggest a lower aluminum oxidation potential for the AOF technology.

Gas and Liquid Flow Patterns

A comparison of gas velocity vectors for the three cases, taken through a horizontal cross-section of the furnace at the burner level, is presented in Figure 3-1. While gas flow patterns predicted by the CFD model are qualitatively similar among the technologies, velocities are highest for air-fuel combustion. The velocity of gases emanating from the burners in this case exceeds the 10 m/sec scale range; hence, the plot simply shows a blank space. The velocity of the burner jet as it hits the back wall of the furnace is also highest for the AF case, approximately 7 m/sec, compared to 5 m/sec for AOF and 3 m/sec for OF. Since combustion rates are slowest for the AF technology, this suggests that direct flame impingement onto the back wall will be most severe in this case.

An important melt phase modeling result is the existence of a stagnant recirculation zone in the rear of the furnace between the two submerged arches connecting the furnace space with the pump and charge wells (see Figure 3-2). This gives rise to local hot spots that may lead to accelerated rates of aluminum oxidation, especially during oxy-fuel operation when gas temperatures and oxygen concentrations are relatively high.

Conclusions

CFD modeling of the Wabash #8 reverb aluminum furnace indicates that peak flame temperatures with AOF technology (at 35% oxygen enrichment) are much closer to those achieved with OF technology than for air-fuel operation. This suggests that AOF thermal performance also more closely approximates that of OF technology. Another key result was that, at a firing rate of 14 MMBTU/hr, refractory temperatures predicted for OF firing were above the material limit, implying that a reduction in firing rate would be necessary to avoid refractory damage. Although calculated average refractory temperatures were lowest for air-fuel technology, melt rates were not high enough to sustain a 12,000 lb/hr melting rate. An increase in firing rate would be required, thereby increasing the risk of direct flame impingement on the furnace back wall. Computed oxygen concentration above the gas melt was lowest in the air-oxy-fuel case, a condition favorable for producing high furnace yields. Results thus suggest air-oxy-fuel technology can, in this application, lead to production rates comparable to oxy-fuel firing, with higher yield, lower oxygen costs and less potential for furnace refractory damage.

Virtual Reality Simulation of Wabash Furnace #8

The CFD results presented above provide some useful insights into differences among the various combustion technologies evaluated herein. However, there are inherent limitations in the ability to visualize and compare highly complex, three-dimensional flow fields within a two-dimensional framework. These limitations were overcome by utilizing the three-dimensional visualization capability and advanced analysis tools of the CAVE at Argonne National Laboratory. The CAVE (see Figure 3-3) is an open-ended, ten-foot cube with stereo images projected onto three walls and the floor. Users entering the CAVE are immersed in the projection of these images, and given the sensation of actually standing within the environment

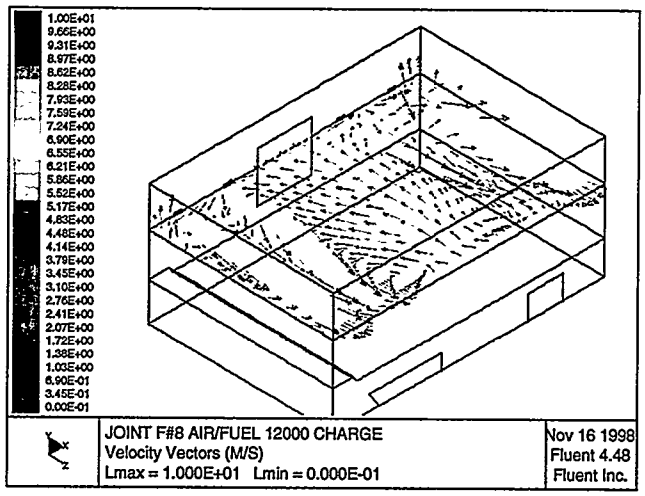

a. Air/Fuel Case

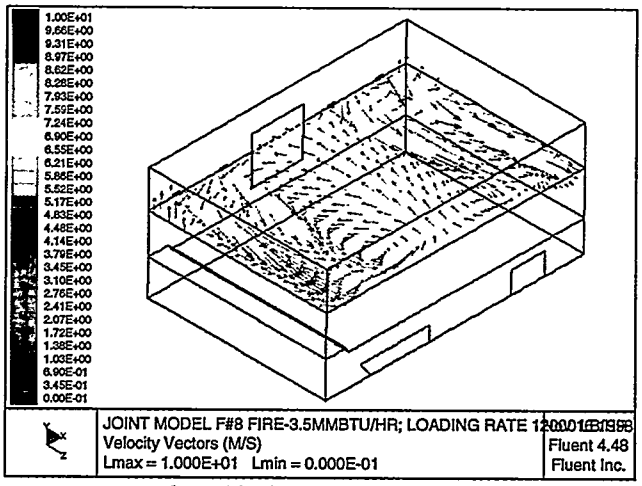

b. Air-Oxy/Fuel Case

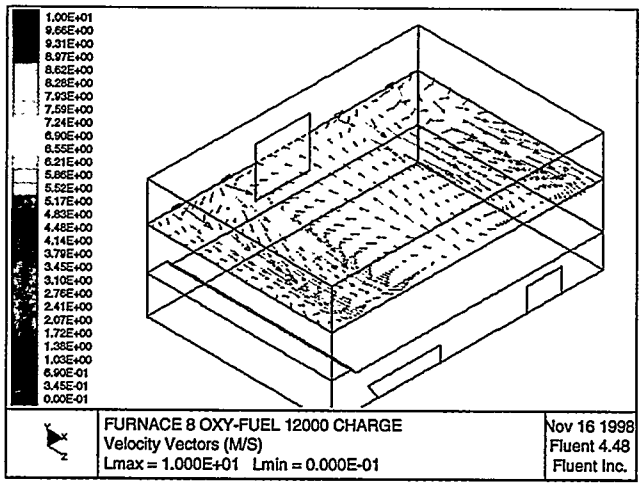

c. Oxy/Fuel Case

FIGURE 3-1 Gas velocity vectors at the burner level.

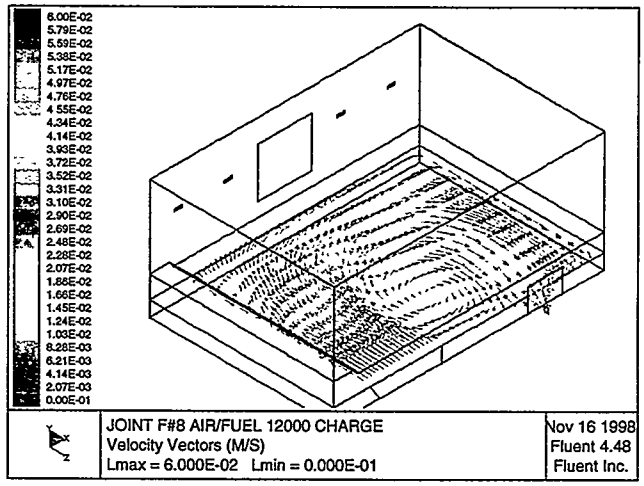

a. Air/Fuel Case

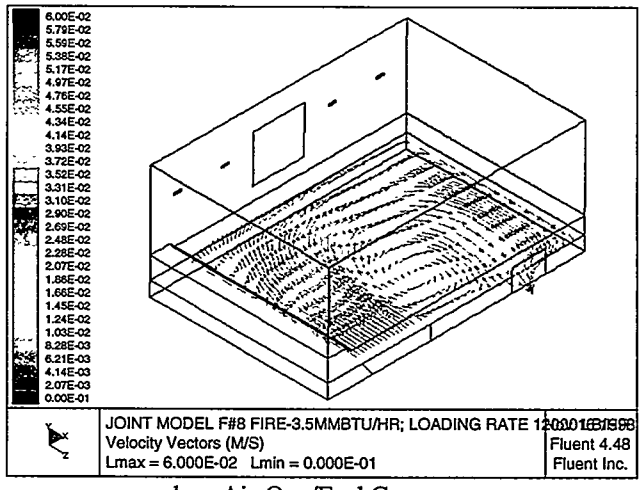

b. Air-Oxy/Fuel Case

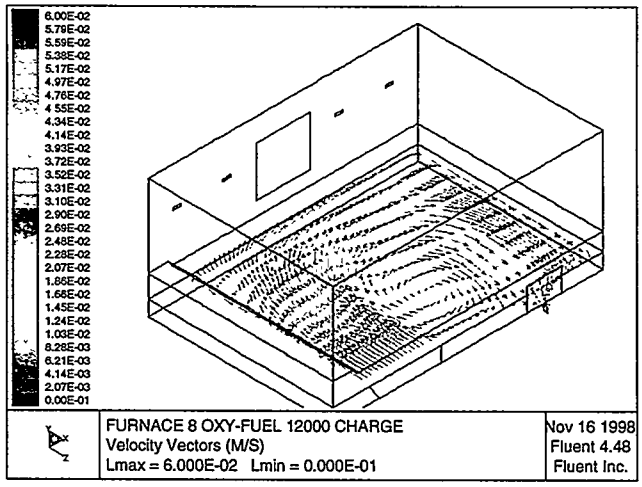

c. Oxy/Fuel Case

FIGURE 3-2 Horizontal velocity vector field in the melt

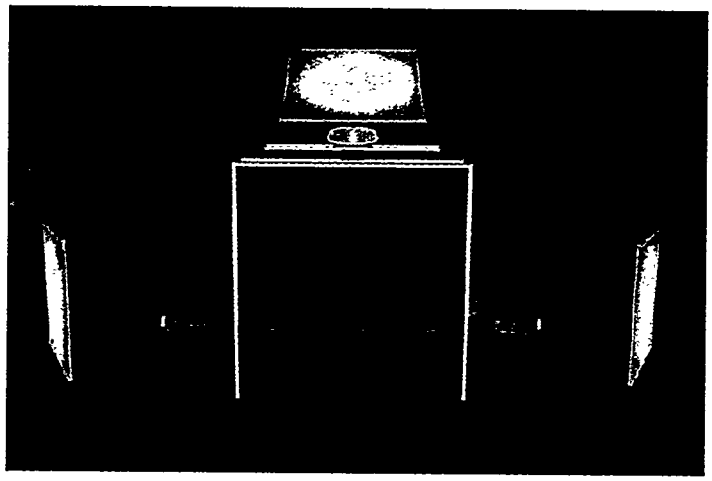

Figure 3-3. Schematic of the CAVE display device (image courtesy of the Electronic Visualization Laboratory, University of Illinois at Chicago)

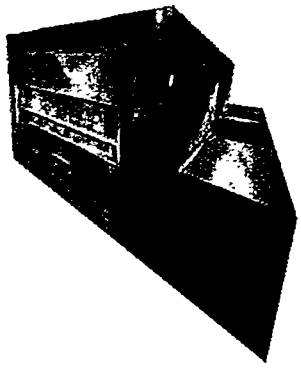

Figure 3-4. Texture-mapped exterior of the virtual aluminum melting furnace

being simulated. One user wears a magnetic tracking device, which sets the reference point for image orientation, and handles a joystick to navigate through the virtual reality environment.

To provide a realistic frame of reference for engineers developing and analyzing computational results, a virtual aluminum smelting furnace was constructed using texture-mapped polygons. The texture images consist of digital pictures of Wabash furnace #8 and include, for example, the melt surface, charging bins, and exhaust stack. Figure 3-4 shows an oblique view of the texture-mapped virtual model of the aluminum smelting furnace. To obtain an unimpeded view of the simulation data, the texture-mapped polygons are replaced with a wireframe representation of the furnace where key reference points, such as the burners and exhaust stacks, are retained (see Figure 3-5).

Data analysis capabilities within the CAVE include interactive comparisons of multiple data sets, dynamic tracking of individual fluid particles and advanced data manipulation techniques such as magnification, culling (i.e., filtering) and exaggeration. For example, Figure 3-6 shows a comparison of furnace gas temperatures for the three combustion technologies taken at a horizontal plane cutting through the burners. The air-fuel case is shown in red; the air-oxy-fuel case in green and the oxy-fuel case in blue. This type of presentation illustrates very graphically how relatively small amounts of oxygen enrichment secure a large percentage of the overall heating potential of full oxy-fuel operation. Additional details of the CAVE model and illustrations of its capabilities are provided in Appendix 3. The completed simulation is available for demonstration at Argonne National Laboratories.

Figure 3-5. Wireframe representation of aluminum reverb furnace

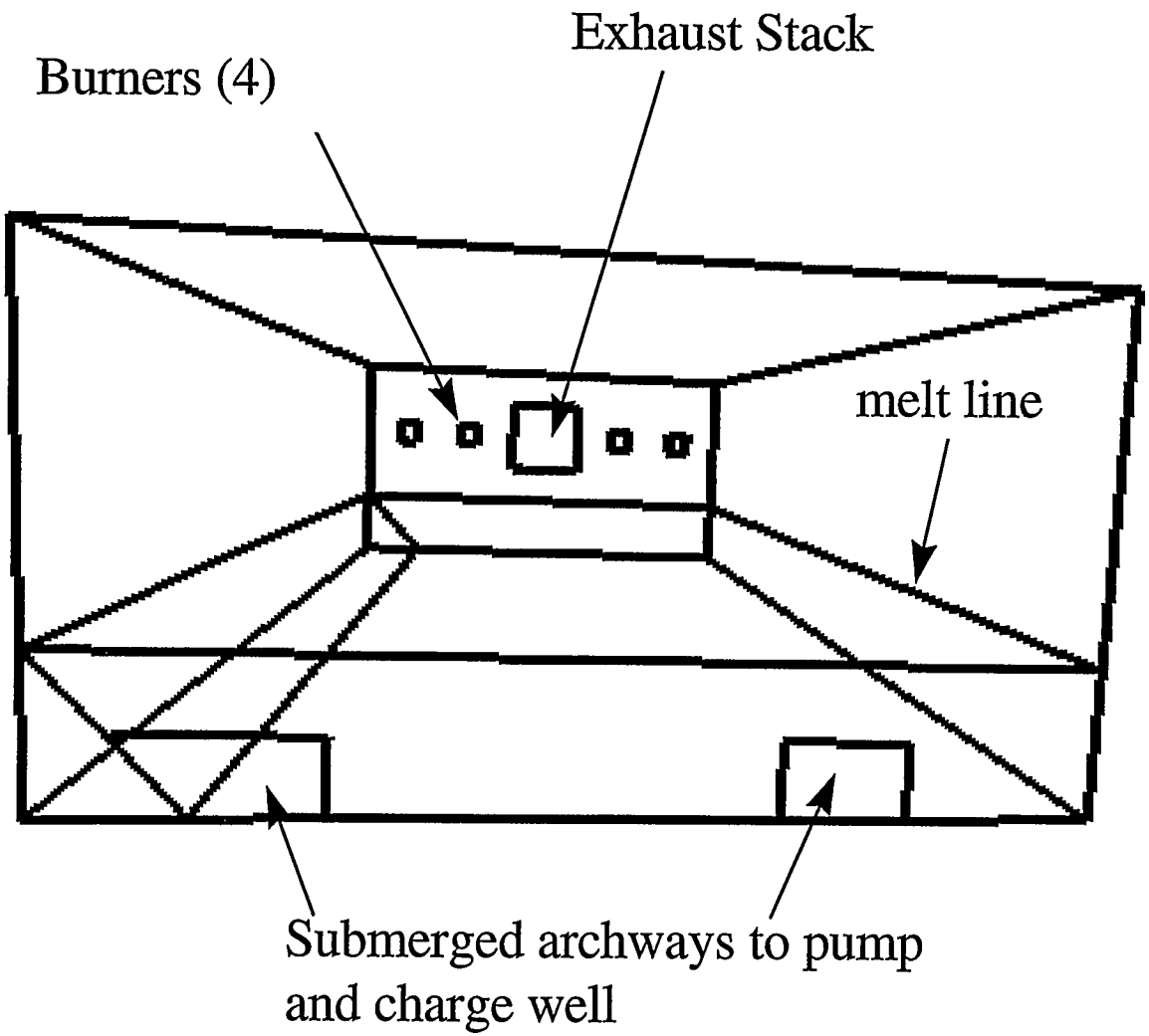

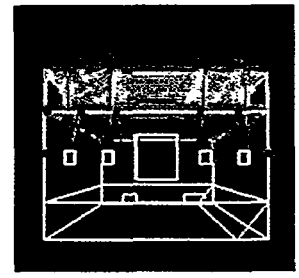

Figure 3-6. CAVE-generated comparison of furnace gas temperatures at horizontal plane cutting through burner axis. Red: Air-fuel; Green: Air-oxy-fuel; Blue: Oxy-fuel

Section 4
Integrated Oxygen Supply with Sieve-Assisted Storage System

Benefits of New Technology

Production of oxygen using VSA technology has the advantage of significantly lower capital and operating costs in comparison with similarly sized cryogenic air separation plants. Moreover, on-site production of oxygen eliminates the logistical problems associated with oxygen delivery, further lowering costs to the end user. However, there are challenges, both technical and economic, in using an on-site O_2 VSA that the new technology developed in this project seeks to overcome.

One challenge is in synchronizing oxygen generation with customer demand. The Wabash plant has three oxygen-enriched furnaces and one air-fuel furnace that, because of varying scrap quality, sharing of casting lines and numerous other factors, produces large and rather irregular fluctuations in oxygen usage (see Figure 4-1). The novel technology developed under this project addresses this challenge by employing a low-pressure accumulator filled with a commercially available adsorbent to store excess oxygen from the on-site plant during periods of low furnace demand. The stored oxygen is used when customer demand exceeds VSA output, thereby allowing for a smaller VSA design, which saves both capital and operating costs. Moreover, the added storage capacity achieved by using an adsorbent, or sieve, means that smaller vessels can be employed.

Another challenge in the use of on-site VSA technology for combustion applications is the generation of NOx emissions. Test data presented in Section 2 showed that lowering the purity of the primary oxidizer increases NOx. However, it was also proven that NOx can be lowered in the new low-NOx burner technology by blending the low oxygen content (~ 12 percent O_2) VSA waste stream with air as the secondary oxidizer. Field data showed the NOx generated with a primary purity of 80 percent O_2 and a secondary purity of 18 percent O_2 was essentially the same as that generated with pure oxygen as the primary oxidizer and pure air as the secondary oxidizer.

Because the integrated oxygen generator and low-NOx combustion technology allows for usage of low-purity oxygen without incurring an environmental penalty, it therefore becomes possible to take advantage of an additional economic benefit, which is the reduced power requirement for the VSA. Figure 4-2 provides results of calculations performed by Air Products for a pilot-scale VSA, showing relative specific power (typically measured in KWh/ton O_2) and product purity versus relative VSA product flow. This graph shows a dramatic reduction in specific power, and a simultaneous decrease in product purity, associated with VSA operation at higher than design flow rates. For example, a 40 percent reduction in specific power, relative to the design condition, can be achieved by operating at twice the design flow, while product purity decreases from 93 to 82 percent. The VSA installed at Wabash does not incorporate this low-purity operating strategy, since the concept has not reached the commercialization stage of product development.

Figure 4-1. Typical O2 Usage Pattern at Wabash

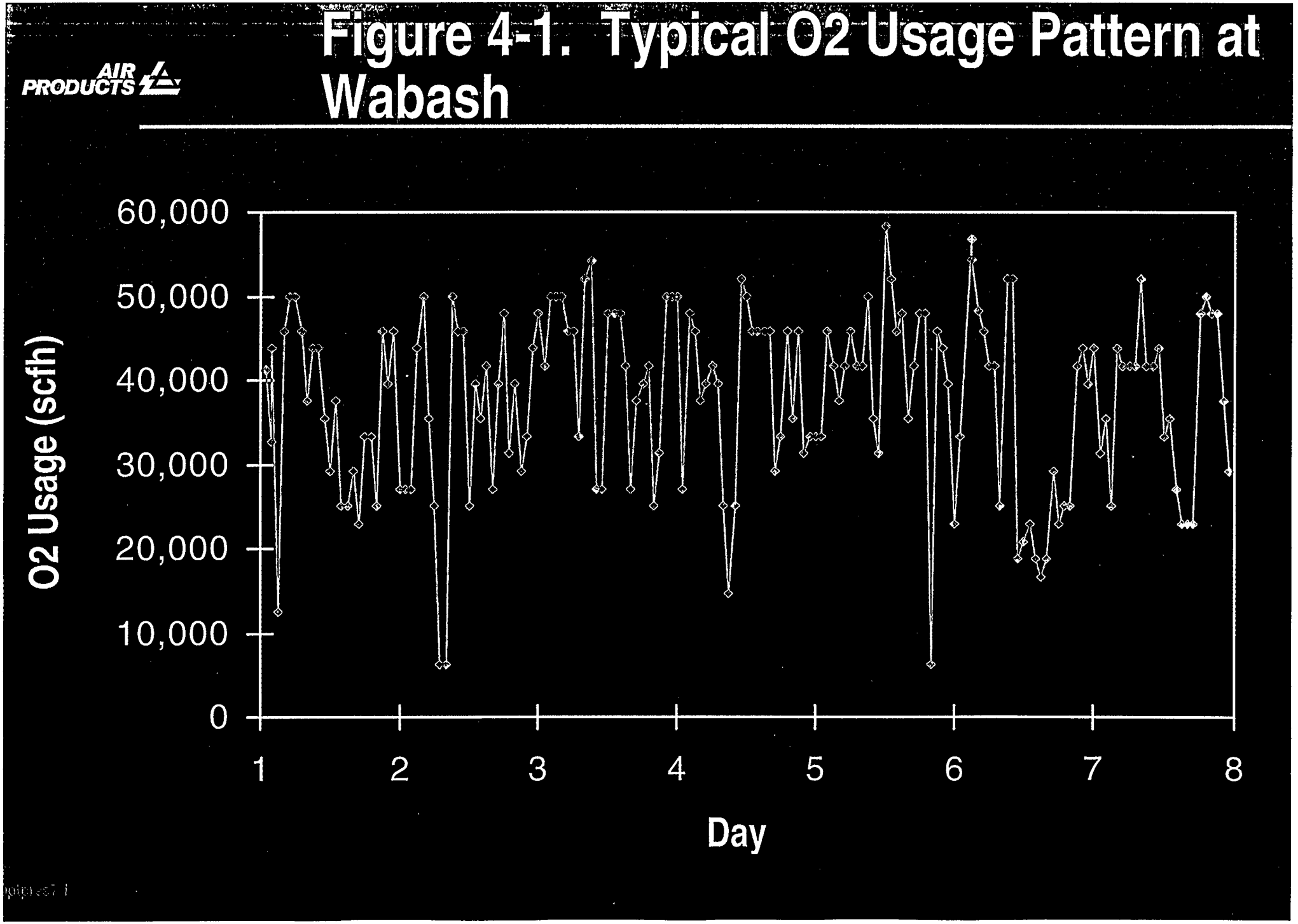

Figure 4-2. Relative Specific Power and Product Purity vs Product Flow for O2 VSA Designed for 93% O2 Purity

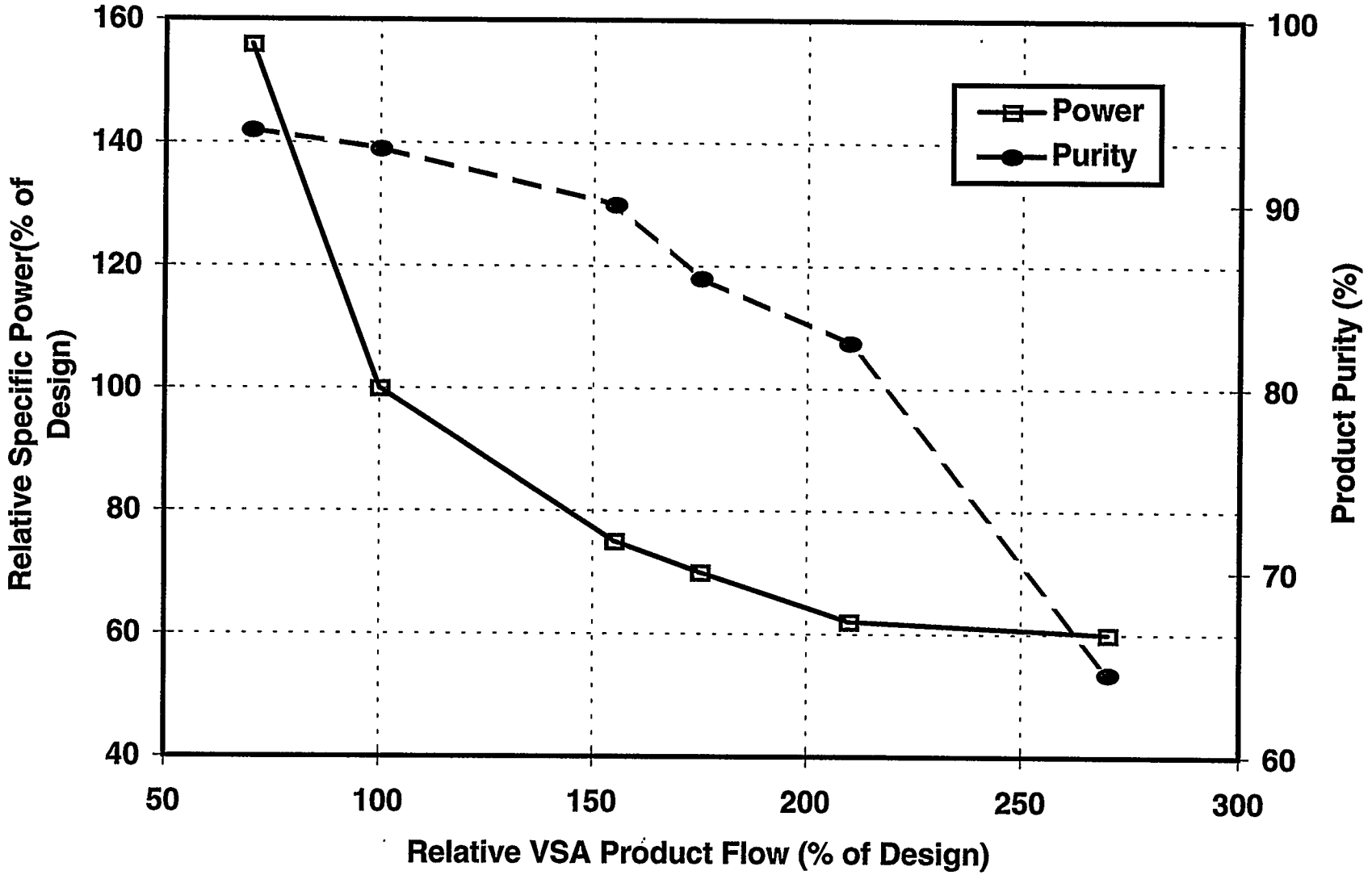

The remainder of this section provides details concerning the design and operation of the integrated VSA technology, and also describes results of field performance tests wherein the effectiveness of the sieve-assisted storage system was evaluated.

System Design and Operation

The VSA consists of two adsorbent beds designed to remove CO_2, H_2O and N_2 from incoming low-pressure (<5 psig) air. The unit operates in cyclic fashion, with one bed in an adsorbing mode and the other in a desorbing, or regenerative mode. The cycle time is of the order of one minute. The low-purity stream can be compressed and delivered to the furnace as a secondary oxidizer. Although the technical feasibility of using this low-purity stream to reduce burner NOx emissions was proven in a field trial at Wabash, the current design vents the waste gas to atmosphere. The high-purity O_2 stream is fed first to a buffer tank, then to an oxygen compressor. LOX is blended into the primary oxidizer stream, if necessary, to supplement the oxygen supply to the furnace. The primary and secondary oxidizers and fuel are delivered to the burner flow controls, and from there they are directed to the individual burners. A sketch of the integrated system is provided in Figure 4-3.

A more detailed sketch of the piping run for the sieve tank and high-purity oxygen stream is shown in Figure 4-4. Oxygen is able to flow in either direction through a single access port connecting the pipeline to the sieve tank. The direction of flow depends on system pressure and furnace oxygen demand. When furnace demand is decreasing, the main flow control valve closes, causing an increase in upstream line pressure, and forcing oxygen into the sieve tank. Conversely, increasing furnace O_2 demand causes the flow control valve to open, reducing pressure and drawing oxygen from the tank. The total amount of oxygen stored in the tank at any time depends on system pressure and temperature via the adsorption isotherm. Pressure upstream of the control valve normally varies between 30 and 75 psig. When pressure falls below 35 psig, the inventory in the sieve tank is significantly reduced, and the control system begins to draw oxygen from the LOX backup supply.

Performance of the Sieve-Assisted Storage System

The task of the sieve-assisted storage system is to provide oxygen to the furnace during periods of operation when furnace demand exceeds VSA output. The ability of the system to effectively execute this task depends on the storage capacity of the sieve tank, proper functioning of the control system and the magnitude and duration of oxygen peak demand levels. Two field tests were carried out to assess system performance; the first test was designed to verify sieve tank capacity, and the second was designed to determine the effectiveness of the system in reducing backup LOX consumption.

Sieve Tank Capacity Test

The sieve tank itself is an 18 foot high (tangent to tangent) by 9 foot diameter pressure vessel with a maximum allowable working pressure of 105 psig. The tank is filled to an internal height of approximately 15 feet with a TOSOH type SA-500 adsorbent. A test was run with the VSA off-stream (main shutoff valve in Figure 4-4 closed) to determine the useful oxygen storage capacity of the sieve-filled tank. The "useful" capacity is defined here as that which can be drawn from during normal operation. Specifically, this means the differential oxygen capacity of

Figure 4-3. Integrated O2 Supply with Low NOx Combustion System at Wabash Aluminum Alloys

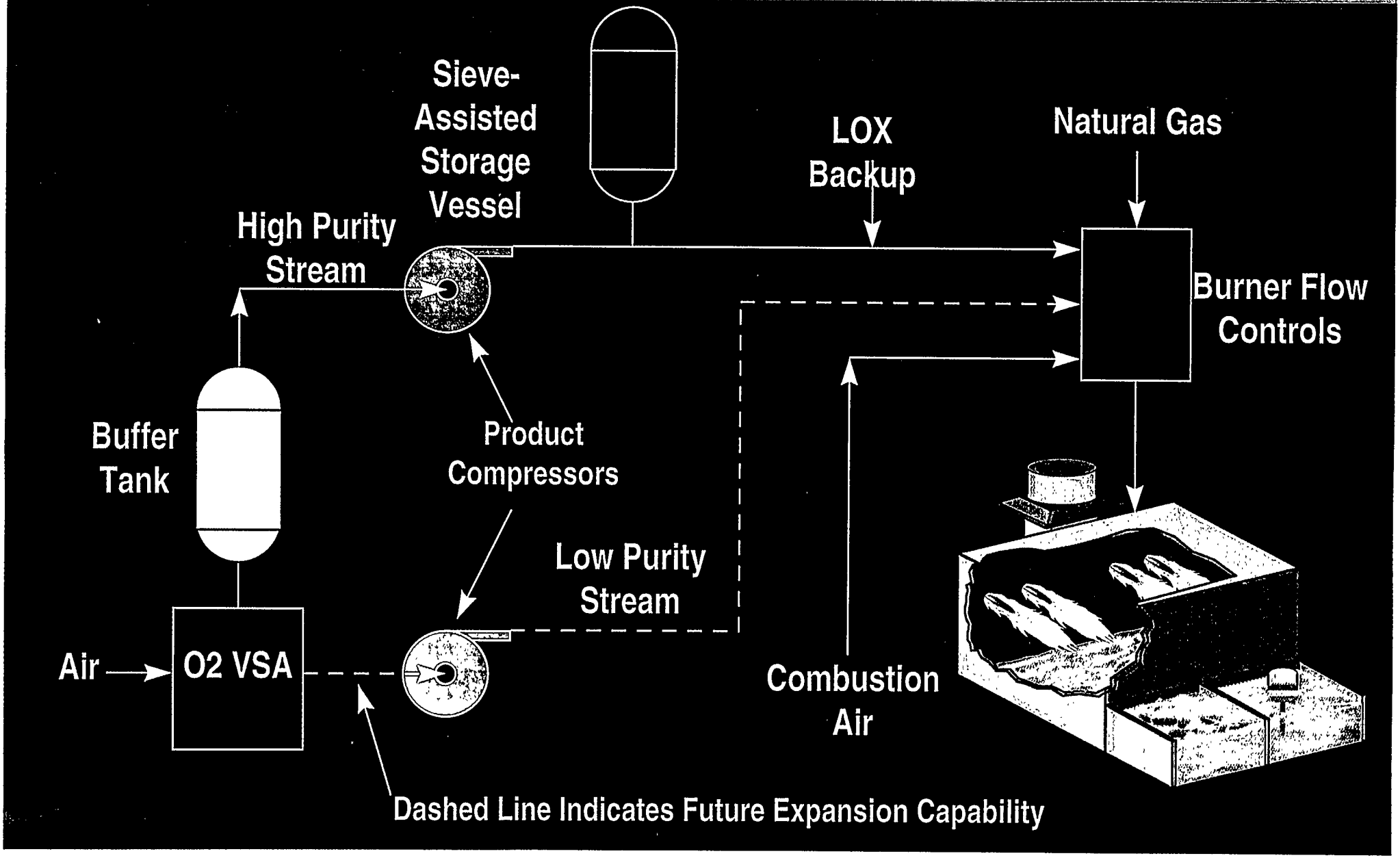

Figure 4-4. Detail of O2 Piping Run in the Vicinity of Sieve Storage Tank

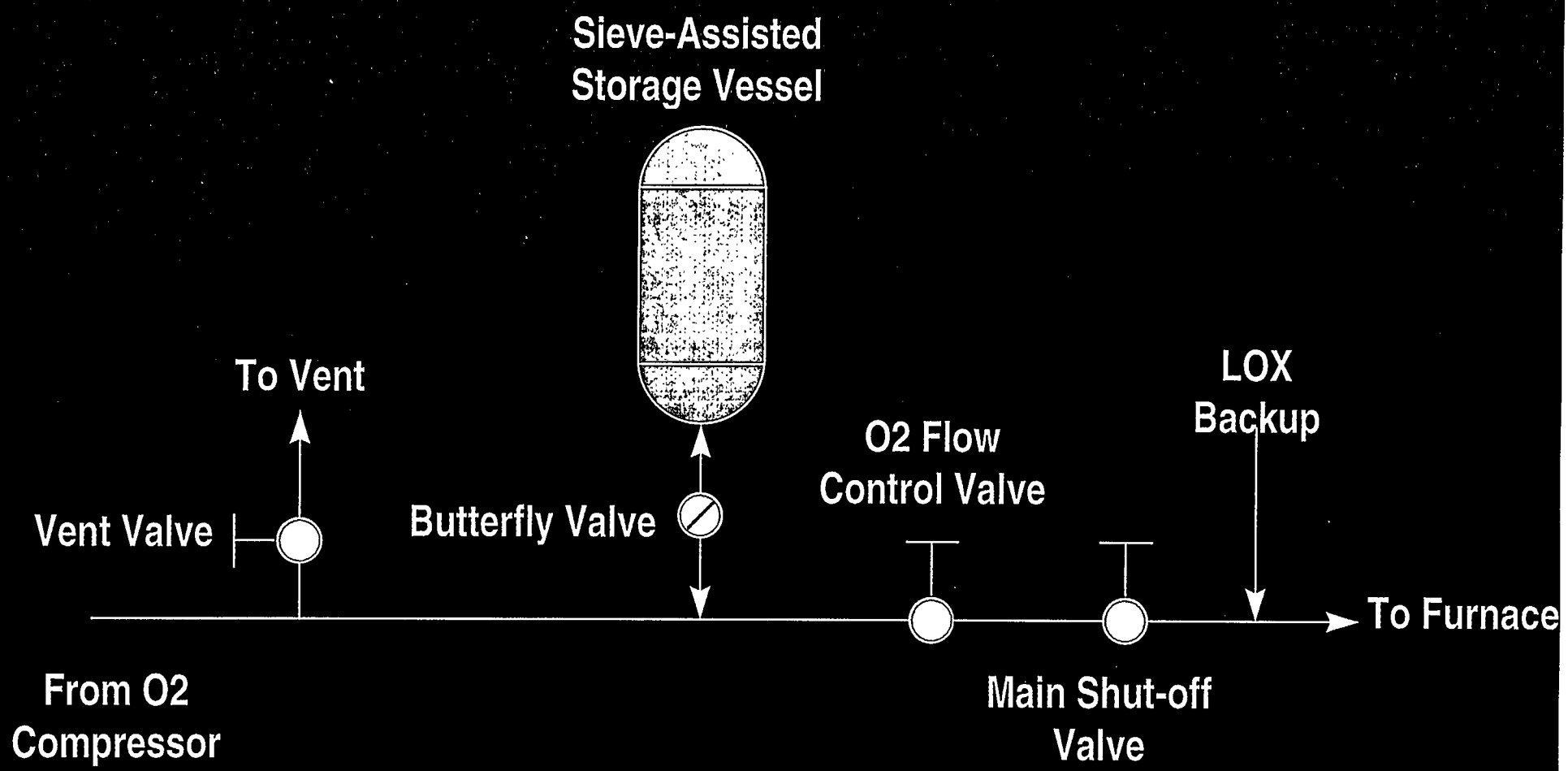

Figure 4-5. Illustration of Typical Peak Oxygen Event

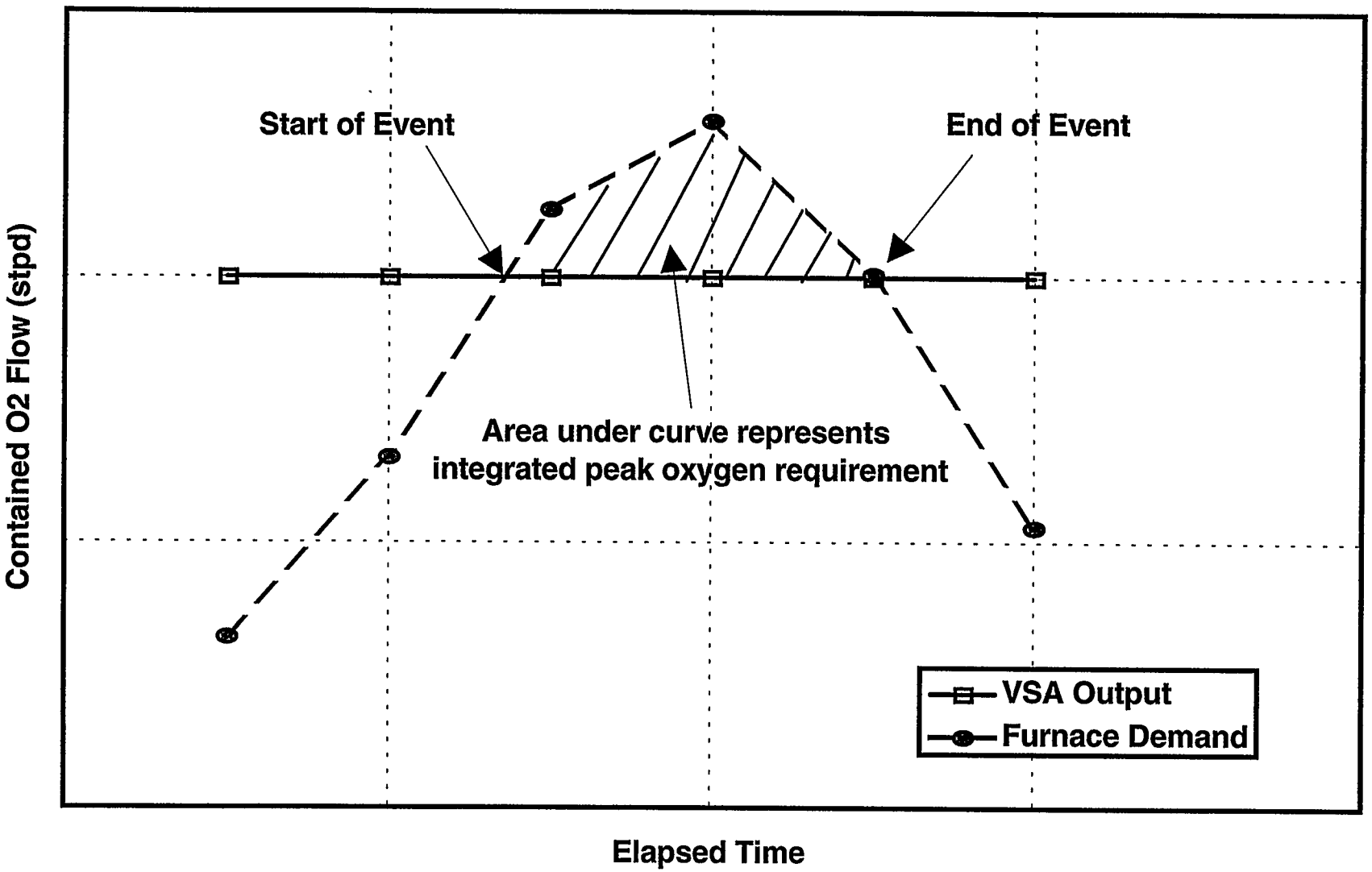

Figure 4-6. VSA Output and Furnace Demand During Sieve Tank Utilization Tests Tank Open: Events 1 through 3

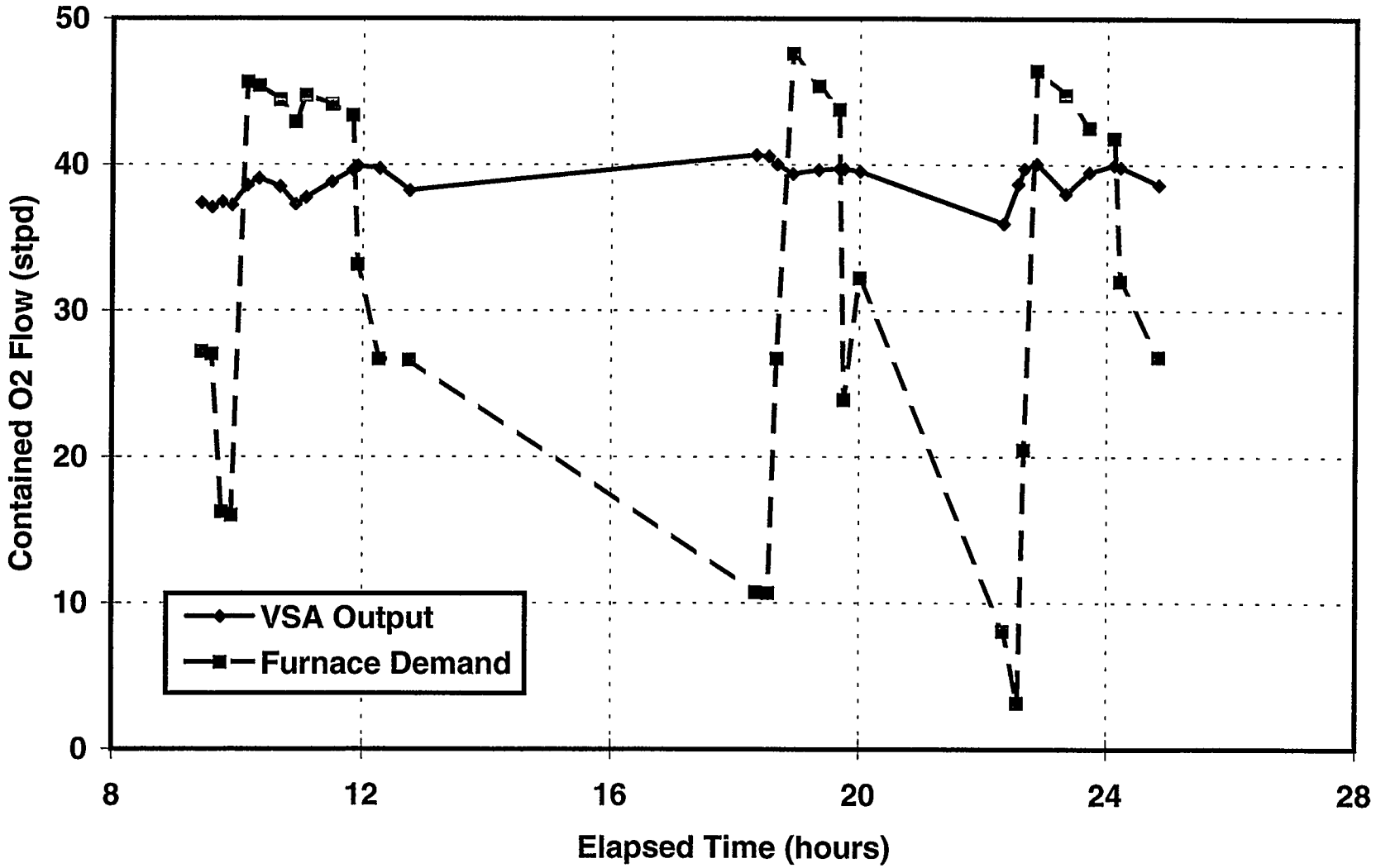

Figure 4-7. VSA Output and Furnace Demand During Sieve Tank Utilization Tests Tank Open: Events 4 through 6

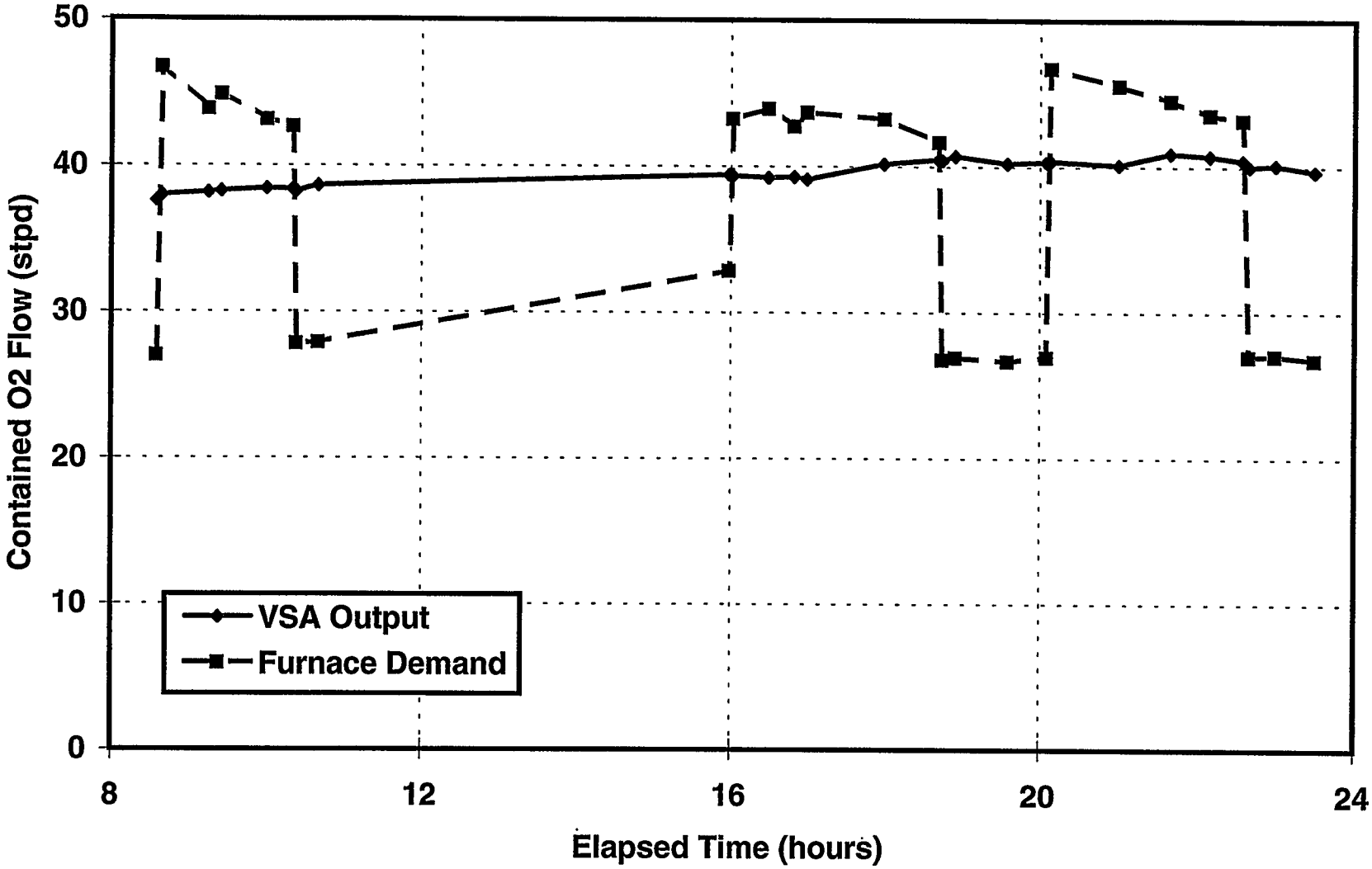

Figure 4-8. VSA Output and Furnace Demand During Sieve Tank Utilization Tests Tank Closed: Events 1 through 6

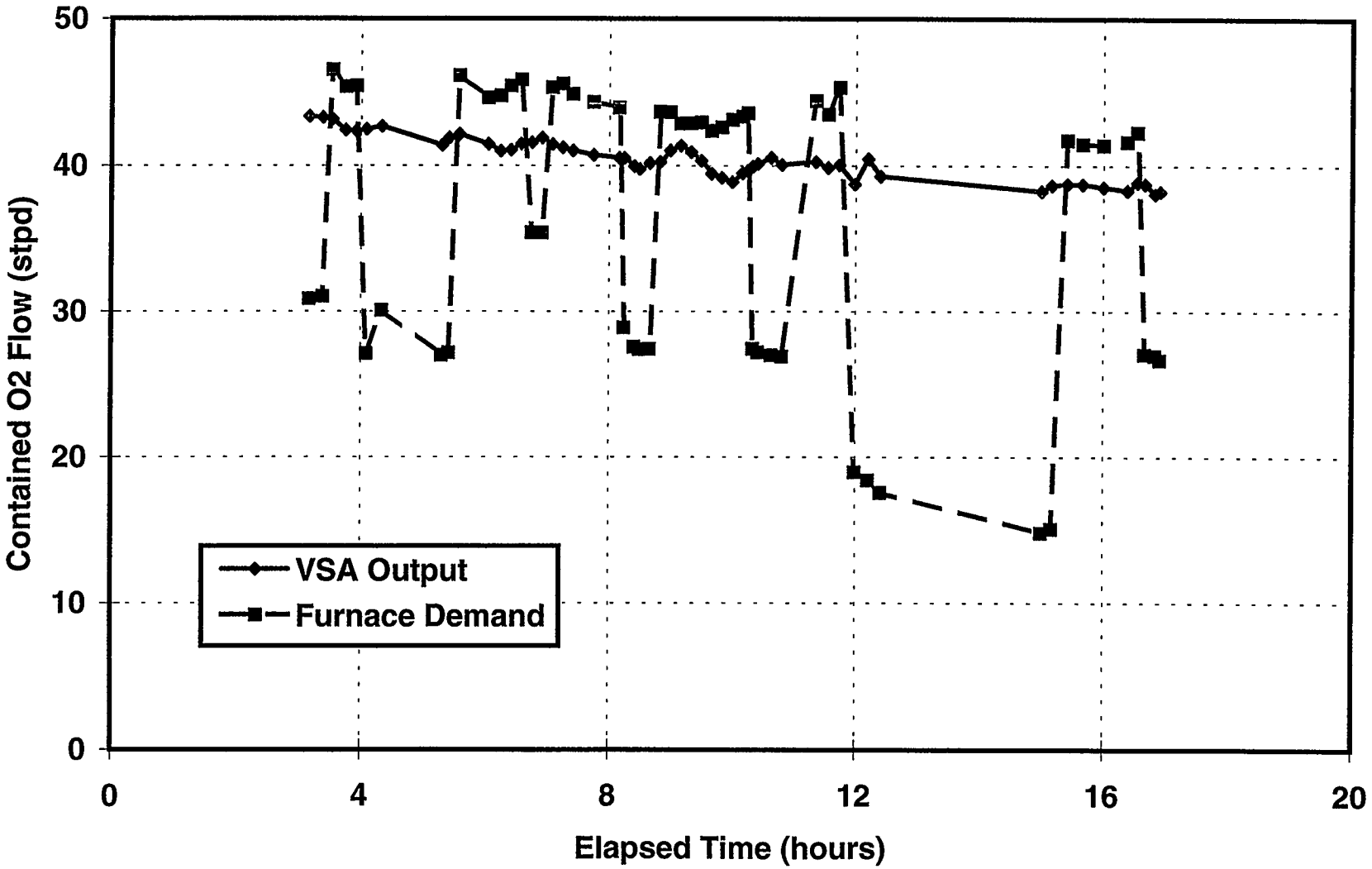

Figure 4-9. VSA Output and Furnace Demand During Sieve Tank Utilization Tests Tank Closed: Events 7 and 8

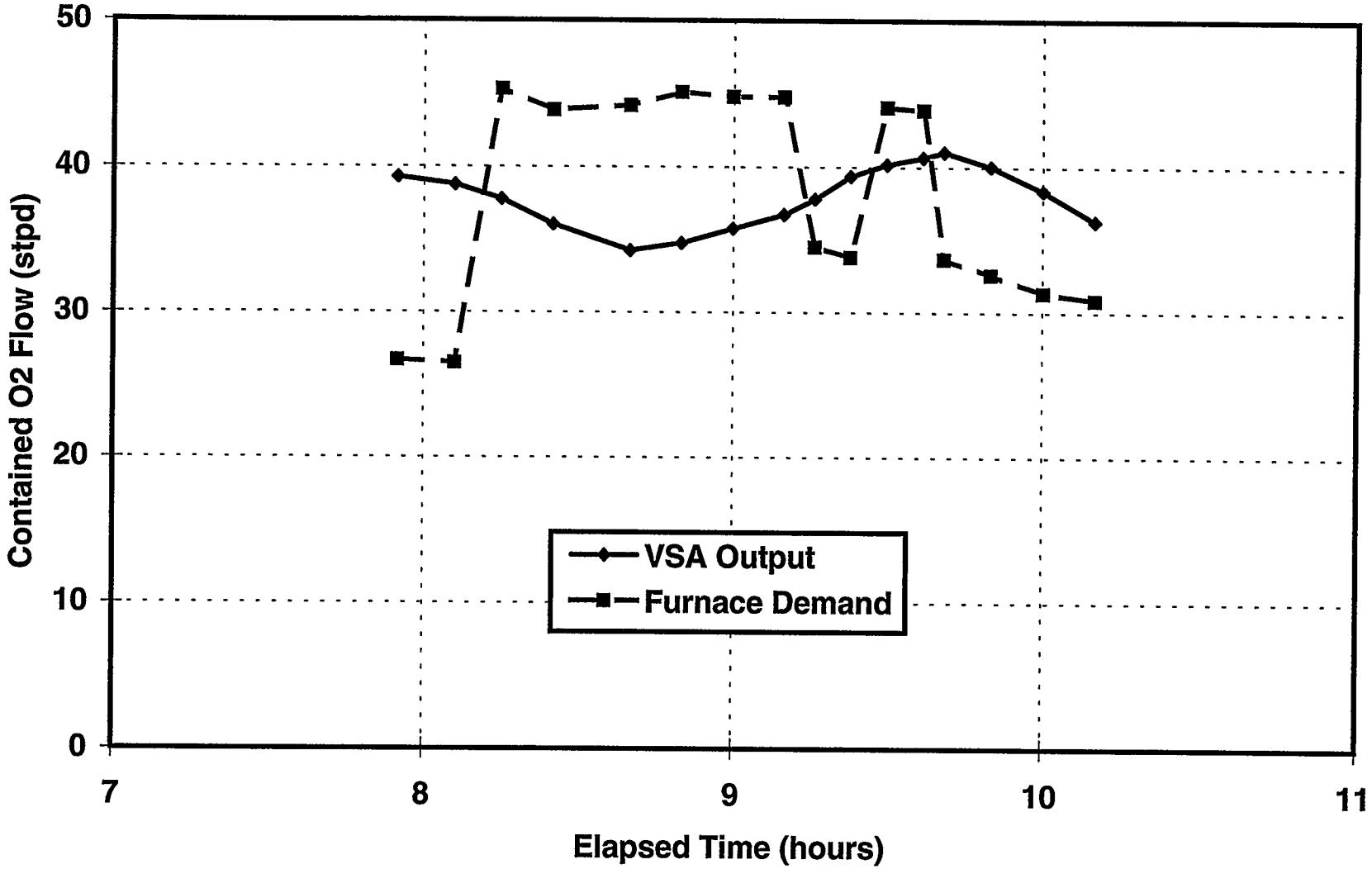

the vessel between the normal working pressures of 30 and 75 psig. The test was therefore conducted by measuring the total amount of oxygen discharged from the oxygen compressor into the tank as the tank pressure increased between the working pressure limits. Standard flow, purity and pressure instruments from the plant were used to make the measurements. Results showed a tank capacity of 8057 standard cubic feet of oxygen. With a working volume of approximately 1000 ft^3 within the sieve tank, this amounted to roughly 2.65 times the storage capacity of the empty vessel over the same pressure range.

Sieve Tank Utilization Test

Effectiveness of the sieve-assisted storage system in supplying peak O_2 demand requirements was evaluated by comparison of backup LOX consumption during two periods of normal furnace operation, one with the sieve tank open and one with the tank closed. Measurements made during this field trial included LOX tank level, VSA oxygen flow rate (supply), furnace oxygen flow rate (demand) and various other process parameters such as system pressures and valve positions. Quantification of sieve tank effectiveness was carried out by identifying peak oxygen "events," wherein furnace oxygen demand exceeded the VSA oxygen supply. Illustration of a typical event is shown in Figure 4-5. The event was characterized by a start time during which furnace oxygen demand initially exceeded VSA output, an end time during which furnace demand again fell below VSA output, and a total peak oxygen requirement, which was the area between the demand and output curves during the event.

There were, in total, six events for the open-tank period and eight events for the closed-tank period. Transient furnace oxygen demand and VSA output data during these events are summarized in Figures 4-6 through 4-9. These figures clearly illustrate variations in characteristics among the events, with ranges of event duration from 15 minutes to 3 hours, and peak oxygen requirement from 0.02 to 0.42 standard tons (roughly 500 to 10,000 scf). These differences precluded a direct comparison between individual "open" and "closed" events. The comparison was thus based on summing the LOX consumption and peak oxygen requirement for all events in the open and closed periods. The specific LOX consumption for each period was then calculated by dividing the total LOX consumption by the total peak oxygen requirement. Calculated values of specific LOX consumption for the open and closed periods are listed in Table 4-1. Results indicate that a 33 percent reduction in normalized LOX consumption was achieved through utilization of the sieve tank. As the peak oxygen requirement during this test was approximately 1 standard ton/day (24,000 scf), use of the sieve tank reduced LOX consumption by 1/3 ton LOX per day. Although this represents a significant reduction in LOX usage, it also suggests that additional storage capacity is needed for this facility. However, we should caution that each operating period during which these tests were conducted spanned approximately one to two days, and therefore may not accurately represent long-term trends in peak oxygen requirement. The economic impact of these test results is addressed in Section 5 of this report.

Table 4-1
Specific LOX Consumption for Sieve Tank Open and Closed Periods

Period	Total LOX Consumption	Total Peak Oxygen Requirement	Specific LOX Consumption
	std tons O_2	std tons O_2	tons LOX/ton peak O_2 required
Open	1.45	2.16	0.67
Closed	1.16	1.16	1.00

Summary
A novel integrated O_2 VSA with sieve-assisted storage system has been successfully built and operated at the Wabash East Syracuse, N.Y. facility. Field test results showed that the tank oxygen storage capacity is in excess of 2.5 times the capacity of an empty tank of equal volume, and that utilization of the tank reduced backup LOX consumption by 33 percent. The system currently operates at a design purity of approximately 93 percent and vents the VSA waste stream to atmosphere. The feasibility of lowering furnace NOx emissions by using the VSA vent stream as a low-purity secondary oxidizer in the new low-NOx burner technology was proven during on-site testing. Calculations also indicate that operating the VSA at lower than design purity will significantly lower the VSA power requirement per unit of oxygen product. Further development would be necessary to commercialize these offerings.

Section 5
Process Economic Evaluation

Overview of Reverb Furnace Economics

Profitability of aluminum melting operations in a reverb furnace is strongly influenced by combustion system performance. To a large extent, the combustion system controls fuel efficiency and productivity, which directly affects the cost of raw materials and utilities. The combustion system can also influence furnace yield, which is the mass ratio of furnace output (product) to input (charge). Another important economic factor is the price of oxygen, which influences overall furnace profitability and, in particular, affects the relative profitability of air-fuel combustion versus oxygen-enriched combustion. Oxygen pricing depends on such commercial factors as oxygen generation technology and logistical issues relating to oxygen supply.

Profit margins are relatively small in secondary aluminum melting. This fact is illustrated by the pie chart in Figure 5-1, which shows that the operating return on investment, OROI, which is essentially the profit margin, is only of the order of 2 percent of the gross revenue for air-fuel operation, whereas raw materials amount to 88 percent of gross revenue. It is also instructive to break down raw material and utility costs. This is accomplished for an air-oxy-fuel installation in Figure 5-2, showing the predominance of scrap aluminum cost (96 percent) relative to fuel (2 percent) and oxygen (1 percent) costs. This disparity helps to explain why oxygen enrichment is normally justified based on potential gains in furnace productivity rather than improvements to fuel efficiency.

Reverb Furnace Economic Model

The economic model developed for reverb aluminum melting takes account of several major cost categories, including raw materials, utilities, capital, labor and overhead, as well as revenue derived from product sales. Raw materials consist essentially of scrap aluminum and fluxes used to segregate and remove impurities from the molten bath. Included in the category of utilities are the cost of electricity (including the cost to drive air blowers), fuel, oxygen, and waste (i.e., dross) disposal. The principal capital costs are in the handling and pre-processing of scrap (i.e., conveyors, de-volatizers); construction of the furnace, including refractory, burners, instrumentation and pollution control equipment; and casting lines for drawing molten aluminum from the furnace into product vessels. The model can be used for evaluating both retrofit and new-build (green field) applications. The present task for this model was to compare the economics of air-fuel technology at Wabash furnace #8 to the retrofitting of an air-oxy-fuel or oxy-fuel combustion system. Model description and results are described in the remainder of this section.

Model Description

The economic model uses input data on the various costs for each operating scenario to perform a series of calculations, culminating with the determination of PBIT, profit before interest and taxes. PBIT is the product of OROI and the annual aluminum production rate. OROI, in turn, is the product selling price minus corporate overhead, depreciation of capital, and plant cash outlay.

Major Cost Components for Air-Fuel Operation in Reverb Furnace

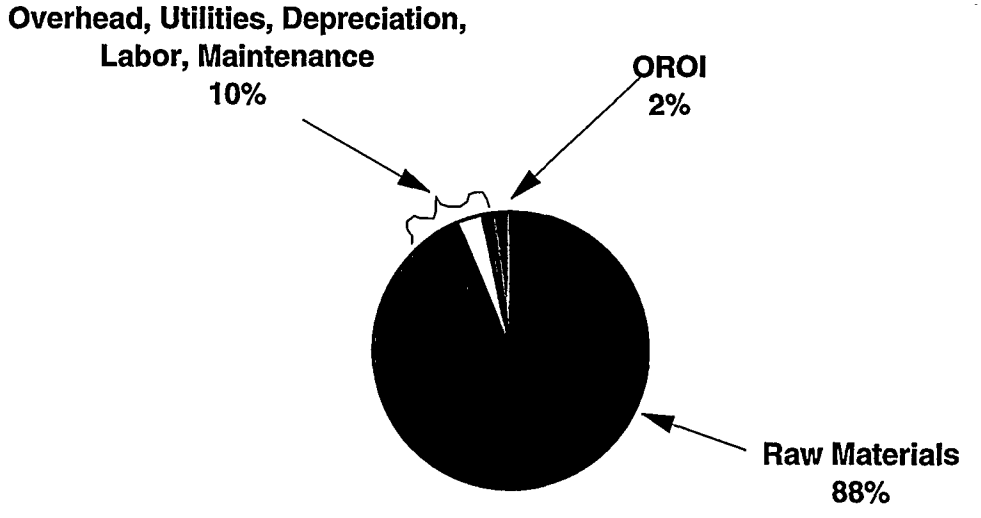

Figure 5-2. Typical Raw Materials and Utilities Cost Breakdown for Air-Oxy-Fuel Operation in Reverb Furnace

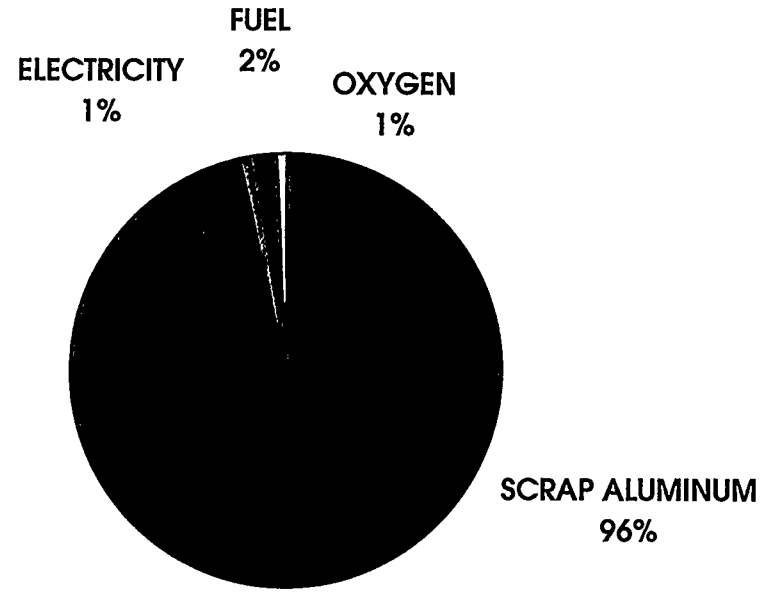

This latter quantity includes the cost of raw materials, utilities, dross disposal, labor, maintenance and miscellaneous plant overheads such as insurance and taxes.

Results Comparison for Air-Fuel, Air-Oxy-Fuel and Oxy-Fuel Cases

The furnace economic model was applied to three basic operating strategies, air-fuel, air-oxy-fuel with 35 percent oxygen enrichment and 100 percent oxy-fuel combustion operating in Wabash furnace #8. The incremental cost for burners and control equipment was estimated at $250,000 per furnace for both the AOF and OF operating scenarios. Four process economic parameters were systematically varied in each of the two OEC modes: furnace productivity, specific energy usage and yield (all relative to air-fuel operation), and oxygen price (cents per hundred standard cubic feet). Data for furnace productivity and specific energy usage in an AOF-fired furnace, relative to air-fuel operation, were based on performance data collected during this project. Ranges for the same performance parameters using oxy-fuel technology were estimated based on unpublished performance data from a commercial OF-fired reverb furnace. No sources were available for obtaining accurate furnace yield data in OEC relative to air-fuel technology. Estimates were therefore based on furnace CFD modeling results carried out under this project. The range of oxygen prices was set based on expected variations due to differences in oxygen generator technology, supply logistics and commercial factors. A summary of parameter ranges for the model calculations is provided in Table 5-1.

Table 5-1
Range of Economic Parameters for Furnace Economic Model Calculations

Parameter	Air-Oxy-Fuel @ 35% Oxygen Enrichment	100 % Oxy-Fuel Combustion
Furnace Productivity	+25-30% relative to air-fuel technology	+30-35% relative to air-fuel technology
Specific Energy Usage	-30% relative to air-fuel technology	-40% relative to air-fuel technology
Furnace Yield	No change from air-fuel technology	0 to -1/2 % relative to air-fuel technology
Oxygen Price	15-35 cents/100 scf	15-35 cents/100 scf

Results of sensitivity calculations with the economic model are summarized in Figures 5-3 through 5-7. All model results are presented as ΔPBIT, the profit of either AOF or OF technology relative to air-fuel technology, versus the price of oxygen. Figure 5-3 illustrates the sensitivity of the relative operating profit to furnace productivity for the air-oxy-fuel case. The two production levels used for this case were increases of 25 and 30 percent relative to air-fuel combustion. Furnace yield and specific energy utilization were held fixed at -30% and +0%, respectively, relative to air-fuel operation. Results indicate a significant increase in profit associated with AOF technology across the entire range of production rate and oxygen price, varying from a maximum of $64,000/month for higher production/lowest oxygen price to $36,000/month for lower production/highest oxygen price. At fixed oxygen price, profit increases by approximately $10,000/month for a 5 percent production increase, while at fixed

Figure 5-3. Results of Reverb Furnace Economic Model Calculations
Effect of Productivity: Air-Oxy-Fuel Case

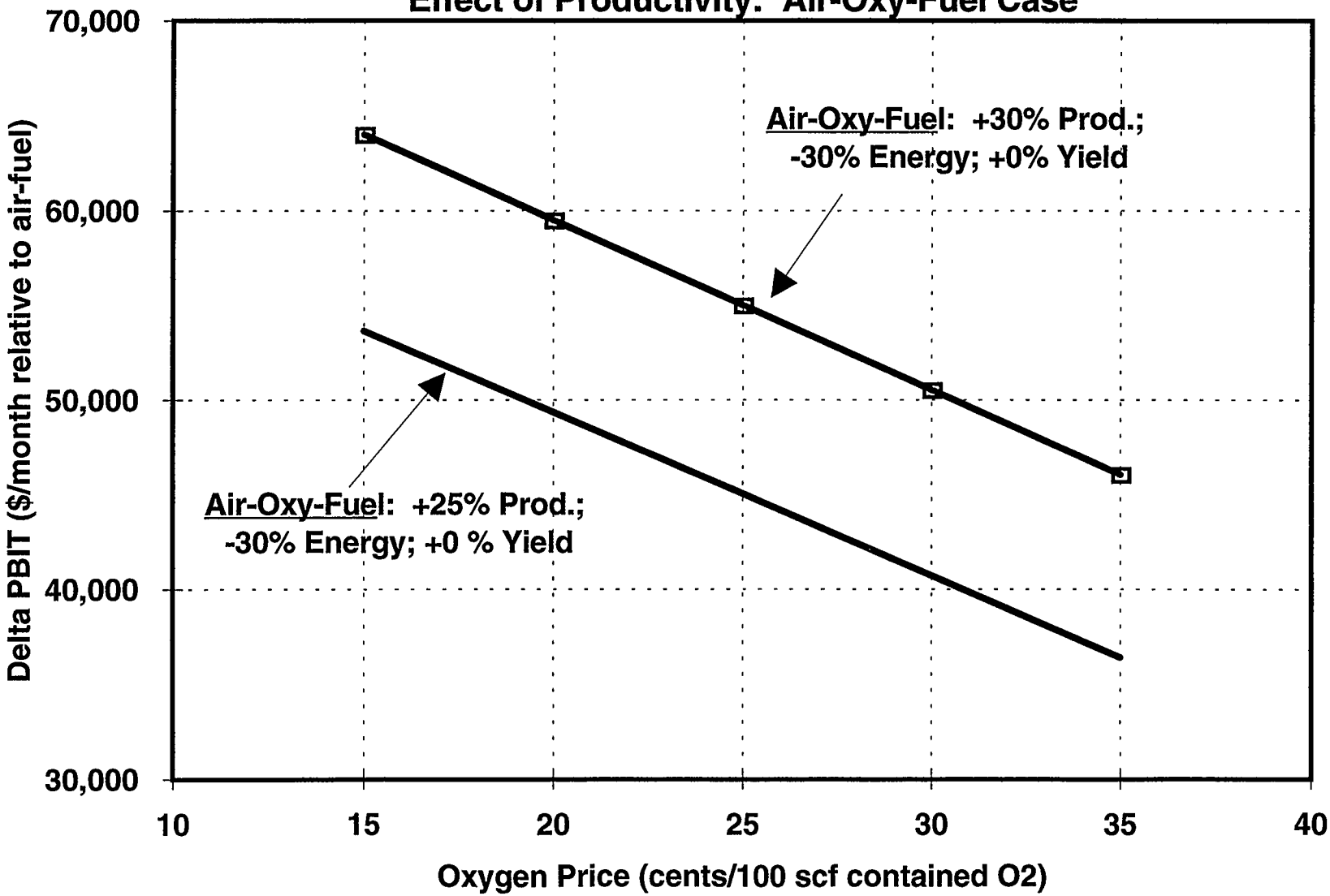

Figure 5-4. Results of Reverb Furnace Economic Model Calculations
Effect of Yield: Oxy-Fuel Case

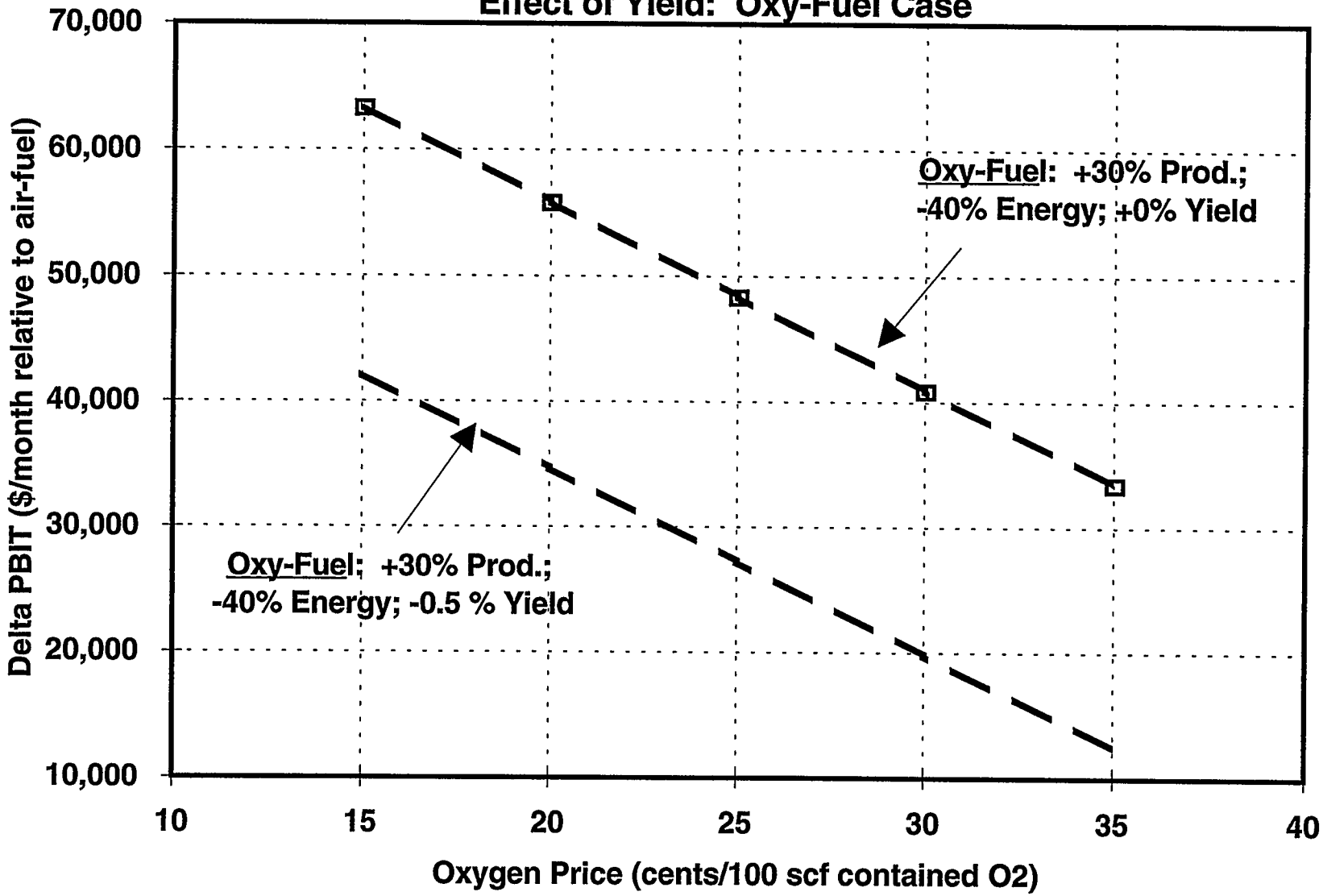

Figure 5-5. Results of Reverb Furnace Economic Model Calculations
Air-Oxy-Fuel vs Oxy-Fuel Comparison #1

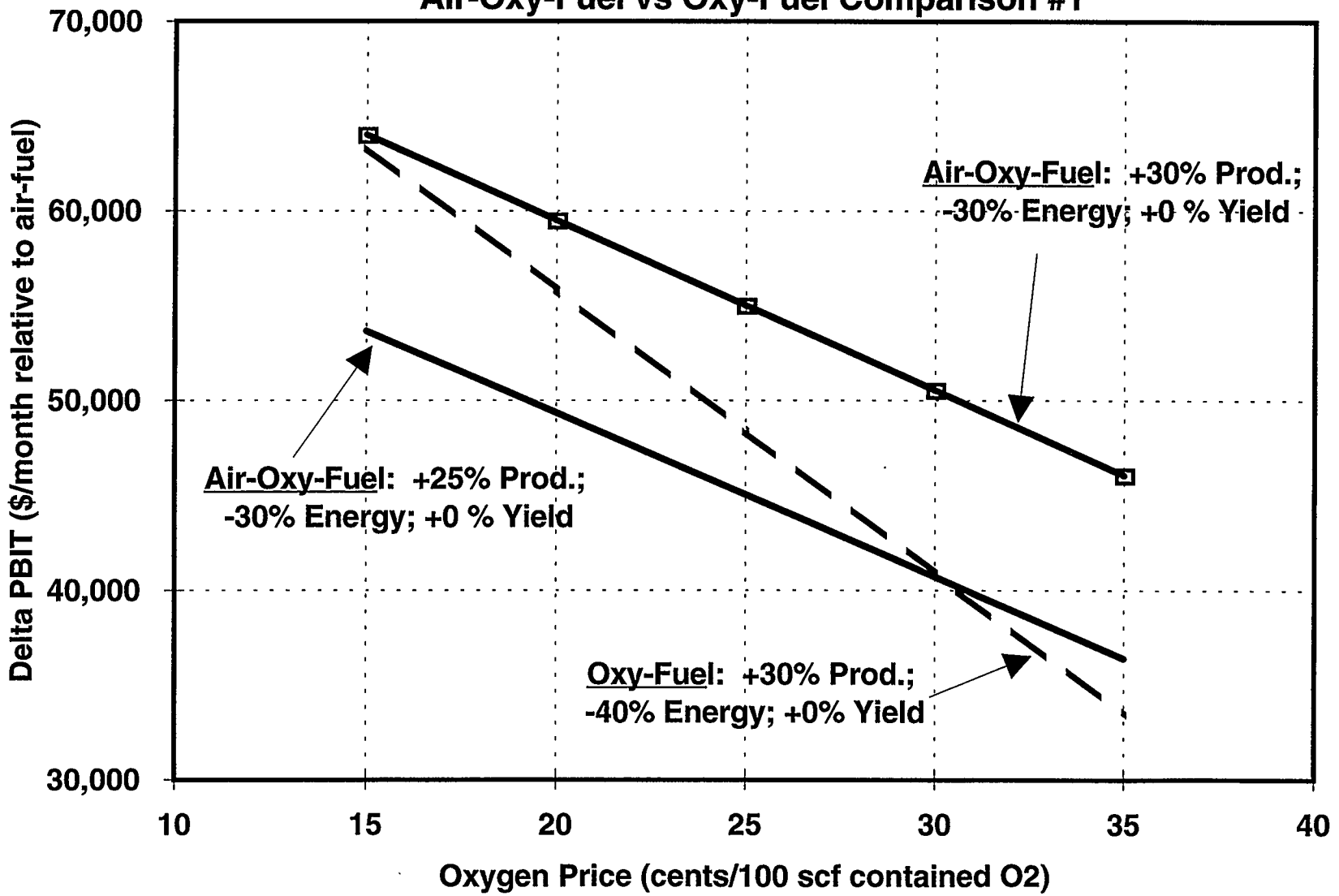

Figure 5-6. Results of Reverb Furnace Economic Model Calculations
Air-Oxy-Fuel vs Oxy-Fuel Comparison #2

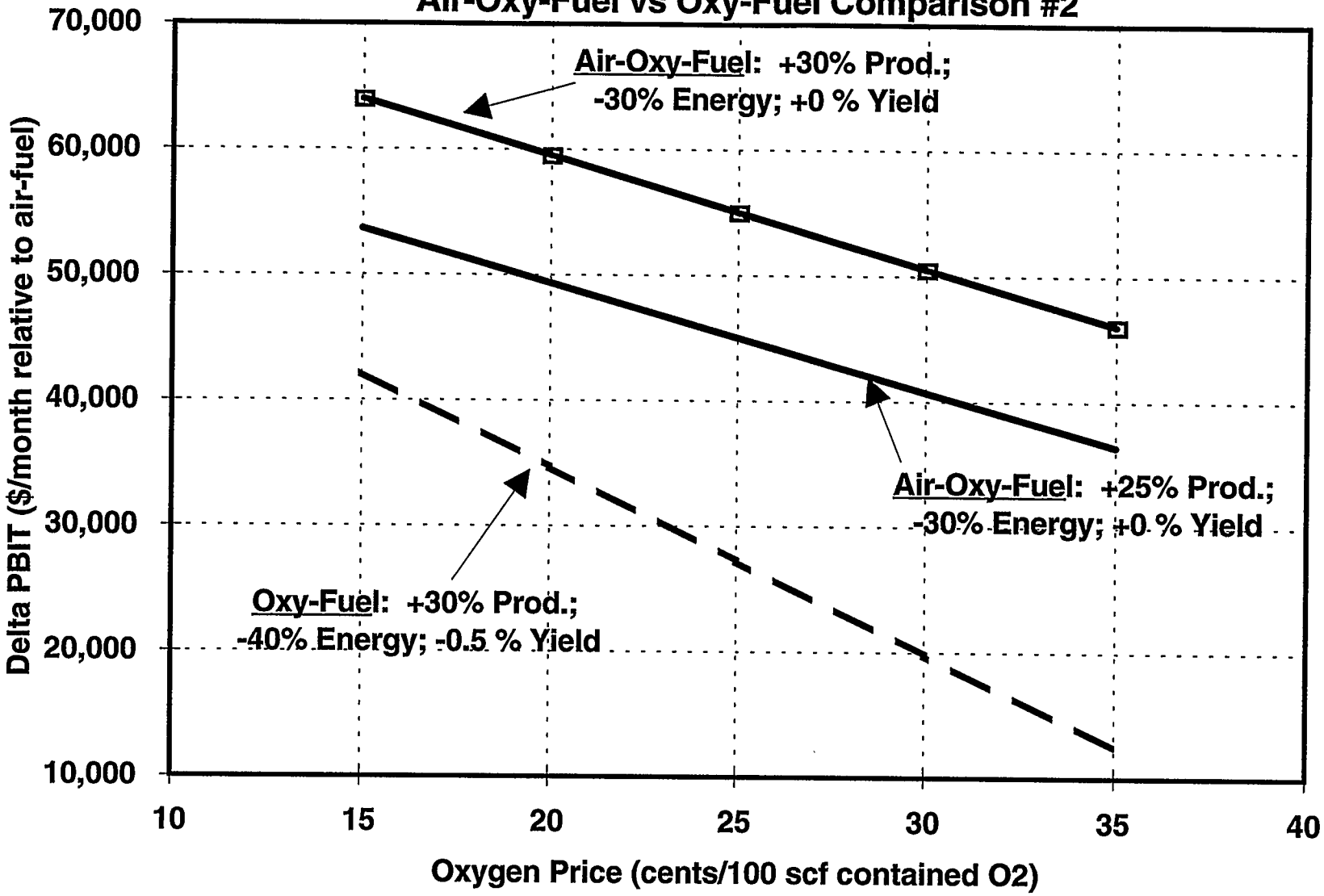

Figure 5-7. Results of Reverb Furnace Economic Model Calculations
Air-Oxy-Fuel vs Oxy-Fuel Comparison #3

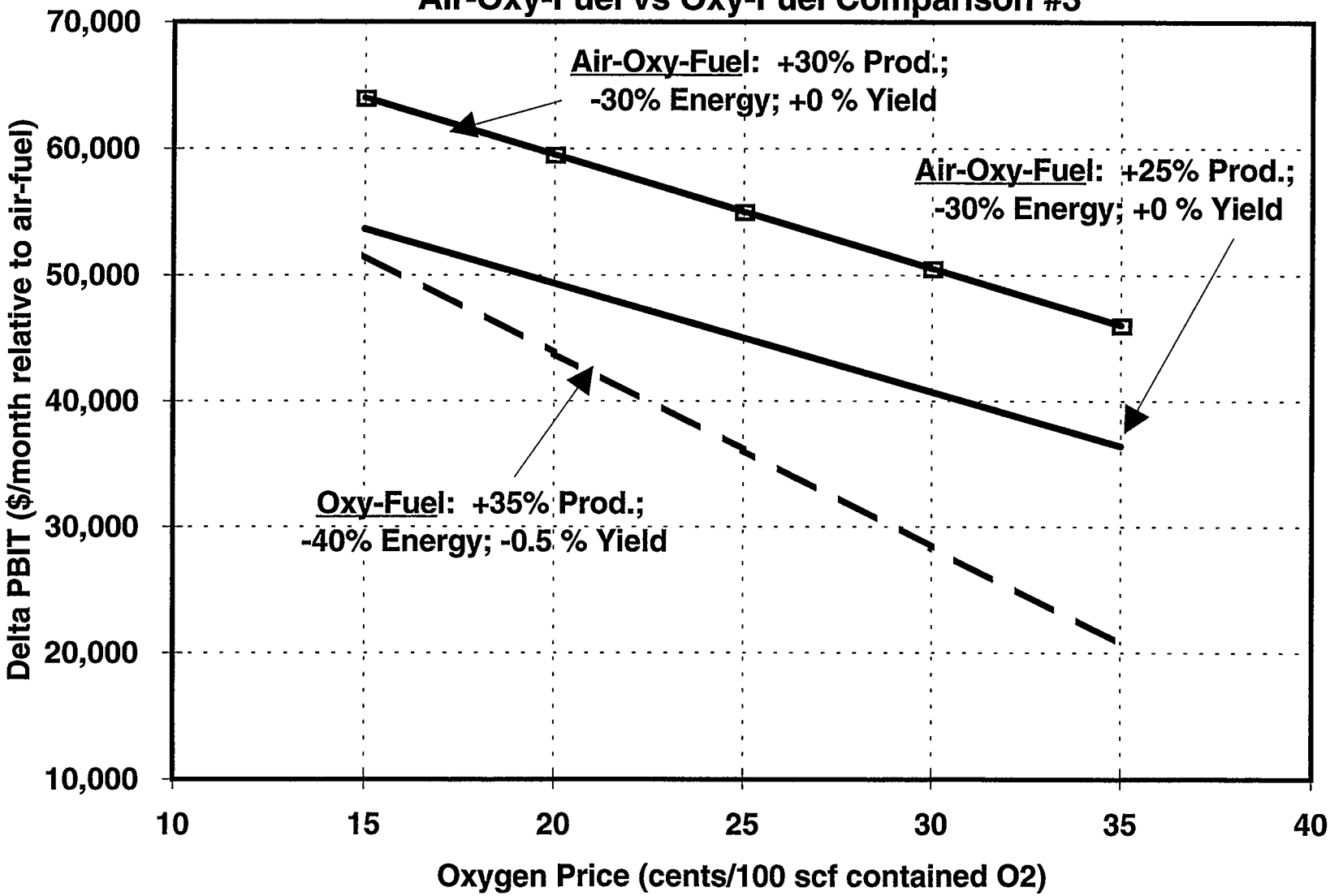

productivity, profits decrease by roughly $8500/month for every 10 cent/100 scf increase in oxygen price.

Figure 5-4 shows the sensitivity of relative profit to furnace yield for oxy-fuel technology. The two yield levels used here were 0% and -0.5% relative to air-fuel technology, while relative furnace productivity and specific energy utilization were held fixed at +30 and -40%, respectively. The oxy-fuel mode rather than the air-oxy-fuel mode was used as the test case here since there is a higher susceptibility for reductions in furnace yield with this technology. As with the air-oxy-fuel comparison of Figure 5-3, Figure 5-4 indicates a substantial increase in profit with oxy-fuel technology relative to air-fuel over the entire range of parameters. Profits vary from $63,000/month for 0% relative yield and 15 cents/100 scf oxygen to $12,000/month for -0.5% yield and 35 cents/100 scf oxygen. At fixed oxygen price, profit decreases by approximately $21,000/month due to the 0.5% yield reduction, illustrating the extremely strong economic penalty associated with degradation to furnace yield. With yield held constant, profits decrease by approximately $15,000/month for every 10 cent/100 scf increase in oxygen price. The sensitivity to oxygen price is greater here than for air-oxy-fuel combustion due to the much larger flow rates of oxygen required for the process.

Figures 5-5 through 5-7 present comparisons between air-oxy-fuel and oxy-fuel technology. Each graph contains model results for three cases. The comparison in Figure 5-5 includes two air-oxy-fuel cases and one oxy-fuel case with the following conditions:

Air-Oxy-Fuel case A: +25% production; -30% specific energy usage; +0% yield
Air-Oxy-Fuel case B: +30% production; -30% specific energy usage; +0% yield
Oxy-Fuel case: +30% production; -40% specific energy usage; +0% yield

It is noted first that model calculations predict substantial increases in profit, relative to air-fuel operation, for all OEC options. Further, results show that, at equal furnace yields and productivity levels, despite the better energy efficiency of the oxy-fuel process, AOF technology is more profitable over the entire range of oxygen pricing. The assumption of equal productivity for the AOF and OF cases is quite reasonable for retrofit applications since, as explained by CFD modeling results, oxy-fuel firing rates and, hence, furnace productivity, are likely to be limited due to refractory temperature constraints. Nevertheless, if it is assumed that air-oxy-fuel technology produces a +25% rather than a +30% increase in melt rate, the relative profitability of AOF versus OF technology then depends on oxygen price, with OF technology more profitable at pricing less than 30 cents/100 scf O_2 and AOF more profitable above this level.

Figure 5-6 examines the model predictions assuming a -0.5% reduction in furnace yield for oxy-fuel firing, while maintaining the same productivity and energy efficiency as in Figure 5-5. Results indicate this relatively small yield reduction lowers the profitability of OF technology to the point that even AOF case A, with reduced productivity, is now significantly more profitable over the entire range of oxygen pricing.

Finally, in Figure 5-7, the OF production rate is increased from +30 to +35%, while furnace yield is maintained at -0.5%. Model calculations show that this increase in OF productivity does not

sufficiently compensate for the profit loss due to the yield reduction, thus rendering AOF technology still more profitable across all oxygen prices.

Summary of Reverb Furnace Economic Model Calculations

Economic model results showed that both air-oxy-fuel and oxy-fuel combustion technologies have the potential to be considerably more profitable than air-fuel technology for secondary aluminum melting in reverb furnaces. This principally results from the fact that the increase in operating costs due to the purchase of oxygen and associated combustion equipment is far outweighed by the gain in revenue due to increased productivity. Results also showed that the relative profitability between AOF and OF technologies is sensitive to assumed values for oxygen pricing, yield and productivity. However, as the retrofitting of OF technology into an existing air-fuel furnace is more susceptible than AOF technology to furnace yield reductions and production constraints due to material limitations, the air-oxy-fuel technology appears to provide the most certain economic advantage for the range of conditions investigated.

Overview of VSA O_2 Storage Economics

The irregular oxygen usage pattern inherent in operation of an aluminum reverb furnace (see Figure 4-1) requires frequent and rapid modulation of oxygen supply, which poses a challenge in the operation of an on-site O_2 VSA. Modulation of oxygen production in the VSA is not a technically feasible option due to the de-stabilizing effect it has on product purity, as well as turndown limitations on air blowers and oxygen compressors. This leaves four basic options, which are:

1. sizing the VSA to meet the peak oxygen demand and venting the excess product when it is not needed,
2. sizing the VSA for less than peak demand and providing a backup LOX supply for satisfying peak demand,
3. sizing the VSA for less than peak demand and storing excess production in an empty vessel for use during peak demand periods,
4. sizing the VSA for less than peak demand and storing excess product in an adsorbent-filled vessel for use during peak demand periods.

There are benefits and drawbacks to each option. Sizing the VSA to provide peak demand and venting the excess product is a simple approach, yet it requires the most expensive VSA and largest specific power requirement per unit of oxygen delivered to the end user. Options 2 through 4 offer reduced capital cost and power requirement due to the use of a smaller VSA. However, depending on the particular backup method selected, complexity is added to the system, and supplemental capital and/or operating costs are incurred. For example, option 2 relies entirely on liquid oxygen backup which, depending upon supply logistics and the amount of LOX required, may represent a substantial incremental operating cost. By contrast, options 3 and 4 require excess capital equipment in the form of gas storage tanks and compressors, while additional operating costs are kept at a minimum.

Economic Decision Model for VSA Oxygen Storage

A model was developed to compare capital and operating costs among the four "storage" options. The primary model input variables investigated in this study were the oxygen usage pattern, the price of LOX and the price of sieve (adsorbent for the storage vessel). In addition to these, there are several economic and process-related parameters. Baseline values for these are summarized in Table 5-2. Capital equipment and power costs for the VSA were estimated from Air Products' commercial data base. Capital costs for the storage vessel were estimated from available commercial data and scale factors.

Table 5-2
Parameter Values Used in Economic Decision Model

Parameter	Value or Range
Sieve Price	$0.50 - $1.50 /lb
LOX Price	$0.25 - $0.30 /100 scf
Oxygen Usage Pattern	See Model Results
VSA Oxygen Purity	94%
Maximum Operating Pressure of Storage Vessel	75 psig
Minimum Operating Pressure of Storage Vessel	30 psig
Project Life	15 years
Interest Rate	9.5%

Input data are used to calculate the present value (PV) of each option. The present value represents the current worth of all payments made over the life of the project, including both capital and operating costs. The present value is calculated from the interest rate per payment period, RATE; the total number of payments over the life of the project, N; and the dollar value of each periodic payment, PMT, through the following equation:

$$PV = PMT*[(1+RATE)^{N}-1]/RATE/(1+RATE)^{N} \qquad (5\text{-}1)$$

The payment, PMT, is a composite of annualized power and capital costs. Capital costs include those of the base VSA, backup LOX supply and storage system (options 3 and 4 only). Note that a backup LOX supply was included for all four options, since this is a standard commercial practice. Options 1 and 2 utilize low-pressure (nominally 20 psig) VSA units, while options 3 and 4 assume that higher pressure units (nominally 70 psig) are required for economical product storage.

The model allows input of a two-stage idealized oxygen usage pattern consisting of high oxygen demand/duration and low oxygen demand/duration. VSA sizing for option 1 was based on the peak oxygen demand, while the time-averaged oxygen demand was used for options 2 through 4.

Model Results

Model calculations, summarized in Figures 5-8 through 5-12, examined the effects of sieve price, oxygen (LOX) price and oxygen usage pattern on the economic viability of sieve-assisted storage versus the other three VSA supply/storage options. Figures 5-8 and 5-9 show the present value of each option versus sieve price for the following oxygen usage pattern:

high demand: 2 hours @ 45 stpd contained O_2
low demand: 6 hours @ 25 stpd contained O_2

This usage pattern simulates that which occurred during the sieve storage utilization tests (see Figures 4-6 through 4-9). The results in Figure 5-8 represent a LOX price of $0.25/100 scf. The costs (i.e., present value) of options 1 through 3 are naturally constant since they do not depend on sieve price, whereas the cost of option 4 decreases with decreasing sieve price. For this set of input conditions, option 4 becomes the least expensive when the sieve price falls beneath $0.55/lb. Of the remaining three options, option 2 (small VSA with LOX backup) is least expensive, with a present value of $4.02 MM, option 3 (small VSA with empty tank) is $4.05 MM, and option 1 (large VSA) is the most expensive at $4.59 MM. The reason the relative economics of option 1 are so poor is that the maximum VSA output of 45 stpd is substantially larger than the time-averaged value of 30 stpd. Figure 5-9 illustrates results for a LOX price of $0.30/100 scf with the same usage pattern. The change in LOX price affects only option 2, which increases in present value from $4.02 MM to $4.14 MM. This change improves the relative economics of sieve storage. Instead of $0.55/lb, as was the case in Figure 5-8, the sieve price must fall below $0.75/lb if option 4 is to be the least expensive. The current price of sieve used in the Wabash VSA is approximately $1.00/lb.

Figures 5-10 and 5-11 examine model results for a different oxygen usage pattern:

high demand: 4 hours @ 47 stpd contained O2
low demand: 4 hours @ 27 stpd contained O2

This usage pattern is closer to that represented in Figure 4-1. The overall storage or "backup" oxygen requirement is essentially equal to that of the first usage scenario; however, the average oxygen demand for this case is closer to the maximum demand (37 stpd average, 47 stpd maximum). Hence, the large VSA sized for option 1 is not as over-priced as in Figures 5-8 and 5-9. Also, the average demand for this case (37 stpd) is significantly larger than for the previous case (30 stpd). This increases the difference in price between the small, low-pressure VSA used for option 2 and the small, high-pressure unit used in options 3 and 4. The net result is that, for a LOX price of $0.25/100 scf (Figure 5-10), option 2 (LOX backup) is the least expensive option over the entire range of sieve prices. However, with a LOX price of $0.30/100 scf (Figure 5-11), the sieve storage option becomes the most economical below a sieve price of $0.75/lb, while LOX backup becomes the most expensive.

One final model case presented herein is the cost of combined sieve storage with LOX backup. Figure 5-12 shows the present value of this option as a function of the percent of peak oxygen requirement delivered from the sieve tank. The sieve tank in this analysis was sized for the

Figure 5-8. VSA O2 Storage Economic Decision Model Results
O2 Usage Cycle: 45 stpd @ 2 hours, 25 stpd @ 6 hours
LOX price = $0.25/100 scf

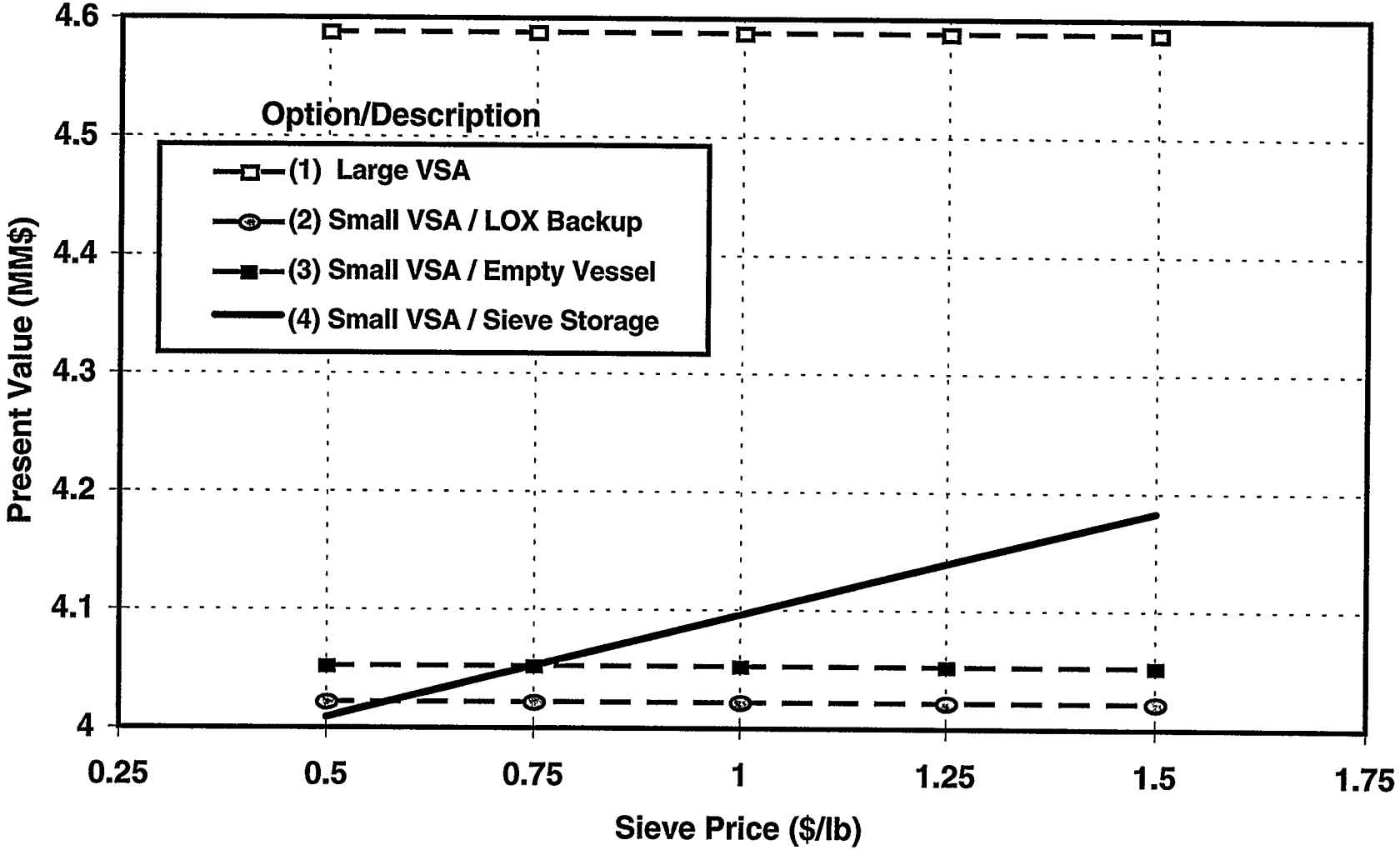

Figure 5-9. VSA O2 Storage Economic Decision Model Results
O2 Usage Cycle: 45 stpd @ 2 hours, 25 stpd @ 6 hours
LOX price = $0.30/100 scf

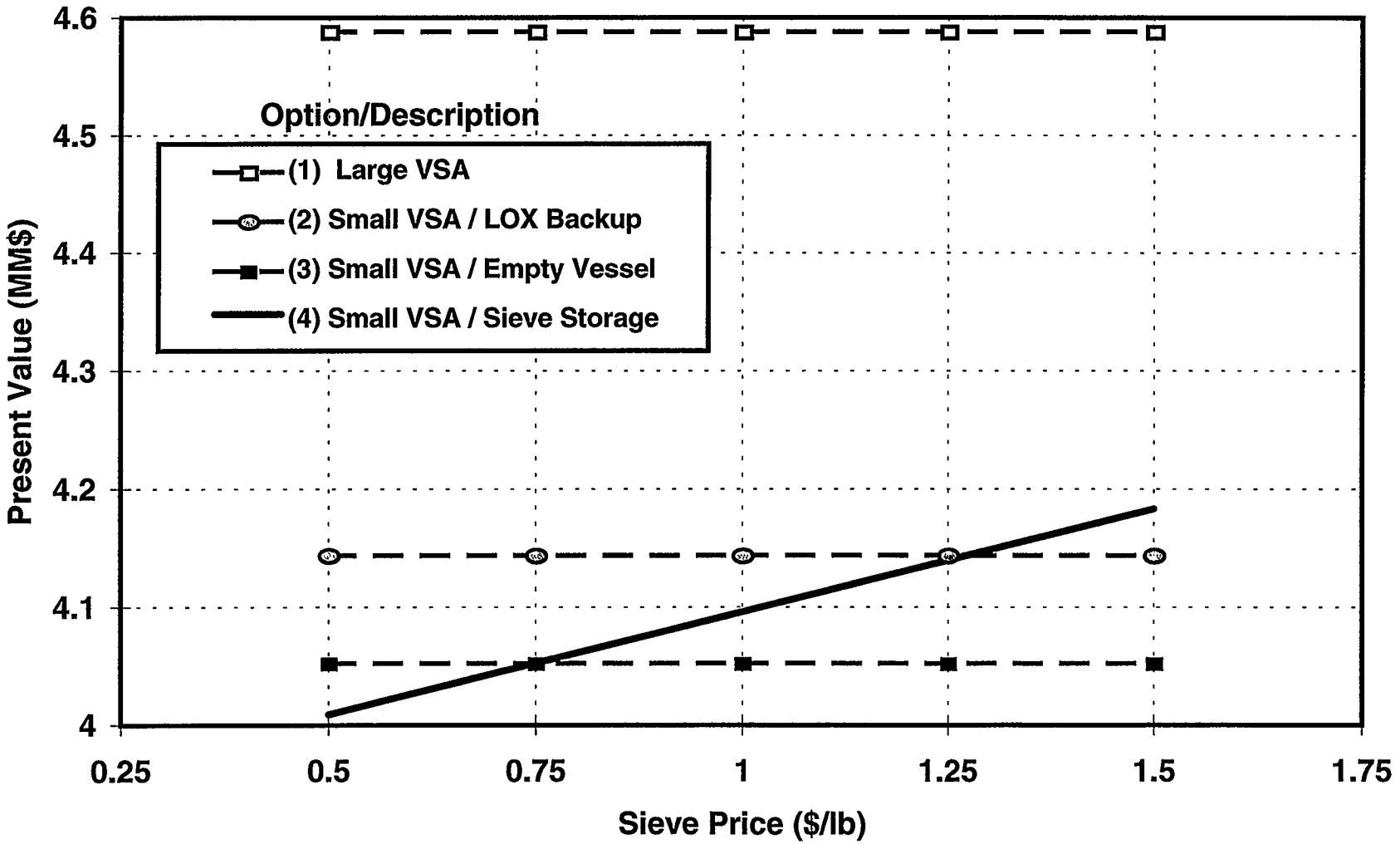

Figure 5-10. VSA O2 Storage Economic Decision Model Results
O2 Usage Cycle: 47 stpd @ 4 hours, 27 stpd @ 4 hours
LOX price = $0.25/100 scf

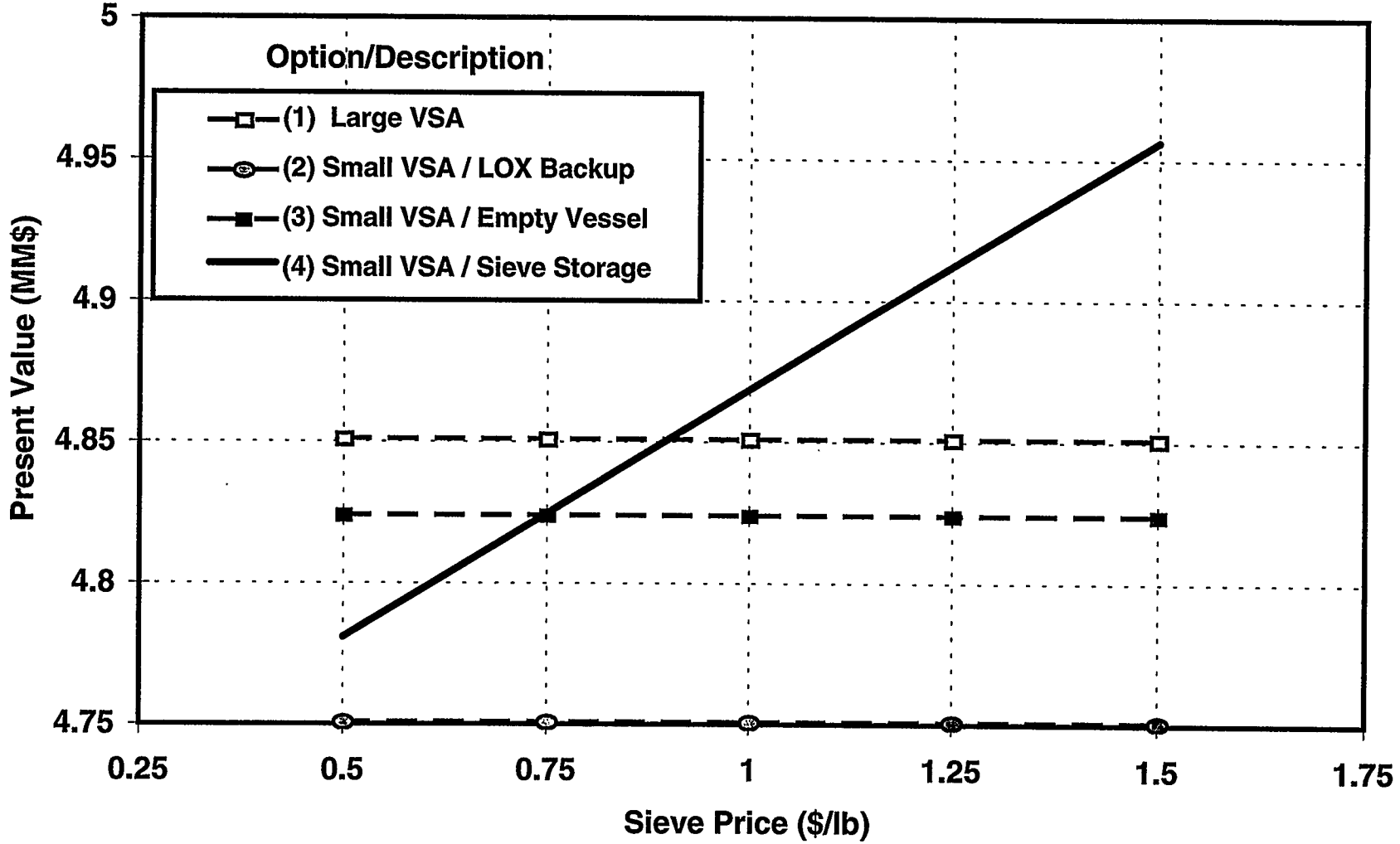

Figure 5-11. VSA O2 Storage Economic Decision Model Results
O2 Usage Cycle: 47 stpd @ 4 hours, 27 stpd @ 4 hours
LOX price = $0.30/100 scf

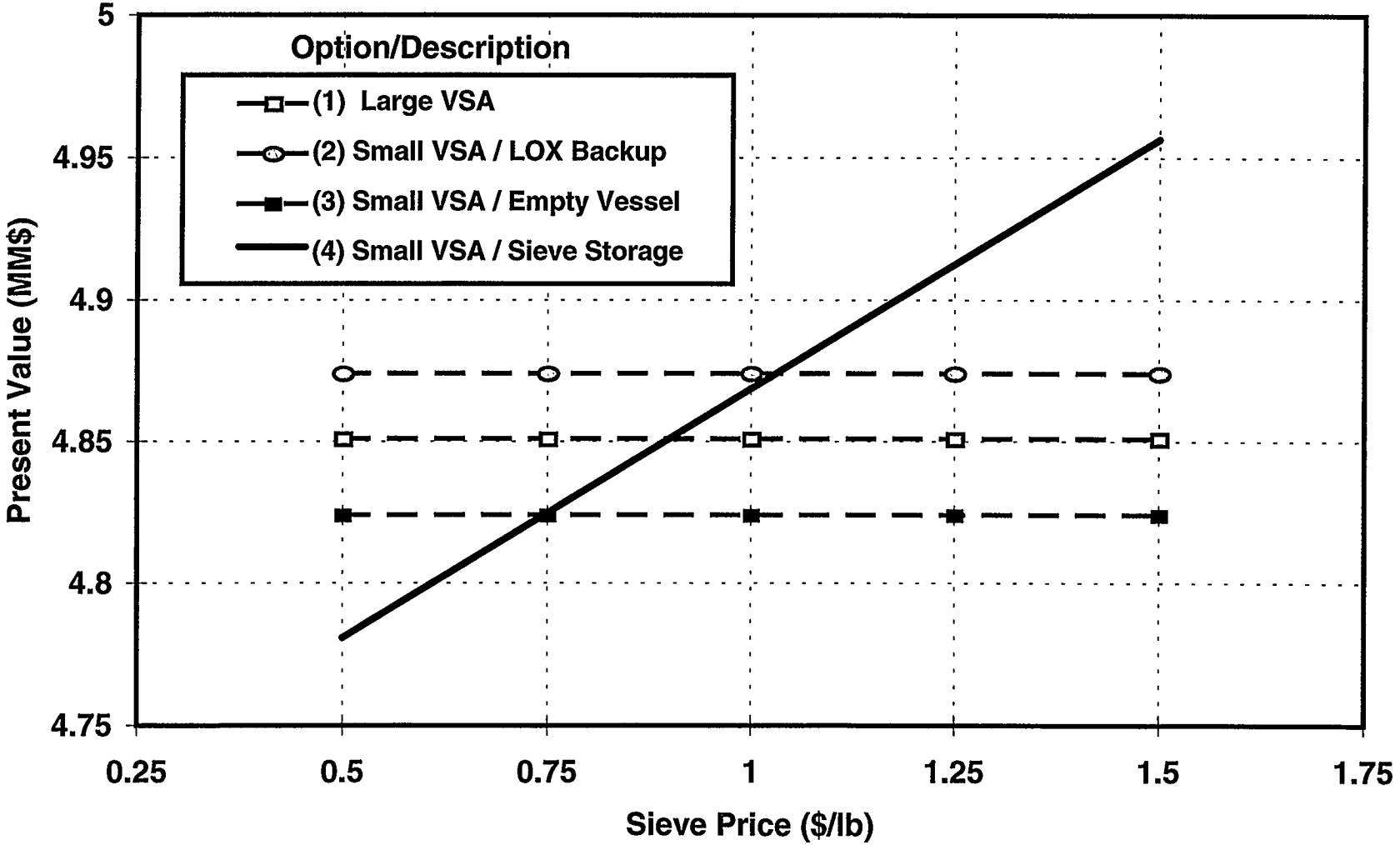

Figure 5-12. Cost of Combined Sieve-Storage with LOX Backup

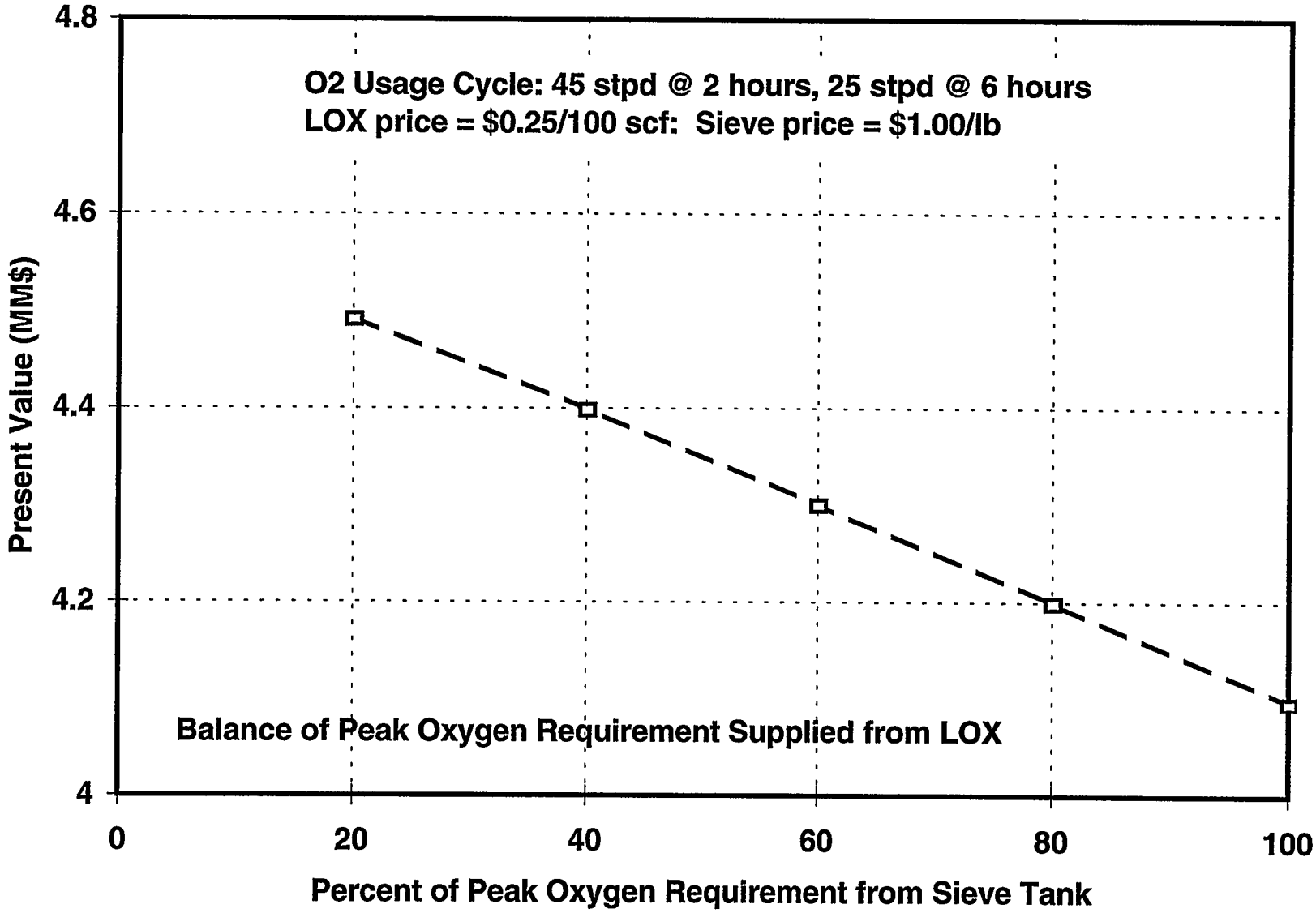

particular fraction of peak oxygen requirement specified. The assumed sieve and LOX prices were $1.00/lb and $0.25/100 scf, respectively, while the oxygen usage pattern was the same as used in Figures 5-8 and 5-9. Results indicate a 10 percent increase in present value (i.e., cost) of this option as tank usage is decreased from 100 to 20 percent of the total peak oxygen requirement. This suggests that sieve-assisted storage is most viable (economically) when it is designed for supplying most or all of the peak oxygen requirement.

Summary of VSA O_2 Storage Economic Decision Model Calculations

Model calculations showed that the economic viability of sieve-assisted storage, as an option for supplying the peak oxygen requirement of an on-site O_2 VSA, is sensitive to factors such as sieve price, price of backup LOX, oxygen usage pattern and design philosophy (i.e., storage of all or part of peak requirement). Conditions that favor using sieve-assisted storage are low sieve price, high LOX price and designing the tank to supply the full peak oxygen requirement. Results showed that, under the most favorable conditions examined herein for implementing sieve storage, the sieve price must be less than $0.75/lb in order for this option to be economically attractive. Even so, model results illustrated that relatively small variations in oxygen usage pattern can significantly alter O_2 storage economics, thereby reducing the viability of the sieve storage option.

Section 6
Summary

Low NOx Combustion System

A novel, low-NOx, air-oxy-fuel burner technology for secondary aluminum melting has been developed under this project. Successful, long-term operation of this technology has been demonstrated in furnace #8 of Wabash Aluminum Alloy's Syracuse, N.Y. plant. The burner incorporates staged injection of a primary, high-purity oxidizer and secondary, low-purity oxidizer and utilizes a unique flow passage design that enhances recirculation of furnace gases into the burner primary combustion zone. These features lead to a long, robust, highly radiant flame with low NOx emissions, high melting capacity and high energy efficiency.

NOx Emissions

Laboratory and field measurements showed burner NOx emissions to be affected by details of the burner design, variations in oxidizer purity and burner operating conditions. When compared to the AOF burner technology in service at the host furnace prior to the start of the project, the new burner technology lowered NOx emissions by more than 80 percent at comparable conditions of burner oxygen enrichment and stoichiometry. Moreover, emissions produced by the new burner technology at several operating conditions were shown to comply with the stringent regulations for both NOx and CO promulgated by Southern California's SCAQMD. Achieving this target had been one of the primary technical objectives of the project.

A field trial was conducted in which variations were made in the purity of the burner's primary and secondary oxidizers by blending nitrogen into streams of pure oxygen and air. Results showed very little change in NOx emissions when the primary oxidizer purity was lowered from 90 to 78 percent, suggesting that operating an O_2 VSA in a high-capacity, low-purity mode with the new burner technology would not result in a significant NOx increase. Results for the secondary oxidizer showed slight reductions in NOx when the purity was reduced from 20.9 percent (air) to 17-18 percent. This implies the possibility of utilizing the low-purity VSA vent stream to further reduce NOx emissions with the new burner technology.

Melting Capacity and Energy Efficiency

The melting capacity and energy efficiency of the new burner technology was evaluated during field tests at the host furnace. Specific energy usage during the melt cycle was shown to vary inversely with scrap charge rate. Peak scrap charge rates in excess of 13,000 lb/hr were achieved, while specific energy usage at these levels was below 1300 Btu/lb aluminum. When extrapolated to complete cycle performance, including both charging/melting and holding/tapping, these performance figures translated into maximum furnace capacity in excess of 210,000 lb/day and optimal specific energy usage at or below 1400 Btu/lb. The capacity target for the new burner technology was 203,000 lb/day, which is a 30 percent capacity increase relative to historic air-fuel operation at the furnace. The efficiency goal for the new burner technology was approximately 1600 Btu/lb, which was the level achieved at the host site with the pre-development AOF technology. Hence, both the melting capacity and the energy efficiency objectives for the new burner technology were met.

Results of CFD Modeling

A CFD model was developed to analyze and compare the characteristics of air-fuel, air-oxy-fuel and oxy-fuel combustion within the host furnace. Model predictions indicate the peak flame temperature with the AOF burner technology operating at 35 percent oxygen enrichment was much closer to that attained with OF technology than in the AF case. This suggested that much of the capacity increase to be derived from oxygen enhancement could be realized with relatively low levels of oxygen enrichment. With respect to refractory temperatures, the model predicted maximum levels in excess of material limits during oxy-fuel furnace operation. This signified that firing rates would have to be lowered in order to avoid excessive refractory wear. Finally, predictions of the oxygen concentration above the aluminum melt were lowest for the air-oxy-fuel case, indicating a potential for improved furnace yield with this OEC technology.

Reverb Furnace Economics

An economic model was developed to systematically assess the effects of combustion system performance, oxygen price and other capital and operating expenses on the overall profitability of reverb furnace operation. Sensitivity calculations performed with the model indicated that melt capacity and furnace yield are the two most important furnace parameters. An analysis was then carried out to compare economics of base air-fuel operation in Wabash furnace #8 with retrofit applications of air-oxy-fuel and oxy-fuel combustion technology. Model results showed strong gains in operating profit for OEC (both AOF and OF) relative to air-fuel technology over the entire input range of oxygen price and combustion system performance. The outcome of the comparison between air-oxy-fuel and oxy-fuel technology was, by contrast, dependent on specific values assumed for productivity and furnace yield. Assuming equal furnace yields and furnace productivity, which was +25 percent (relative to air-fuel) for AOF and +30 percent for OF, air-oxy-fuel was found to be more profitable than oxy-fuel technology when oxygen pricing was above $0.30/100 scf. However, for cases in which AOF productivity was equal to OF, or furnace yield of OF was reduced by 0.5 percent, air-oxy-fuel technology was more profitable than oxy-fuel over the entire range of oxygen pricing.

Integrated VSA Oxygen Supply with Sieve-Assisted Storage

Operation and Performance of Sieve-Assisted Storage System

An on-site VSA was installed at the host site to supply combustion oxygen to several operating furnaces. The VSA was sized for 40 stpd of contained oxygen, which was less than the maximum plant demand. The supply system was therefore equipped with an adsorbent (sieve)-filled vessel for storing excess VSA product during periods of low oxygen demand, and for subsequently supplying the peak oxygen requirement when furnace demand exceeded VSA output. A LOX backup supply was also tied into the oxygen supply pipeline.

Tests were conducted to determine the oxygen capacity of the storage vessel. Results indicated the capacity was approximately 2.5 times that of an empty tank of the same volume operating between the same minimum and maximum pressures. Additional tests were carried out to evaluate the effectiveness of the sieve storage system in meeting the peak oxygen requirement of the furnace. This was accomplished by measuring backup LOX consumption, VSA output and

furnace oxygen demand during extended operating periods with and without the sieve tank in service. Analysis of test data showed backup LOX consumption was reduced by 33 percent through the use of the sieve tank.

VSA Oxygen Supply Economics

A model was developed to assist in selecting the most cost-effective method of supplying on-site generated oxygen from a VSA to the end user. Four options were evaluated: **1)** sizing the VSA output to meet the maximum oxygen demand, or sizing the VSA to meet the average oxygen demand; and **2)** using a backup LOX supply, **3)** an empty storage vessel, or **4)** a sieve-filled storage vessel for meeting peak oxygen requirements. Model inputs included capital and operating costs for the various systems, sieve and LOX prices and oxygen demand profile. Economic predictions were sensitive to the assumed oxygen demand profile. Two profiles that approximated behavior observed at the host site were tested. With a LOX price of $0.30/100 scf, model results indicated that the sieve price would have to be less than $0.75/lb for the sieve-assisted storage system to be the lowest cost option. A sieve price below $0.50/lb would be required if LOX was available at $0.25/100 scf. Current sieve price was estimated to be in the $1.00 to $1.50 per pound range. These results assume that, with option 4, all of the peak oxygen requirement would be supplied from the sieve tank. Additional calculations showed that the economics of sieve storage become progressively less favorable as more LOX is required to augment the oxygen capacity of the storage vessel.

References

1. Baukal, CJ.E., Eleazer, P.B. and Farmer, L.K, "Basis for Enhancing Combustion by Oxygen Enrichment," *Industrial Heating*, February 22, 1992.

2. Becker, J.S., Heffron, J.F., Hewertson, R.J., and Riley, E.K., "Advanced Non-Ferrous Scrap Melter," Proceedings of the 1997 Minerals, Metals & Materials Society Conference, edited by B. Mishra, pp. 673-688.

3. Beer, J.M., and Chigier, N.A., *Combustion Aerodynamics*, Halsted Press Division, John Wiley & Sons, Inc., New York, 1972.

APPENDIX 1

COMBUSTION MEASUREMENTS IN AN INDUSTRIAL GAS-FIRED ALUMINUM RECYCLING FURNACE: PRE-REBUILD RESULTS

by

B.W. Webb and M.Q. McQuay
Mechanical Engineering Department, 242 CB
Brigham Young University
Provo, UT 84602

Phone: (801) 378-6543
Fax: (801) 378-2138
Email: webb@byu.edu

submitted to
Dr. Charles E. Baukal
Air Products and Chemicals Inc.
December 15, 1997

EXECUTIVE SUMMARY

The objective of the work reported here was to characterized the pre-rebuilt combustion performance in the natural-gas-fired, partially oxygen-enriched, aluminum recycling furnace (Furnace 8) operated by Roth Brothers Smelting Corporation in Syracuse, New York. Measurements of gas temperature and species concentration (O_2, CO, NO, and CO_2) were made in the exhaust of the furnace. Local gas temperature, species concentration, incident wall radiant flux and furnace wall temperature measurements were also made in the combustion space. Finally, limited stack measurements were also made in the other three furnaces in operation at Roth Brothers (Furnaces 6, 7, and 9).

In Furnace 8, average exhaust gas temperatures varied between a low of 1558_F (1121K) and a high of 2281_F (1523K) for the conditions of low-fire and highest oxygen enrichment, respectively. It was observed that changes in furnace stoichiometry were important in controlling the overall NO production. The highest NO level (3509 ppmvd) was observed for the normal high-fire condition when the temperatures were high in the furnace and there was enough excess air available (more than 10% excess). A significant reduction in NO production (from 3509 to 1390 ppmvd) was observed when the stoichiometry was reduced (from 2.22 to 2.01). Values of CO concentrations of 10,820 and 7700 ppmvd were measured in the stack with oxygen excess values of 0.5 and 5%, respectively.

Temperatures in the combustion space very quickly reached the service ceiling of the type S thermocouple used in the suction pyrometer (3500_F), which prevented full profiles in all access holes available. Oxygen concentration profiles indicate that typically early in the centerline of the jet flames the concentrations are higher. NO profiles in the combustion space indicate high concentrations in locations where the oxygen concentrations and gas temperatures were high. Peak values of 8000 ppmvd were detected in the flame region. CO concentrations reached values as high as 10 vol% earlier in the flame at the initial stages of combustion and CO_2 values were largest in locations where combustion is complete as indicated by the correspondingly low values of CO concentrations. Near-constant values of wall radiative heat fluxes were measured of 140.5 Btu/h/ft^2 (443 W/m^2).

Exhaust temperatures for Furnaces 6, 7, and 9 were about the same [average value of 1808_F (1260K)] for the three furnaces and the NO levels were low compared to the measured values in Furnace 8. CO concentration values were also negligible in the stack of these three furnaces.

INTRODUCTION

Significant progress has been made in the combustion process in large furnaces over the past two decades in reducing energy consumption and maximizing product yield. Nonetheless, escalating global competition and increasingly restrictive government regulations on pollutants in furnace effluents are prompting the examination of even more aggressive measures to increase combustion efficiency while reducing the impact of the combustion process on the environment. The objective of the work reported here was to characterize the pre-rebuilt combustion performance in the natural-gas-fired, partially oxygen-enriched, aluminum recycling furnace (Furnace 8) operated by Roth Brothers Smelting Corporation in Syracuse, New York. Measurements of gas temperature and species concentration (O_2, CO, NO, and CO_2) were made in the exhaust of the furnace. Gas temperature, species concentrations, wall incident radiant flux, and wall temperature were also measured in the combustion space through a specially designed wall insert placed in an existing side door used for dross removal during the normal operation of the furnace. Stack measurements in this furnace included five operating conditions, *i.e.*, normal high and low firing, high fire with only air as the oxidizing agent, high fire low stoichiometry, and high fire with the highest possible oxygen enrichment (without requiring any manual valve adjustments). Combustion space measurements were made only for the baseline, high-fire operating condition. Limited stack measurements were also made in the other three furnaces in operation at Roth Brothers (Furnaces 6, 7, and 9). These measurements are in support of a DOE-funded project to Air Products and Chemicals, Inc. and Roth Brothers aimed at the development of oxygen-enriched, advanced technology for increased furnace yield and reduced pollutants. The measurements reported here for the pre-rebuild tests in Furnace 8 will be repeated after the new technology is installed providing a means to document the impact of the new technology on furnace performance and emissions. Acknowledgment is made of the support of Roth Brothers during the test preparation and tests, as well as the Air Products personnel.

FURNACE DESCRIPTION

A schematic of the Roth Brothers Smelting Corporation reverberatory aluminum melting Furnace 8 can be seen in Fig. 1. The furnace is generally of rectangular cross-section. The combustion space

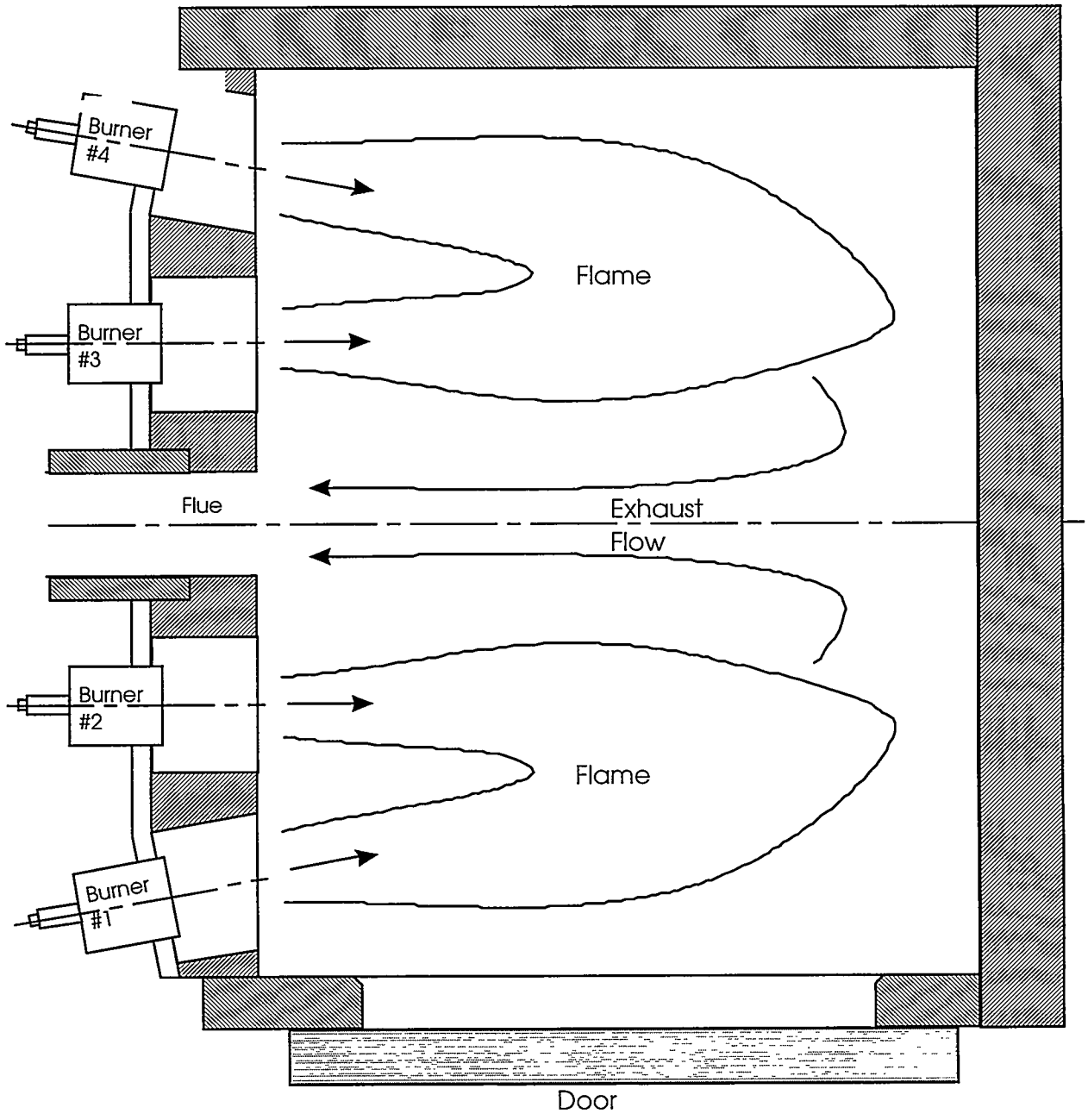

Figure 1. Top-view schematic drawing of the natural gas-fired aluminum melting furnace illustrating the complex reacting flow field including the four burners and exhaust port.

is approximately 49.5 in (1.26 m) high from the melt line (fully charged) to the roof, 12 ft (3.66 m) wide, and 17.5 ft (5.33 m) from front to back. Two Air Products EZ-Fire™ oxygen enrichment burners are located on either side of the exhaust flue. The outer burners (1 and 4) are vectored toward the furnace symmetry line at a 7° angle, while the inner burners (2 and 3) are fired parallel to the symmetry line. All four burners are vectored downward at a 10° angle. The burners are comprised of a central core oxygen/fuel burner, surrounded by an annular air/fuel burner. During high-fire operation, both central and annular burners operate simultaneously in an overall oxygen-enriched combustion mode. When furnace temperatures exceed desired levels or while tapping of the molten aluminum occurs, the furnace is operated in low-fire mode, utilizing only the annular air/fuel burner. A large door, which can be opened for dross removal, forms the front wall of the furnace parallel to the furnace symmetry line.

A furnace wall insert was constructed by Roth Brothers personnel to provide access to the combustion space of Furnace 8 during operation. The insert was constructed of mild steel with five 4 in (10 cm) diameter pipes welded to the wall through which water-cooled probes could be inserted for furnace probing. The insert was centered in the front wall of the furnace, and the five access holes were spaced at 19.5 in (0.5 m) intervals. The flame-exposed face of the insert was wrapped in high-temperature insulation to prevent heat loss from the furnace while the insert was in place. The furnace door was lifted, the insert was placed on the furnace sill, and the door was lowered onto the insert until a relatively tight seal was achieved. The clearance gap between the wall insert and the furnace, as well as unused access holes were plugged with high temperature blanket insulation. Figure 2 shows the position of the wall insert and probe locations relative to the furnace geometry and burner vectoring. The figure is drawn to scale to illustrate the probing locations relative to the anticipated flame.

Effluent species concentration and gas temperature measurements were made in the stack of all four furnaces. These measurements were made by inserting the water-cooled probes through access holes in the refractory flue where available (Furnaces 7, 8, and 9). No access hole was available in the flue of Furnace 6, so the probes were inserted through the top of the flue for measurement.

Fuel (natural gas) flow rates were measured for the oxygen/fuel and air/fuel central and annular segments, respectively, of each burner. The air and oxygen flow rates were metered by the plant.

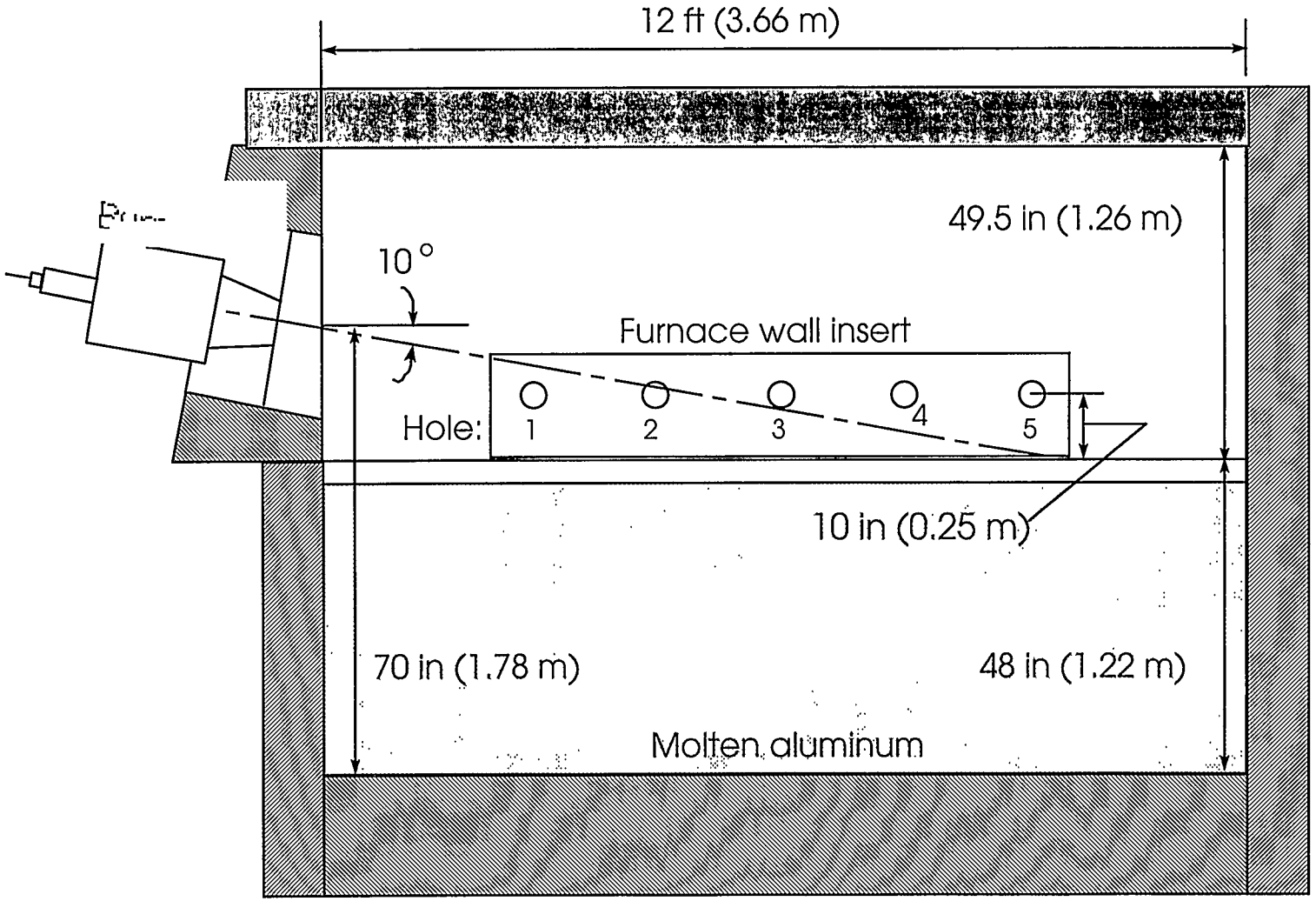

Figure 2. Side-view schematic of the wall insert and probe locations relative to the furnace geometry and furnace vectoring.

These data enabled the calculation of the overall furnace stoichiometry and the level of oxygen enrichment. Stoichiometry is defined here as the total oxygen volume flow through the burners divided by the total fuel flow through the burners. A ratio of 2 is approximately stoichiometric, while less than 2 is fuel-rich and greater than 2 is fuel-lean. Excess air is then calculated as (stoichiometry - 2)/2 × 100%. The overall oxygen enrichment is defined as the total oxygen volume flow through the burners divided by the total volume of air plus oxygen through the burners. An enrichment of 21% is air/fuel combustion, while an enrichment of 100% is oxygen/fuel combustion. Intermediate values represent partial oxygen enrichment.

INSTRUMENTATION AND EXPERIMENTAL PROCEDURE

Gas Velocity

A straight, water-cooled, stainless steel pitot tube was used to measure gas velocities. The instrument consisted of a 0.875 in (22.2 mm) outside diameter, 9.8 ft (3 m) long, water-cooled annular tube with two 0.125 in (3.2 mm) outside diameter tubes running lengthwise through the probe to pressure taps at the end of the probe, as shown in Fig. 3. The pressure taps were located 2 in (5.1 cm) from the end of the probe (two probe diameters) and spaced circumferentially 70° apart. The pressure taps were connected to a lightweight, differential pressure transducer. The transducer produced a voltage proportional to the differential pressure which was measured by a hand-held voltmeter capable of averaging the incoming signal.

Since the probe was not of conventional design, it was calibrated against a standard pitot tube and manometer in a wind tunnel at Brigham Young University. The flow in the wind tunnel was varied through the pressure differential range corresponding to that anticipated in the furnace. From the measured voltage and pressure differentials for both standard pitot tube and velocity probe, a calibration curve was determined for the probe.

Due to the very high concentration of water vapor in the combustion gases there was significant condensation on the velocity probe. This occurred both in the furnace flue and the combustion space. The effect was that the static and stagnation holes were intermittently plugged by water condensation, making velocity measurements impossible.

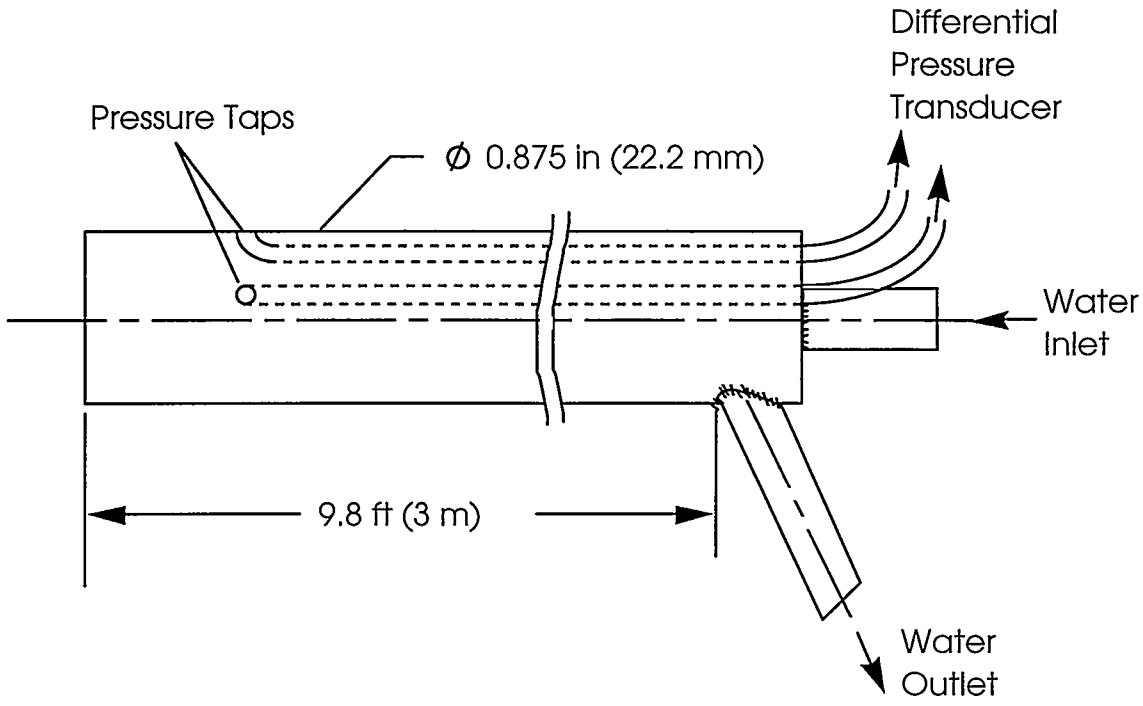

Figure 3. Schematic drawing of velocity probe.

Gas Concentration

Combustion gases were sampled by drawing them through a water-cooled, stainless steel collection probe using a four-head suction pump. As illustrated in Fig. 4, the probe was made of a 0.875 in (22.2 mm) outside diameter, 9.8 ft (3 m) long annular tube with a 0.375 in (9.5 mm) suction tube on the inside. The gases were rapidly quenched upon being drawn into the tube due to the high water-cooling rate in the surrounding annulus. The combustion gases were drawn through the probe and passed through two in-line condenser coils with integral water trap immersed in an ice bath. The two condenser coils eliminated the water from the gases prior to species concentration measurement by the gas analyzers.

The sampled gases were analyzed in real-time with four on-line gas analyzers, yielding measurements in either volume percent (vol%) or parts per million on a dry basis (ppmvd): a Nova 301-BD infrared analyzer for CO_2, two Land Combustion 6500 electrochemical analyzers for O_2, NO, and low (< 2000 ppmvd) and high (> 2000 ppmvd) CO, and a North American Enviromate electrochemi-

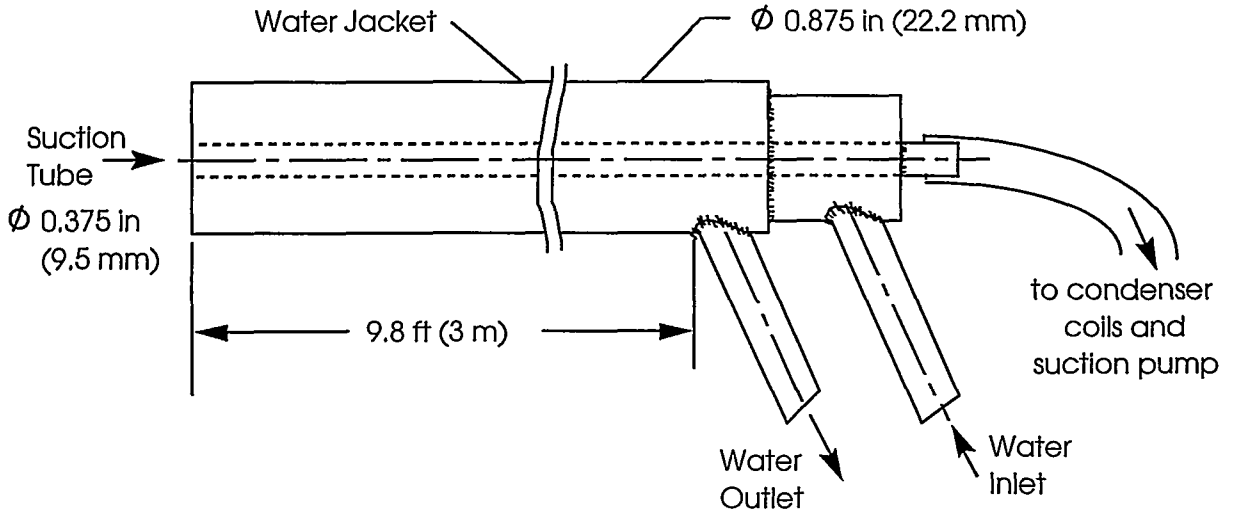

Figure 4. Schematic drawing of gas sampling probe.

cal analyzer for duplicate O_2, NO, and low CO measurements. The measurement limits for the four analyzers used are summarized in Table 1.

Table 1. Measurement limits for the on-line gas analyzers used.

	CO_2	O_2	CO (low)	CO (high)	NO
Nova	30 vol%	-	-	-	-
Land Combustion	-	21 vol%	2000 ppmvd	40,000 ppmvd	4000 ppmvd
North American	-	21 vol%	4000 ppmvd	-	4000 ppmvd

The accuracy reported for the CO_2 measurement is ±0.3%. The manufacturer-specified accuracy for both electrochemical analyzers was ±0.05% for O_2, and ±4% and ±100 ppmvd for CO measurements greater than and less than 2000 ppmvd, respectively.

All units were carefully calibrated before and after each test using research-grade calibration gas standards for O_2, CO_2, CO, and NO. The gas calibration standards were designed to provide instrument calibration over the range of values anticipated. Calibration gas concentrations were:

O_2	21 vol% (atmospheric)
CO:	900 ppmvd and 25,000 ppmvd (2.5 vol%)
CO_2:	10.0 vol%
NO:	900 ppmvd and 1800 ppmvd

Research grade pure nitrogen was also used to test for leakage in the gas sampling train.

Very good agreement was observed throughout the tests in the duplicate measurements for the different electrochemical analyzers. Response time for species measurements was estimated for the sample train used in the tests to be approximately 2 min for the CO_2 measurements, and 1 min for all other gas species.

Higher levels of gas species concentrations than anticipated were encountered in the combustion space. Preliminary concentration measurements revealed that, in several locations in the furnace, the concentrations exceeded the measurement limits of the analyzers. Therefore, a dilution system was used to make measurements in these locations possible. Research grade pure nitrogen was mixed with the sampled combustion gases in known proportions prior to on-line gas concentration analysis. The measured results were then scaled by the appropriate scaling factor using the known combustion gas and dilution nitrogen flow rates.

Gas Temperature

Gas temperatures were measured using a conventional, shielded, water-cooled suction pyrometers illustrated schematically in Fig. 5. The pyrometers were fabricated by the International Flame Research Foundation. A 1.7 in (43 mm) outside diameter, 4.25 ft (1.3 m) long, stainless steel water-cooled pyrometer with 4.7 in (12 cm) long double alumina radiation shields was used for the flue gas temperature measurements. A 2.5 in (63 mm) outside diameter, 13 ft (4 m) long, water-cooled pyrometer with 7 in (18 cm) long triple alumina radiation shields was used for the combustion space measurements. Gas suction for both small and large suction pyrometers was provided by a venturi pump that was attached to a 1 in (2.54 cm) pressure line at 80 psi (550 kPa). The thermocouple voltage was measured with a type-S, cold-junction compensator and amplifier using a hand-held voltmeter. A ninth-order polynomial was used to describe the thermocouple temperature as a function of the voltage output. The accuracy of the pyrometers is reported by the manufacturer to be ±8K when operated at the recommended gas flow rate. The pyrometers have a service temperature ceiling of approximately 3500_F (2200K).

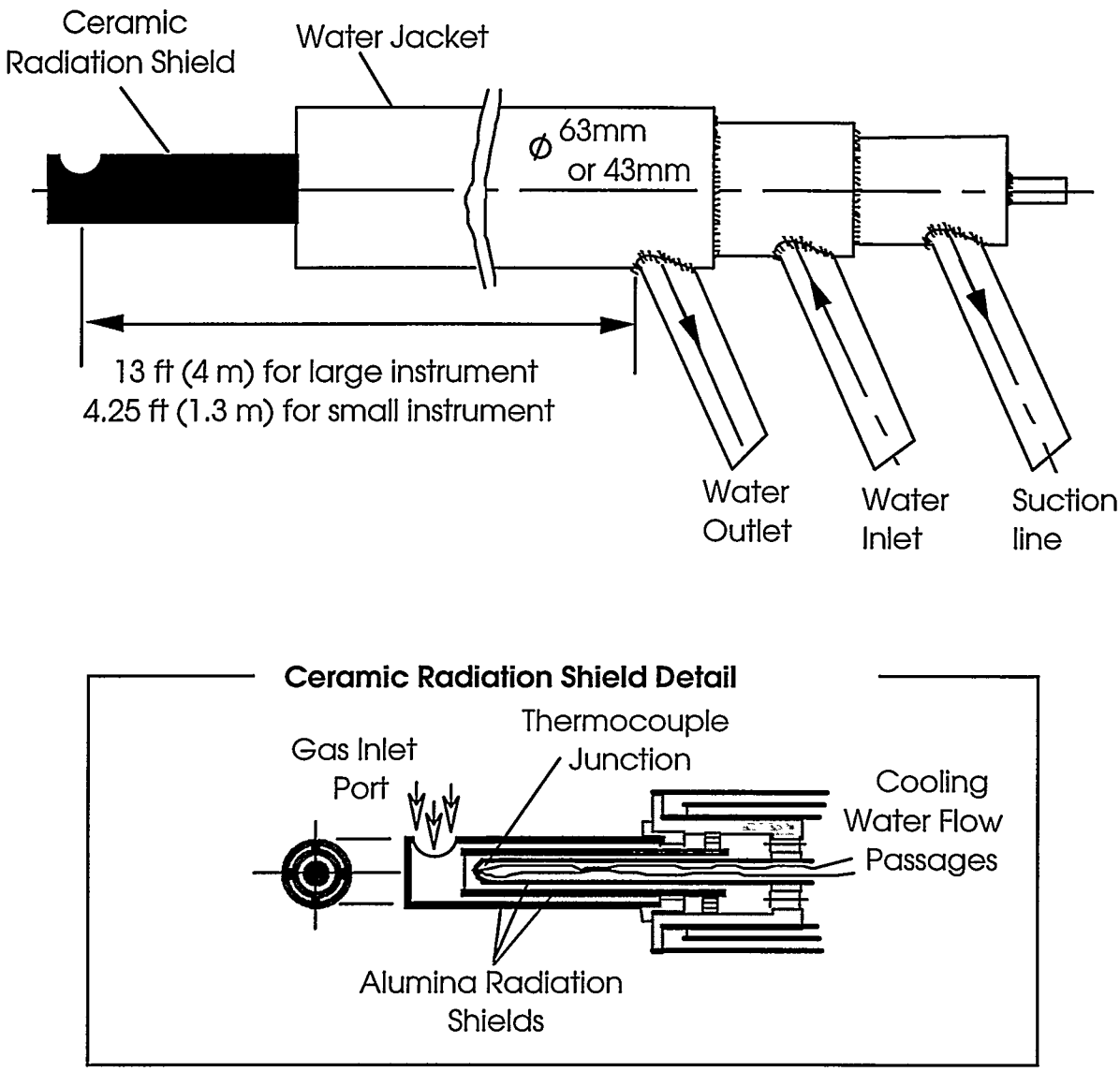

Figure 5. Schematic drawing of suction pyrometer.

Wall Temperature

Refractory wall temperature measurements were made using an Omega OS651 hand-held optical pyrometer with user-selectable emissivity. The instrument has a calibrated range of -20 to 2000_F with an accuracy of ±1%, with estimated accuracy of ±5% to 2400_F. These measurements were made immediately after the furnace door was lifted. Characterization of wall temperature drop during the time

interval for dross removal was also made by making wall temperature measurements after the door was opened, and after some time. An emissivity of 0.8 was assumed in the measurement.

Incident Radiant Flux

A calibrated, water-cooled, hemispherical ellipsoidal radiometer was used to characterize wall incident radiant heat flux at each of the access hole locations. This instrument, shown schematically in Fig. 6, was fabricated by the International Flame Research Foundation. The radiometer consisted of a stainless steel, water-cooled jacket, 1.7 in (43 mm) in diameter and 2 in (0.65 m) long, encasing an inner signal wire tube with the detector head mounted in one end, and cooling water and signal lead connections at the opposite end. The hollow ellipsoidal cavity detector has a 0.12 in (3 mm) diameter aperture at one focus, and a hemispherical sensing pellet at the other. The aperture and sensor head are centered at the foci of the ellipsoidal cavity, which is coated with a layer of polished gold. The ellipsoid is purged with dry nitrogen to prevent combustion products from fouling the highly reflective ellipsoidal cavity surface. The radiometer was calibrated by the manufacturer accurate to ±5% to radiant flux level of 95 Btu/hr/ft^2 (300 kW/m^2). Above this calibrated maximum the manufacturer indicates that the linear calibration curve can be extrapolated to calculate the radiative flux, although the extrapolated value would be below the true value of incident flux if not within the manufacturer-specified 5% error.

RESULTS AND DISCUSSION

Furnace 8 - Exhaust Measurements

Exhaust profile measurements of gas temperature and species concentrations were made for several furnace operating conditions. These settings included: (1) high-fire condition, which is the normal operating condition of the furnace; (2) low-fire condition, which is used when tapping the furnace or when the furnace roof temperature exceeds a predetermined maximum value; (3) high-fire, low-stoichiometry condition, selected to determine its impact on NO emissions; (4) high-fire, highest oxygen enrichment condition (without any manual valve changes); and (5) high-fire, air/fuel-burning condition. Each profile in these tests included six-point measurements in the approximately 4 ft (1.2 m) square cross-section stack. Velocity measurements were also attempted, but failed due to excessive water condensation on the stagnation and static pressure ports of the probe. The gas temperature and species concentration profiles were very flat in the stack (maximum variation from point to point

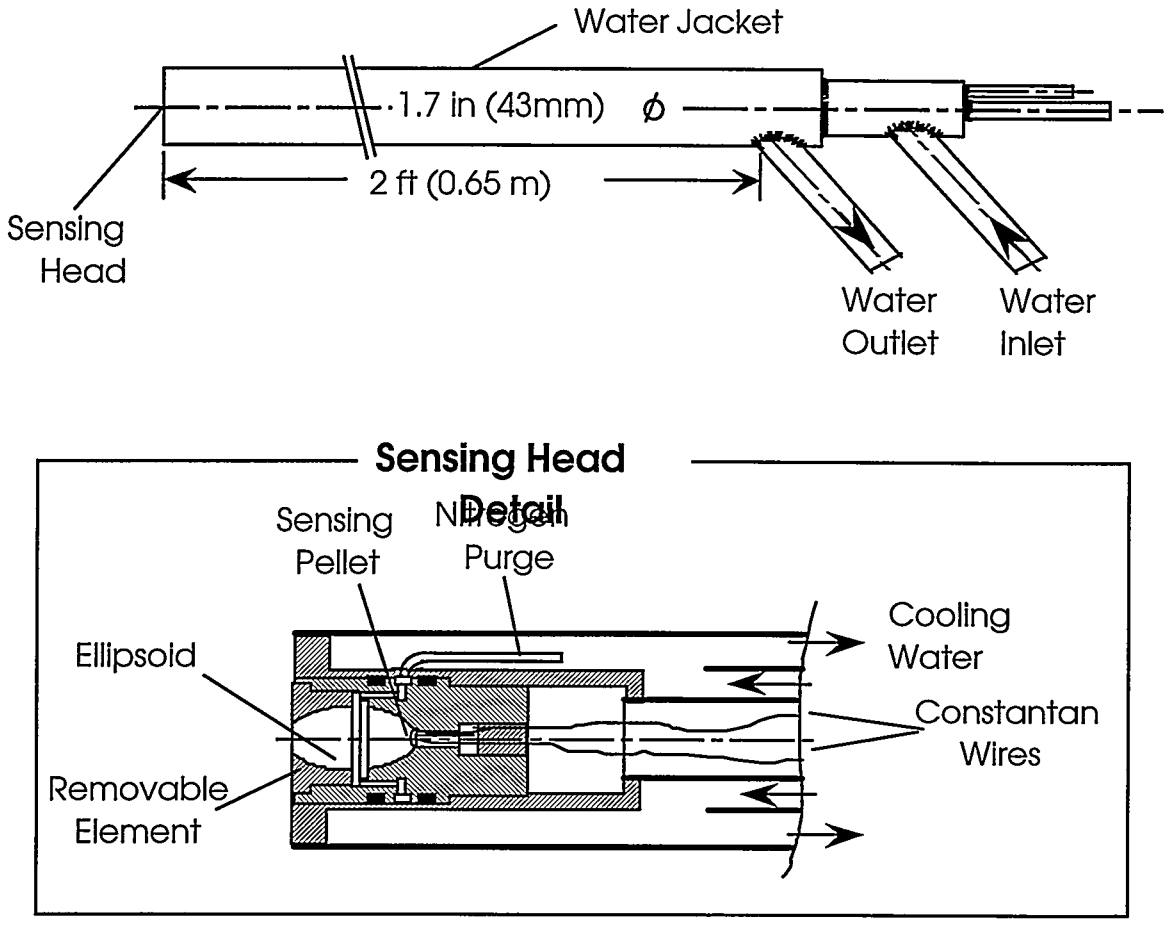

Figure 6. Schematic drawing of hemispherical, ellipsoidal radiometer

less than 5%); therefore, only averaged values are reported here. Table 2 presents a summary of the stack measurements in Furnace 8. It includes the furnace settings for methane, air, and oxygen flow rates in standard cubic feet per hour (SCFH) as obtained from the furnace operators. Based on these flow rates, the overall stoichiometry (the variable "Stoich" included in Table 2) and dry concentrations of oxygen and carbon dioxide were calculated. The last five columns in Table 2 are the average results for the dry concentrations of O_2, CO_2, NO, and CO, and gas temperature. NO concentrations are presented for the actual oxygen concentration (uncorrected for variations in oxygen concentration). Appendix A tabulates in spreadsheet format all raw data for the stack and combustion space measurements discussed in this report.

Table 2. Furnace operating conditions, gas temperature, and calculated and measured species concentrations in the stack of Furnace 8.

	Furnace Settings (SCFH)				Calc. Concentrations[a,b]		Measured Concentrations[a]				
	CH_4	Air	O_2	Stoich[c]	O_2 (vol%)	CO_2 (vol%)	O_2 (vol%)	CO_2 (vol%)	NO (ppmvd)	CO (ppmvd)	Temp (_F)
Normal H. F.	15,000	75,000	17,500	2.22	4.2	19.4	4.4	17.8	3509	5	2153
Normal L. F.	4400	77,000	0	3.68	10.2	6.1	9.1	6.8	48	3	1558
H. F., Low Stoic	16,970	79,000	17,500	2.01	0.2	21.3	0.1	19.5	1390	10,820	2132
Highest Enrichment	16,970	82,000	18,440	2.10	2.1	20.3	0.3	20.3	1775	7700	2281
H. A/F F.	14,900	174,000	0	2.45	4.3	9.4	2.2	11.0	53	13	2118

[a] Both calculated and measured concentrations are on a dry-basis and are uncorrected for varying O_2 concentration.

[b] Calculations are based on complete combustion for the furnace setting of methane, air, and oxygen air flows in SCFH.

[c] The variable Stoich (Stoichiometry) is the ratio of the total moles of oxygen (both from air and pure oxygen) to one mole of methane. Stoich = 2.0 is the value for stoichiometric combustion of methane.

Average exhaust gas temperatures varied between a low of 1558_F (1121K) and a high of 2281_F (1523K) for the conditions of low-fire and highest oxygen enrichment (35.4%), respectively. Furthermore, the differences in exhaust gas temperature for the high-fire conditions were not significant. With the exception of the highest enrichment case, average temperatures were about 2132_F (1440K) for the high-fire settings. It is also observed in Table 2 that changes in furnace stoichiometry were important in controlling the overall NO production. The highest NO level (3509 ppmvd) was observed for the normal high-fire condition when the temperatures were high in the furnace and there was enough excess air available (stoichiometry > 2.2). A significant reduction in NO production (from 3509 to 1390 ppmvd) was observed when the stoichiometry was reduced (from 2.22 to 2.01). Only a small increase in NO levels were observed for the case of the highest oxygen enrichment, which had an excess air of about 5% (Stoich = 2.1) based on the plant settings. It is believed that this NO level could be further reduced by optimizing the stoichiometry of the furnace. CO concentrations were negligible except for cases with minimum oxygen excess. Values of CO concentrations of 10,820 and 7700 ppmvd were measured with oxygen excess values of 0.5 and 5%, respectively.

Generally speaking, there was good agreement between the calculated and measured O_2 and CO_2 concentrations. The only discrepancies observed were for the highest-enrichment and air/fuel conditions, it being larger for the latter experimental condition where the CO_2 concentration agreed well, but for which the O_2 concentration was off by almost 100%. It should be noted here that (*i*) before and after each test the analyzers were calibrated following the procedure previously described in this report, and (*ii*) during all tests there was a very good agreement between the concentration values measured with the three analyzers used for all species. Therefore, the explanation for the differences in measured and calculated O_2 concentrations is related to the possible variation in operating conditions, particularly variations in air flow rates. For example, the high CO concentration value (7700 ppmvd) for a stoichiometry of 2.10 in a gaseous flame (highest enrichment condition) is unexpected. Based on the measured O_2 concentration for that case (0.3 vol%) and accepting the O_2 flow rate as being correct, the stoichiometry should be more nearly 2.0136 instead of the 2.10 calculated based on the furnace settings. This change in stoichiometry corresponds to a variation in air flow rate of less than 9%. If both the air and oxygen flow rates are assumed to have an error associated with them, the furnace stoichiometry should be 2.0146 based on the measured exhaust concentrations of O_2 and CO_2. It is important to point out here that, with

nearly stoichiometric combustion, there is a strong sensitivity of O_2 effluent concentration to errors in measurements of both air and oxygen flow rates. A summary of this sensitivity analysis is presented in Appendix B, where it is shown that an error of 5% in both air and oxygen flow rates can lead to errors in O_2 concentration (dry) of up to 200%, depending on stoichiometry. Moreover, the O_2 and CO_2 concentrations measured are consistent with respect to each other, given the possibility of an experimental error in measuring the supply flow rates of oxygen and air. For the case of the air/fuel firing, assuming that the methane and oxygen flow rates were correct, the measured O_2 concentration of 2.2 vol% would correspond to an air flow of 157,000 SCFH (an error of less than 10% in the reported operating setting of 174,000 SCFH), which would make the overall stoichiometry 2.21 with a corresponding CO_2 concentration of 10.5 vol% (11 vol% was the measured value).

Furnace 8 - Combustion Space Measurements

Detailed profiles of gas concentration, limited profiles of gas temperature, and wall incident radiant heat flux in the combustion space were also measured for the normal, high-fire operating condition. As explained before, these measurements were obtained through the access insert mounted in the furnace door as illustrated in Fig. 2. Figures 7 through 11 show the results for the profiles of gas temperature, O_2, NO, CO, and CO_2 concentrations, respectively. Included in each of these five figures is a top-view schematic (drawn to scale) of one half of the furnace showing the relative position of the profiles with respect to important features in the combustion space. All profiles of a given variable obtained for each of the five access holes are also included in individual plots in Appendix C (Figs. C.1-C.5). As one would expect, the flow structure is very complex in this highly three-dimensional combustion configuration. Interpretation of these experimental results can certainly be enhanced if accompanied by numerical simulations of the flow field in this furnace. In an attempt to aid in the understanding of this complex flow structure, Fig. 2 illustrates the probe locations relative to burner vectoring. Not only are all burners vectored downward by 10_, but the two exterior burners (burners 1 and 4) are also vectored towards the furnace centerline by 7_. A side view of the orientation of the burners with respect to the access insert has been presented in Fig. 2. The same problem of water

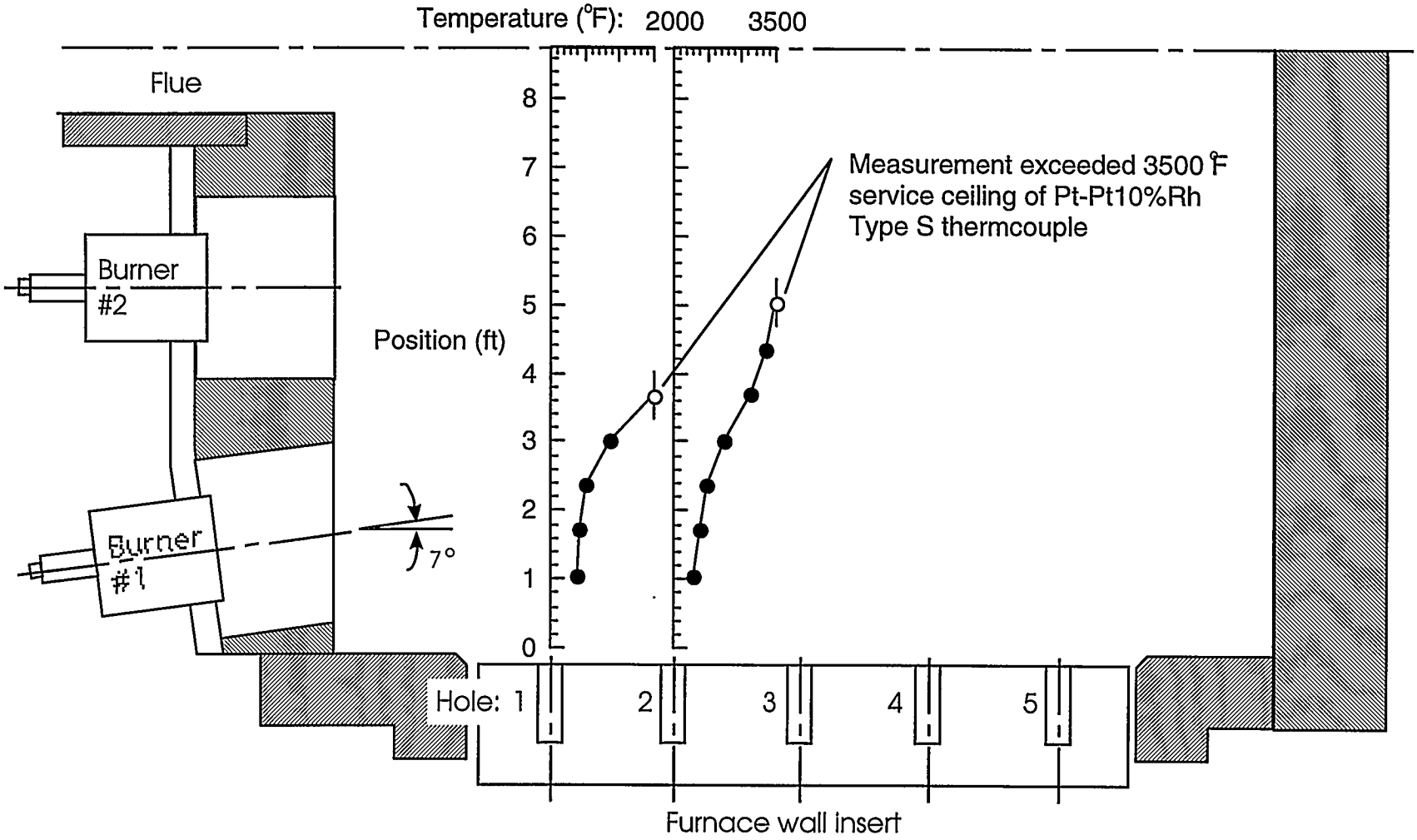

Figure 7. Measured temperature profiles in the combustion space of Furnace 8.

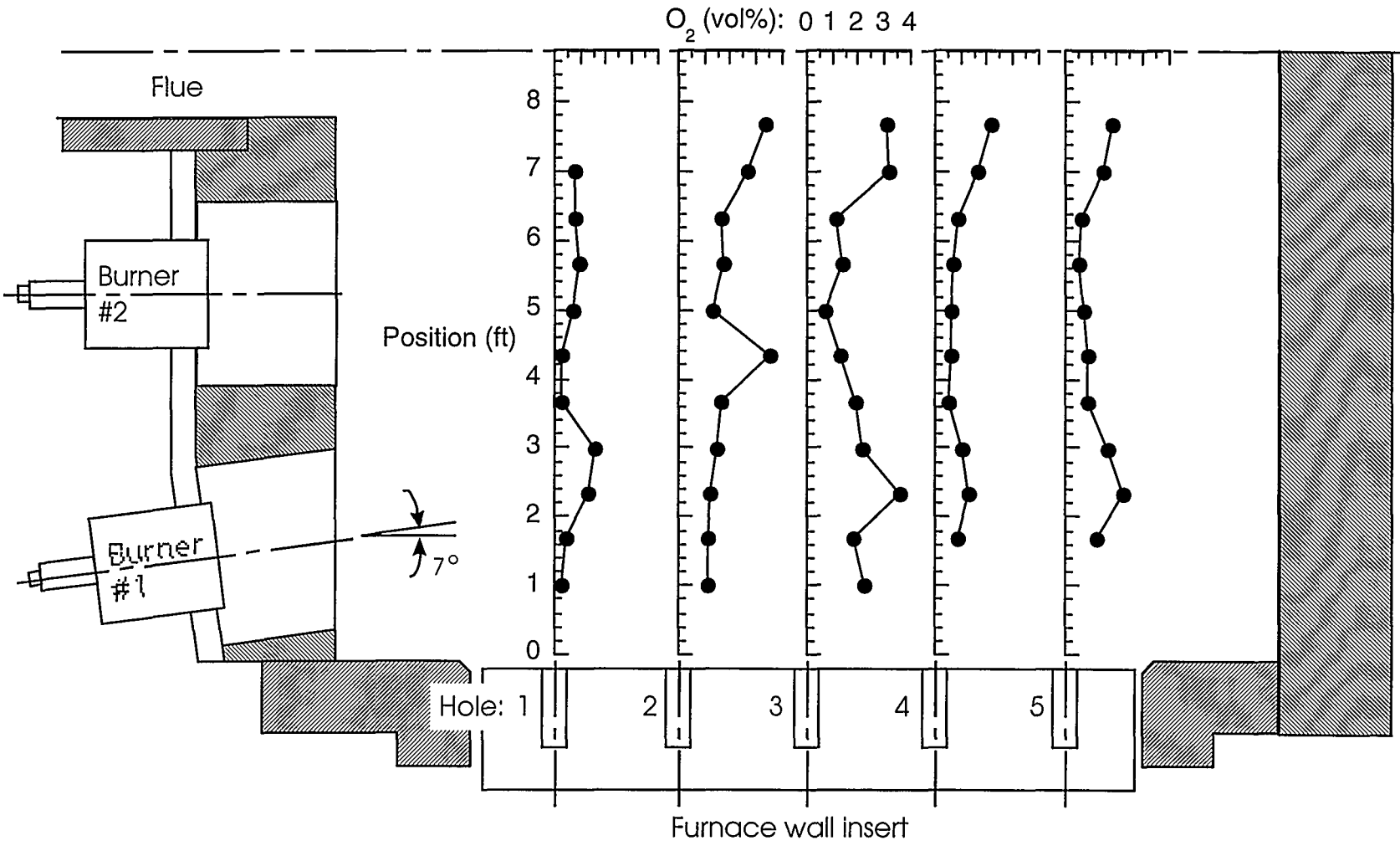

Figure 8. Measured oxygen (O_2) profiles in the combustion space of Furnace 8.

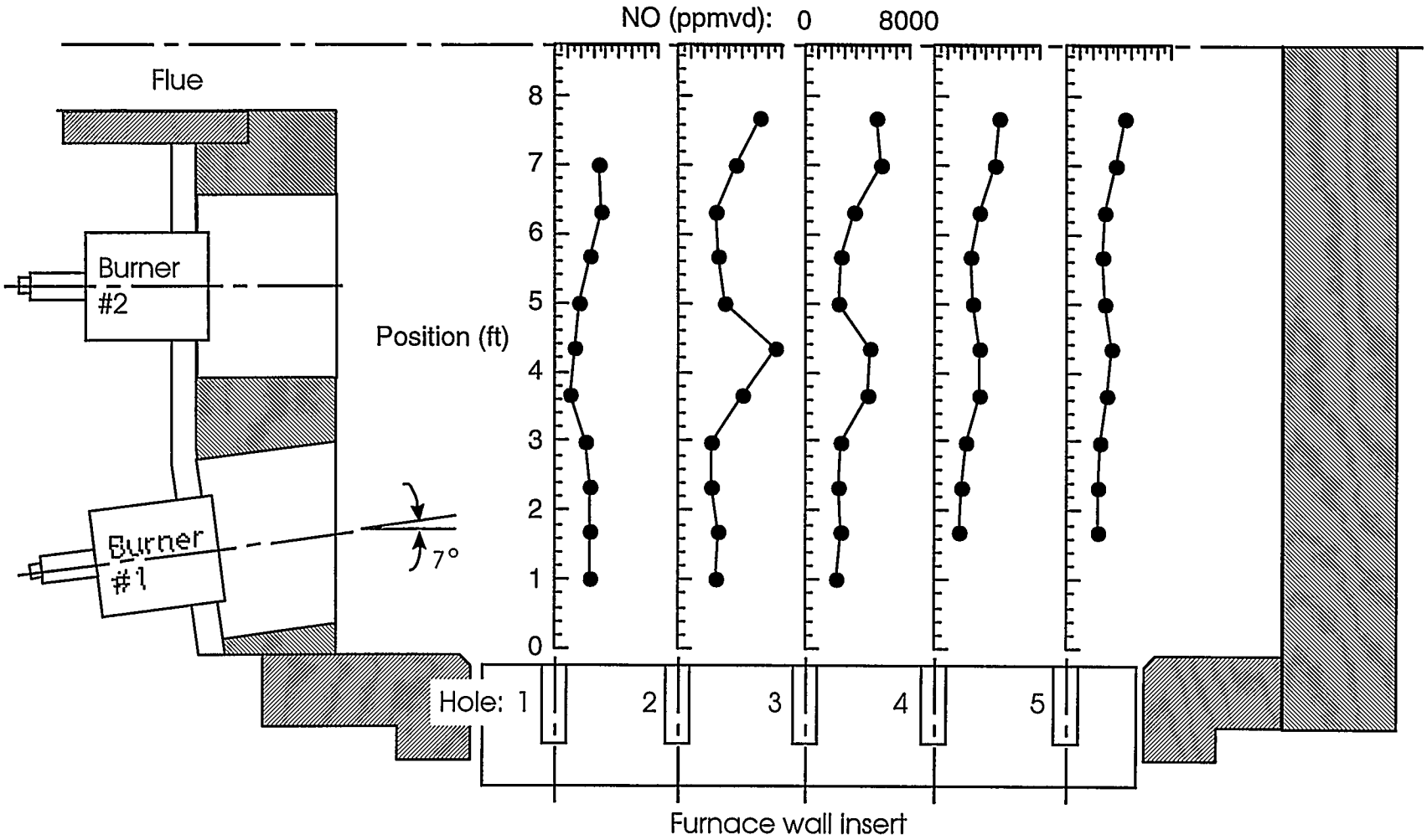

Figure 9. Measured nitrogen oxide (NO) profiles in the combustion space of Furnace 8. (Data are uncorrected for varying oxygen concentration.)

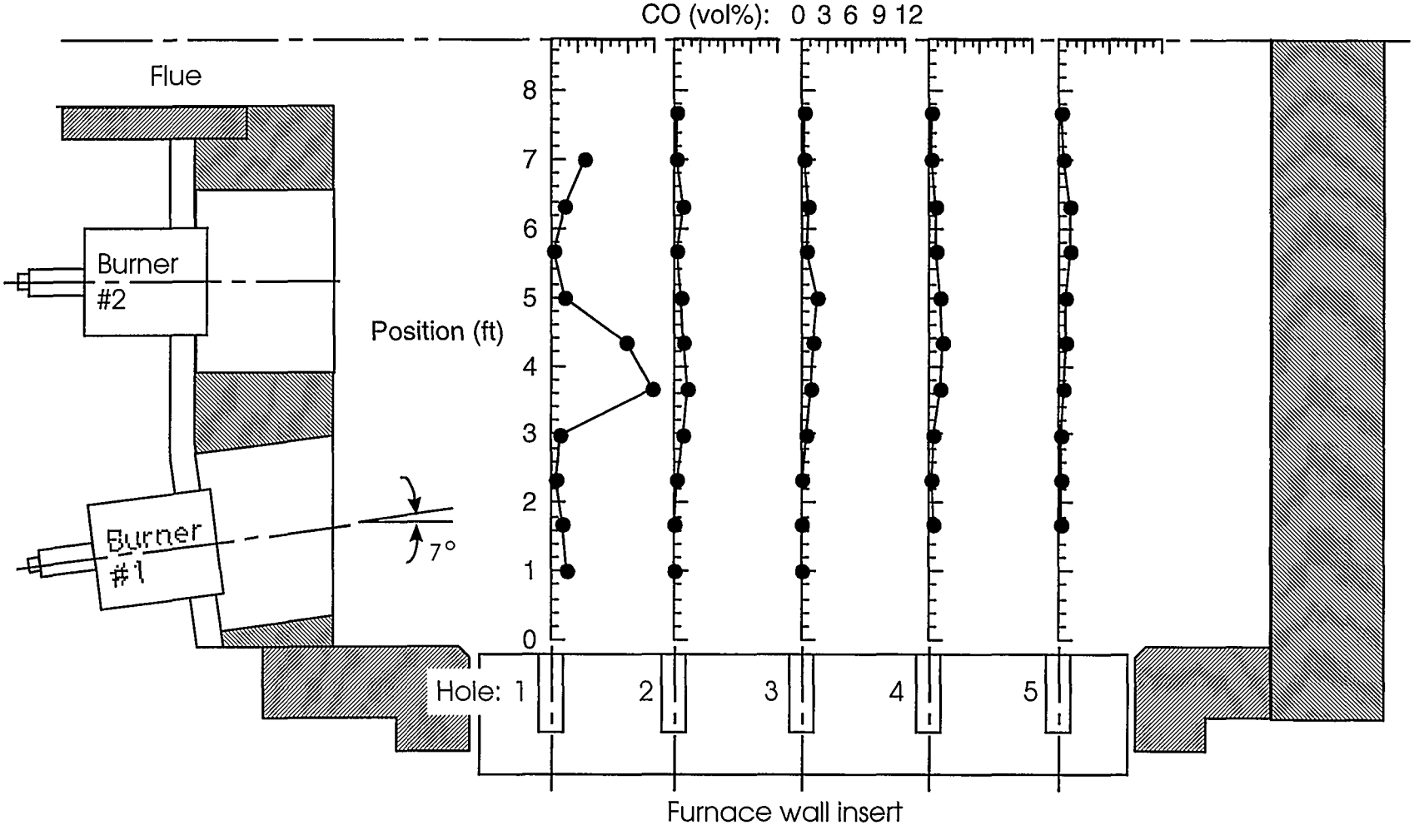

Figure 10. Measured carbon monoxide (CO) profiles in the combustion space of Furnace 8.

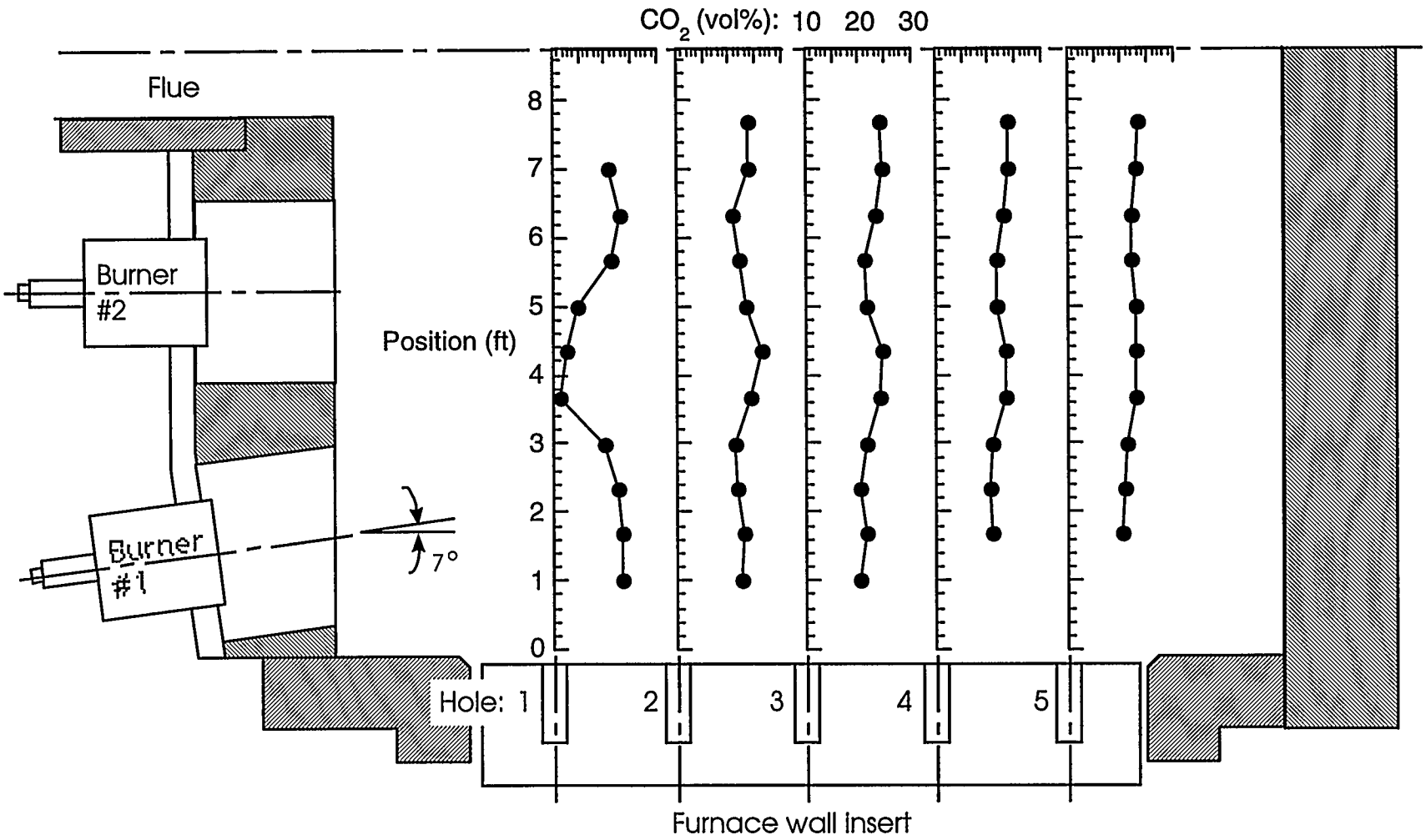

Figure 11. Measured carbon dioxide (CO_2) profiles in the combustion space of Furnace 8.

condensation in the velocity probe encountered in the stack measurements was also observed in the combustion space; therefore, velocity measurements were not possible there.

Temperatures in the combustion space very quickly reached the service ceiling of the type S thermocouple used in the suction pyrometer [3500_F (2200K)] as the probe moved in the direction of the flames as indicated by the large temperature gradients shown in Fig. 7. Typically, the gas temperature increased rather quickly from around 2240_F (1500K) to 3500_F (2200K) in regions close to the flame. Profiles at access holes 3, 4, and 5 were not possible because the high temperature environment in the final measurement position in hole 2 caused the ceramic radiation shields to melt and collapse, eventually fusing the tip and the thermocouple wire, making the suction pyrometer inoperable.

Wall temperatures were measured optically with a hand-held optical pyrometer assuming a furnace refractory emissivity of 0.8 during a period when the furnace door was open for dross removal. Immediately after opening the door the back wall was measured to be 2461_F (1623K). After 46 min the wall temperature in the same location had dropped to 2300_F (1533K).

The highest O_2 concentrations were observed in the profiles of holes 2 and 3, where the probe traversed oxygen-rich, unreacted streams in the flames (see Fig. 2). The quite distinct peaks in the O_2 concentration profiles maybe seen in Fig. 8 for hole 1 coinciding with burners 1 and 2, suggesting independent flame structures early in the reaction, which can be further complicated by the existence of a possible recirculation flow present below the burners. By hole 2, the flames appear to have merged. The oxygen concentrations in the combustion products are low (penetration distances 3 and 6 ft for holes 4 and 5). Although close to the exhaust flow at positions greater than 7 ft the oxygen concentrations were high (between 2 and 3.5 vol% for holes 2, 3, 4, and 5).

NO profiles (Fig. 9) indicate high concentrations in locations where the oxygen concentrations and gas temperatures were high. A peak value of 8000 ppmvd were detected in the flame region in hole 2. CO concentrations reached values as high as 12 vol% early in the flame during the initial stages of combustion (Fig. 10), and CO_2 values were largest in locations where combustion is complete (Fig. 11) as indicated by the correspondingly low values of CO concentrations. It is also interesting to note that of all species measured, CO_2 profiles exhibited the least spatial variation.

Wall radiant heat flux measurements through the five access holes are summarized in Table 3. The incident flux measured varied between 139 and 141 Btu/hr/ft^2 (438 and 446 W/m^2) with an average value of 140 Btu/hr/ft^2 (443 W/m^2).

Table 3. Measured incident radiant flux at the wall for each access hole.

Hole:	1	2	3	4	5
Inc. Rad. Flux, Btu/hr/ft^2 (W/m^2):	139 (438)	141 (444)	141 (446)	140 (441)	141 (446)

Furnace 6, 7, and 9 - Exhaust Measurements

Exhaust measurements of gas temperature and species concentrations were also made at the normal, high-fire operating conditions for Furnaces 6, 7, and 9. Table 4 presents a summary of the furnace operating conditions and stack measurements for these three furnaces. This table includes similar data as those already presented in Table 2. It should be noted here that the burners in Furnace 9 were not designed to support oxygen-enriched combustion. Exhaust temperatures were about the same [average value of 1800_F (1260K)] for the three furnaces and the NO levels were low compared to the measured values in Furnace 8. CO concentration values were also negligible with the exception of the measurements in Furnace 6. The measured NO concentration of 1081 ppmvd was lower than the three NO levels measured in Furnace 8. Closer examination of the raw data for Furnace 6 indicated a possibility that the CO_2 measurement was taken when the CO_2 analyzer had not yet reached a steady state value. The CO_2 concentration corresponding to the stoichiometry calculated based on the O_2 measured concentration (12.3 vol%) would be 28 vol% instead of the 11.8 vol% recorded in the raw data. Note also that for Furnace 7 the measured O_2 concentration (4 vol%) corresponds to an overall stoichiometry of 2.21, which is supported by the measured CO_2 concentration of 18.9 vol% and by the absence of CO in the stack.

CONCLUSIONS

The objective of the work reported here was to characterized the pre-rebuilt combustion performance in the natural-gas-fired, partially oxygen-enriched, aluminum recycling furnace (Furnace 8)

Table 4. Furnace operating conditions, gas temperature, and calculated and measured species concentrations in the stack of Furnaces 6, 7, and 9.

	Furnace Settings (SCFH)				Calc. Concentrations[a,b]		Measured Concentrations[a]				
	CH_4	Air	O_2	Stoich[c]	O_2 (vol%)	CO_2 (vol%)	O_2 (vol%)	CO_2 (vol%)	NO (ppmvd)	CO (ppmvd)	Temp (_F)
Furnace No. 9[d]											
Normal A/F H. F.	19,100	208,000	0	2.29	2.9	10.1	2.3	10.4	69	0	1844
Furnace No. 7											
Normal H. F.	14,250	47,000	16,000	1.82	0	17.5	4.0	18.9	753	0	1845
Normal L.F.	13,900	146,000	0	2.21	2.2	10.5	N/A	N/A	N/A	N/A	N/A
Furnace No. 6											
Normal H.F.	9210	32,000	17,250	2.60	13.8	23.2	12.3	[-][e]	1081	105	1743
Normal L.F.	11,500	121,000	0	2.21	2.2	10.5	N/A	N/A	N/A	N/A	N/A

[a] Both calculated and measured concentrations are on a dry-basis and are uncorrected for varying O_2 concentration.

[b] Calculations are based on complete combustion for the furnace setting of methane, air, and oxygen air flows in SCFH.

[c] The variable Stoich (Stoichiometry) is the ratio of the total moles of oxygen (both from air and pure oxygen) to one mole of methane. Stoich = 2.0 is the value for stoichiometric combustion of methane.

[d] The normal operating condition for Furnace No. 9 does not include any oxygen enrichment at the present time.

[e] This particular concentration is not reported here because the CO_2 analyzer had not reached steady state when the concentration values were recorded.

operated by Roth Brothers Smelting Corporation in Syracuse, New York. Measurements of gas temperature and species concentration (O_2, CO, NO, and CO_2) were made in the exhaust of the furnace. Gas temperature, species concentration, wall incident radiant heat flux, and furnace wall temperature were made in the combustion space through a specially designed wall insert placed in an existing side door used for dross removal during the normal operation of the furnace. Stack measurements in this furnace included five operating conditions, *i.e.*, normal high and low firing, high fire with only air as the oxidizing agent, high fire low stoichiometry, and high fire with the highest possible oxygen enrichment. Combustion space measurements were only made for the baseline, high-fire operating condition. Limited stack measurements were also made in the other three furnaces in operation at Roth Brothers (Furnaces 6, 7, and 9).

Average exhaust gas temperatures varied between a low of 1560_F (1121K) and a high of 2280_F (1523K) for the conditions of low fire and highest oxygen enrichment, respectively. Furthermore, the differences in exhaust gas temperature for the high-fire conditions were not significant. Changes in furnace stoichiometry were important in controlling the overall NO production. The highest NO level (3509 ppmvd) was observed for the normal high-fire condition when the temperatures were high in the furnace and there was enough excess oxygen available (more than 10% excess). A significant reduction in NO production (from 3509 to 1390 ppmvd) was observed when the stoichiometry was reduced (from 2.22 to 2.01). Only a small increase in NO levels was observed for the case of the highest oxygen enrichment which had an excess air of about 5% based on the plant settings. Values of CO concentrations of 10,820 and 7700 ppmvd were measured with oxygen excess values of 0.5 and 5%, respectively.

As one would expect, the flow structure is very complex in this highly three-dimensional combustion configuration. Interpretation of these experimental results can certainly be enhanced if accompanied by numerical simulations of the flow field in this furnace. Temperatures in the combustion space very quickly reached the service ceiling of the type S thermocouple used in the suction pyrometer (3500_F/2200K). Typically the gas temperature increases rather quickly from around 2250_F (1500K) to values exceeding 3500_F (2200K) in regions close to the flame. Profiles at access holes number 3, 4, and 5 were not possible because the high temperature environment in the last position in hole 2 caused the ceramic radiation shields to melt and collapse, eventually fusing together the tip and the thermocouple wire, making the suction pyrometer inoperable.

The highest O_2 concentrations were observed in the profiles of holes 2 and 3, where the probe traversed oxygen-rich, unreacted streams in the flames. The quite distinct peaks in the O_2 concentration profiles in hole 1 may suggest independent flame structures early in the reaction. By hole 2 the flames appear to have merged. NO profiles in the combustion space indicate high concentrations in locations where the oxygen concentrations and gas temperatures were high. Peak values of 8000 ppmvd were detected in the flame region. CO concentrations reached values as high as 10 vol% earlier in the flame at the initial stages of combustion and CO_2 values were largest in locations where combustion is complete as indicated by the low values of CO concentrations. It is also interesting to note that from all species measured, CO_2 profiles were the ones with the least amount of spatial variations. Wall radiant heat flux measurements through the five access holes are presented in Table 3. As shown in this table an almost constant heat flux of 140 Btu/hr/ft^2 (442 W/m^2) was measured during the test in the combustion space of Furnace 8.

Exhaust temperatures for Furnaces 6, 7, and 9 were about the same [average value of 1800_F (1260K)] for the three furnaces and the NO levels were low compared to the measured values in Furnace 8. CO concentration values were also negligible with the exception to the measurements in Furnace 6.

ACKNOWLEDGMENTS

The support of the Roth Brothers Smelting Corporation personnel is gratefully acknowledged, with particular thanks to Neal Schwartz, Robert Hubbert, and John Sessler. Significant pre- and post-test support was provided by Dr. Chuck Baukal from Air Products and Chemicals, Inc. Financial support of the project was provided by Air Products and Chemicals, Inc., and the U.S. Department of Energy. The help of student assistants Jacob Peart and Raj Dubey is also gratefully acknowledged.

APPENDIX A

Tabulation of Raw Data

This is the only page for Appendix A.

APPENDIX B

Sensitivity Analysis for O_2 and CO_2 Measurements

In order to quantify the sensitivity of measured effluent oxygen and carbon dioxide concentrations to errors in inlet air and oxygen flow rate measurements, the following analysis was performed for a generalized lean complete combustion of methane for variable volumetric amounts of air and oxygen, a and b, respectively. The combustion equation is

$$CH_4 + a(O_2 + 3.76\,N_2) + b\,O_2 \rightarrow CO_2 + 2\,H_2O + (a+b-2)O_2 + 3.76\,a\,N_2 \tag{B.1}$$

For this equation, the dry concentrations in volume percent of oxygen and carbon dioxide are, respectively:

$$[O_2]_{dry} = \left(\frac{a+b-2}{b+4.76a-1}\right) \tag{B.2}$$

$$[CO_2]_{dry} = \left(\frac{1}{b+4.76a-1}\right) \tag{B.3}$$

Assuming an error in the measurements of a and b, given by e_a and e_b, the expression for the total error in the concentration of oxygen or carbon dioxide, e_t, is given by

$$e_t^2 = \sum_n \left(\frac{\partial F}{\partial n}\right)^2 e_n^2 \tag{B.4}$$

where F is the functional dependence of both concentrations on a and b as given by Eqs. (B.2) and (B.3). Evaluating the partial derivatives of Eqs. (B.2) and (B.3) to be used in Eq. (B.4) one obtains

$$\frac{\partial[O_2]_{dry}}{\partial a} = \frac{8.52-3.76b}{(b+4.76a-1)^2} \quad \text{and} \quad \frac{\partial[O_2]_{dry}}{\partial b} = \frac{3.76a+1}{(b+4.76a-1)^2} \tag{B.5}$$

$$\frac{\partial[CO_2]_{dry}}{\partial a} = \frac{-4.76}{(b+4.76a-1)^2} \quad \text{and} \quad \frac{\partial[CO_2]_{dry}}{\partial b} = \frac{-1}{(b+4.76a-1)^2} \tag{B.6}$$

The fractional errors, ε, given by evaluating Eq. (B.4) using Eqs. (B.5) and (B.6) and the concentrations of oxygen and carbon dioxide [Eqs. (B.2) and (B.3)] are then

$$\varepsilon_{O_2} = \frac{e_{O_2}}{[O_2]_{dry}} = \frac{1}{b+4.76a-1}\left[\left(\frac{8.52-3.76b}{a+b-2}\right)^2 e_a^2 + \left(\frac{3.76a+1}{a+b-2}\right)^2 e_b^2\right]^{1/2} \tag{B.7}$$

$$\varepsilon_{CO_2} = \frac{e_{CO_2}}{[CO_2]_{dry}} = \frac{1}{b+4.76a-1}\left[(-4.76)^2 e_a^2 + (-1)^2 e_b^2\right]^{1/2} \tag{B.8}$$

Plots of the concentrations of oxygen and carbon dioxide in the products of combustion [Eqs. (B.2) and (B.3)] and the accompanying relative error in each measurement [Eqs. (B.7) and (B.8), respectively] assuming a 5% error in air and oxygen flow rates (e_a and e_b = 0.05) are shown in Figs. B.1 and B.2, and B.3 and B.4 for combustion supported by air only and oxygen and air (50/50), respectively.

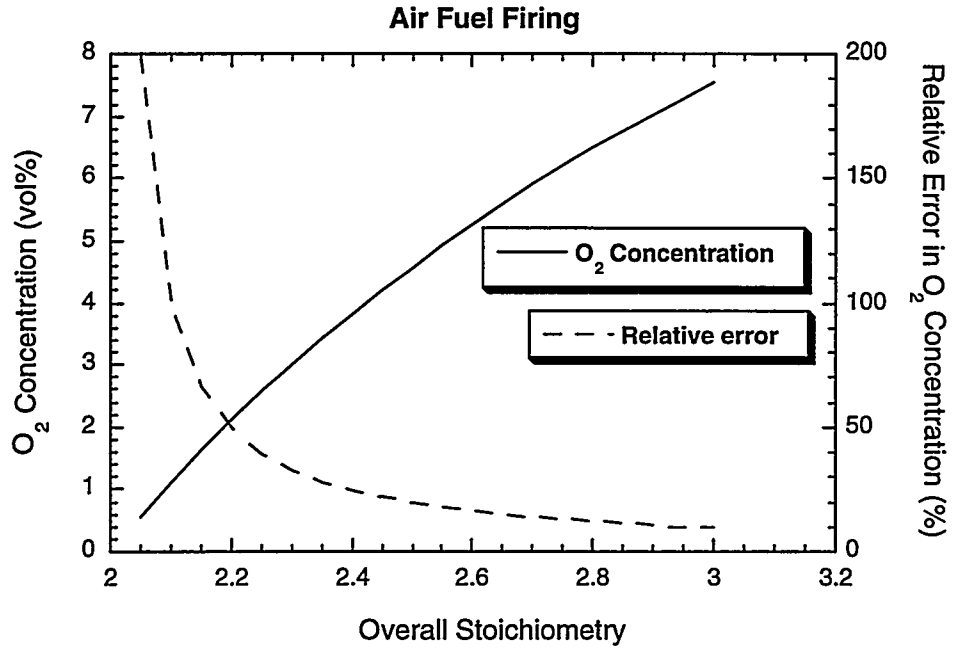

Figure B.1 Oxygen concentration (vol% dry) in the combustion products and relative error in oxygen concentration as a function of stoichiometry for methane combustion in air assuming a 5% error in air flow rate.

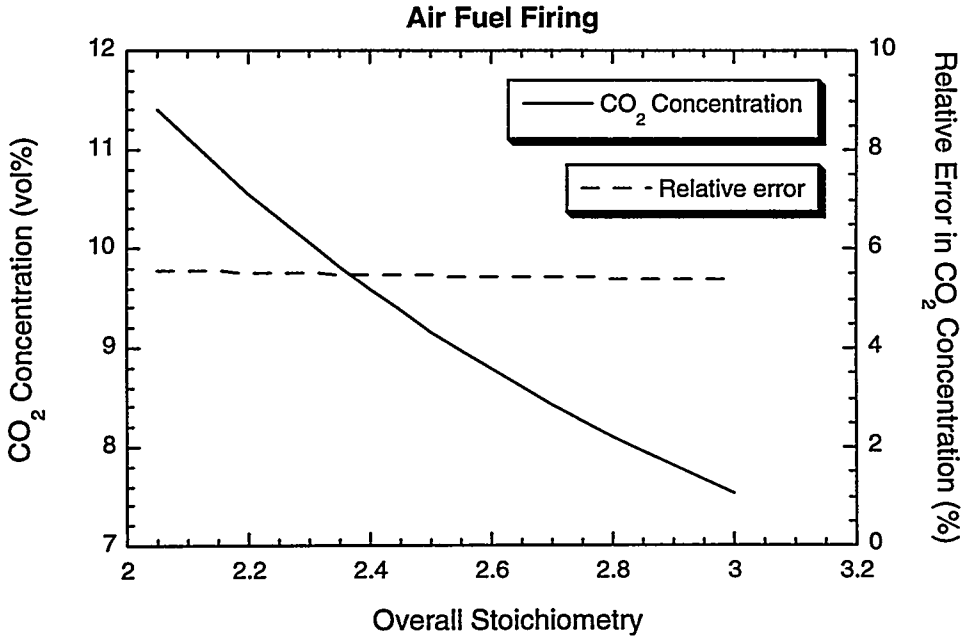

Figure B.2 Carbon dioxide concentration (vol% dry) in the combustion products and relative error in carbon dioxide concentration as a function of stoichiometry for methane combustion in air assuming a 5% error in air flow rate.

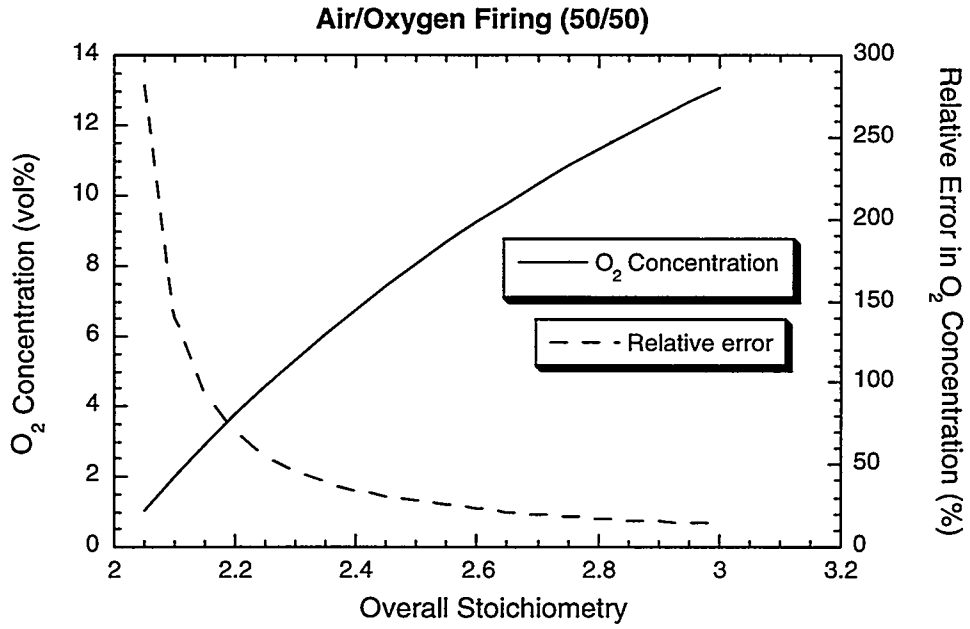

Figure B.3 Oxygen concentration (vol% dry) in the combustion products and relative error in oxygen concentration as a function of stoichiometry for methane combustion in air and oxygen (50/50) assuming a 5% error in air and oxygen flow rates.

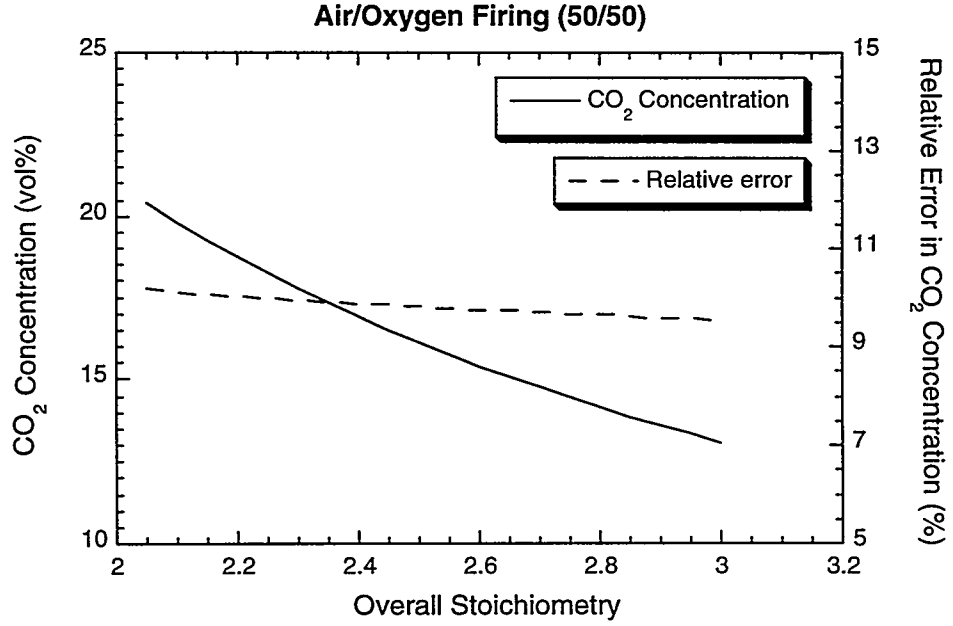

Figure B.4 Carbon dioxide concentration (vol% dry) in the combustion products and relative error in carbon dioxide concentration as a function of stoichiometry for methane combustion in air and oxygen (50/50) assuming a 5% error in air and oxygen flow rates.

APPENDIX C

Plots of Combustion Data Measured in Furnace 8

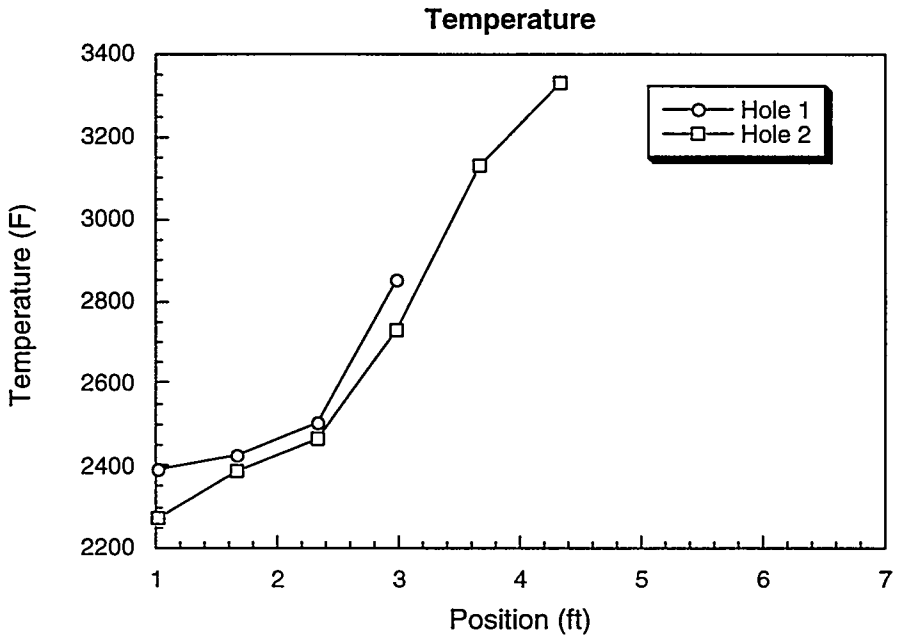

Figure C.1 Measured temperature profiles in the combustion space of Furnace 8.

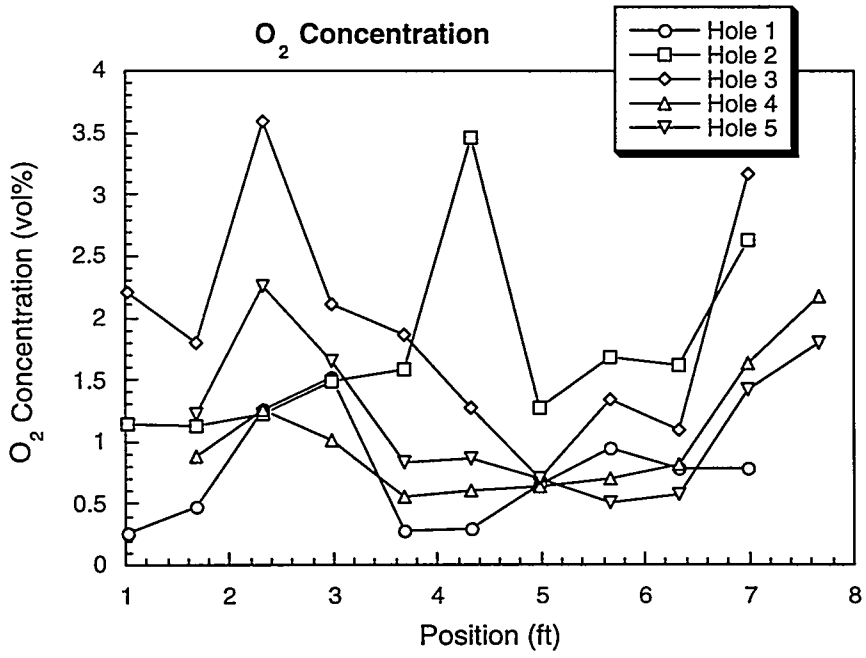

Figure C.2 Measured oxygen (O_2) profiles in the combustion space of Furnace 8.

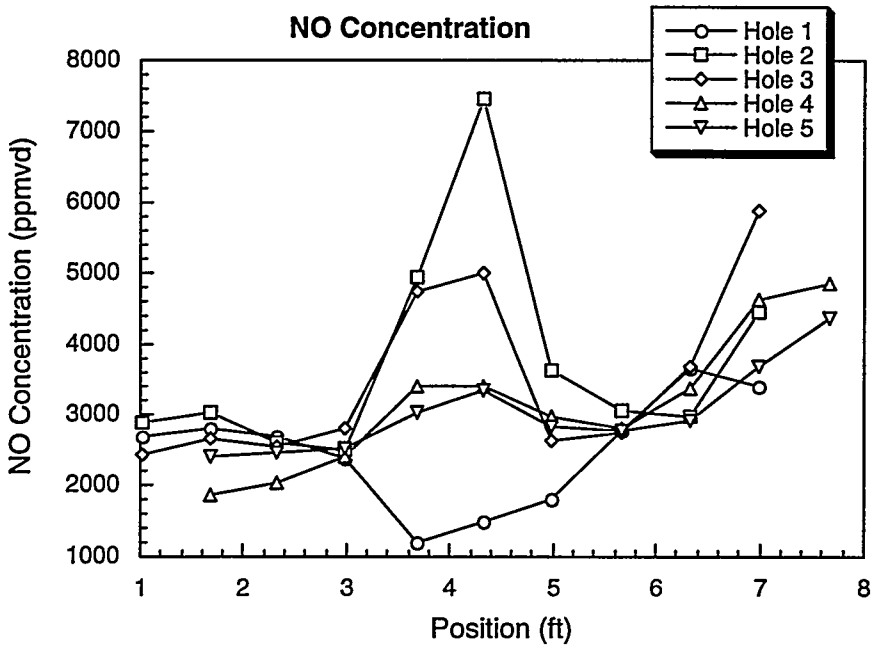

Figure C.3 Measured nitrogen oxide (NO) profiles in the combustion space of Furnace 8. Data are uncorrected for varying oxygen concentration.

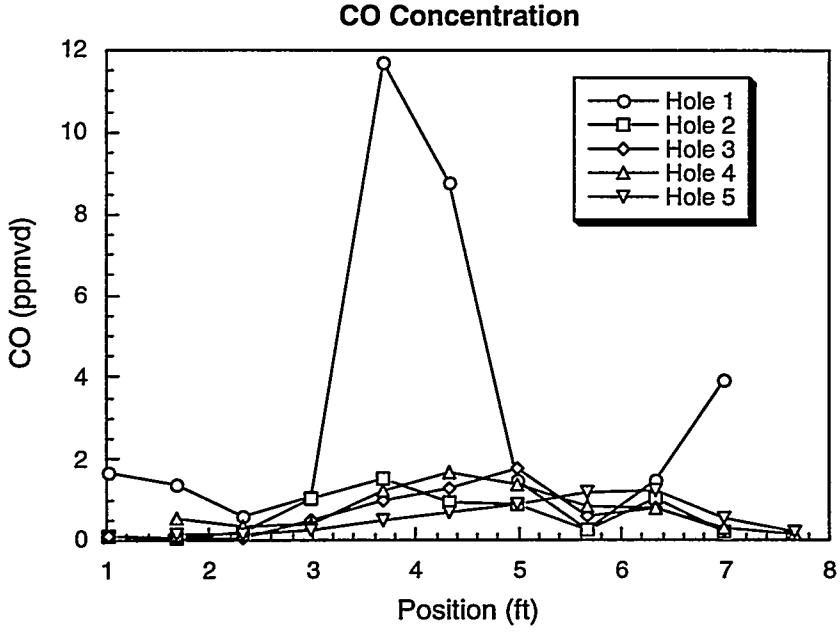

Figure C.4 Measured carbon monoxide (CO) profiles in the combustion space of Furnace 8.

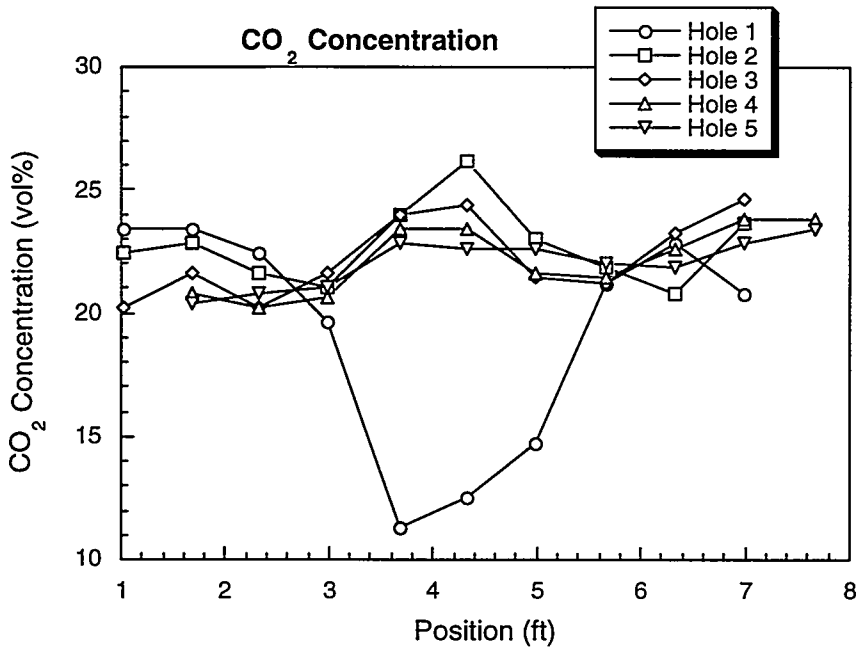

Figure C.5 Measured carbon dioxide (CO_2) profiles in the combustion space of Furnace 8.

APPENDIX 2

COMBUSTION MEASUREMENTS IN AN INDUSTRIAL GAS-FIRED ALUMINUM RECYCLING FURNACE: POST-REBUILD RESULTS

by

B.W. Webb and M.Q. McQuay
Mechanical Engineering Department, 242 CB
Brigham Young University
Provo, UT 84602

Phone: (801) 378-6543
Fax: (801) 378-2138
Email: webb@byu.edu

submitted to
M. DíAgostini and V. Gershtein
Air Products and Chemicals Inc.

EXECUTIVE SUMMARY

The objective of the work reported here was to characterized the post-rebuilt combustion performance in the natural-gas-fired, partially oxygen-enriched, aluminum recycling furnace (Furnace 8) operated by Roth Brothers Smelting Corporation (now Wabash Alloys) in Syracuse, New York. Measurements of gas temperature and species concentration (O_2, CO, NO, and CO_2) were made in the exhaust of the furnace for several operating conditions of interest. Local species concentration measurements were also made in the combustion space for the furnace/burner design condition: Stoichiometry at or near 2.0 with 35% oxygen enrichment.

The combustion space measurements showed clear evidence of the flame zone with oxygen depletion and high carbon monoxide (as high as 13% in the flame core). The new low-NO_x burner designs yielded NO concentrations below 350 ppm at all locations in the furnace. The corresponding stack NO concentration was 267 ppm. CO_2 concentrations showed little variation in the combustion space except in hole 1 of the insert, where some flame structure was observed.

The stack measurements were performed for a range of furnace operation conditions: Oxygen enrichment values ranging from 32 to 40% and combustion stoichiometries ranging from 1.94 to 2.22 (with 2.0 being stoichiometric combustion). NO concentrations ranged from 103 ppm (for *Stoich* = 1.98, 33% O_2 enrichment) to 651 ppm (for *Stoich* = 2.11, 41% O_2 enrichment). Exhaust temperatures were a maximum for the near-stoichiometric combustion cases, reaching a maximum of 2056°F for *Stoich* = 1.94, 39% O_2 enrichment. Complete combustion was observed (absence of CO in the exhaust) for all fuel-lean conditions. A peak CO concentration of 12,250 ppm was measured for *Stoich* = 1.98, 33% O_2 enrichment.

A mass-balance analysis of the effluent species concentration data was conducted to estimate the true air and oxygen flow rates into the furnace. Deviations from the differential pressure orifice air flow measurement may be due to error in the orifice plate measurement and/or infiltration into the furnace by leakage. The data analysis suggests that the actual air flow is, on average, 10% above the measured air flow rate. The same analysis shows that the metered oxygen flow is within 4% of the actual values.

INTRODUCTION

Significant progress has been made in the combustion process in large furnaces over the past two decades in reducing energy consumption and maximizing product yield. Nonetheless, escalating global competition and increasingly restrictive government regulations on pollutants in furnace effluents are prompting the examination of even more aggressive measures to increase combustion efficiency while reducing the impact of the combustion process on the environment. The objective of the work reported here was to characterize the post-rebuild combustion performance in the natural-gas-fired, partially oxygen-enriched, aluminum recycling furnace (Furnace 8) operated by Roth Brothers Smelting Corporation (recently acquired by Wabash Alloys) in Syracuse, New York. Measurements of gas temperature and species concentration (O_2, CO, NO, and CO_2) were made in the exhaust of the furnace. Local species concentrations were also measured in the combustion space through a specially designed wall insert placed in an existing side door used for dross removal during the normal operation of the furnace. Stack measurements in this furnace included ten high-fire operating conditions over a range of combustion stoichiometries and oxygen enrichment. Combustion space measurements were made only for the burner design condition. These measurements are in support of a DOE-funded project to Air Products and Chemicals, Inc. and Roth Brothers aimed at the development of oxygen-enriched, advanced technology for increased productivity and energy efficiency and reduced pollutants. The measurements reported here for the post-rebuild tests in Furnace 8 compliment pre-rebuild measurements reported previously (see "Combustion Measurements in an Industrial Gas-Fired Aluminum Recycling Furnace: Pre-Rebuild Results," December 15, 1997). Acknowledgment is made of the support of Roth Brothers during the test preparation and tests, as well as the Air Products personnel.

FURNACE DESCRIPTION

A schematic of the Roth Brothers Smelting Corporation reverberatory aluminum melting Furnace 8 can be seen in Fig. 1. The furnace is generally of rectangular cross-section. The combustion space

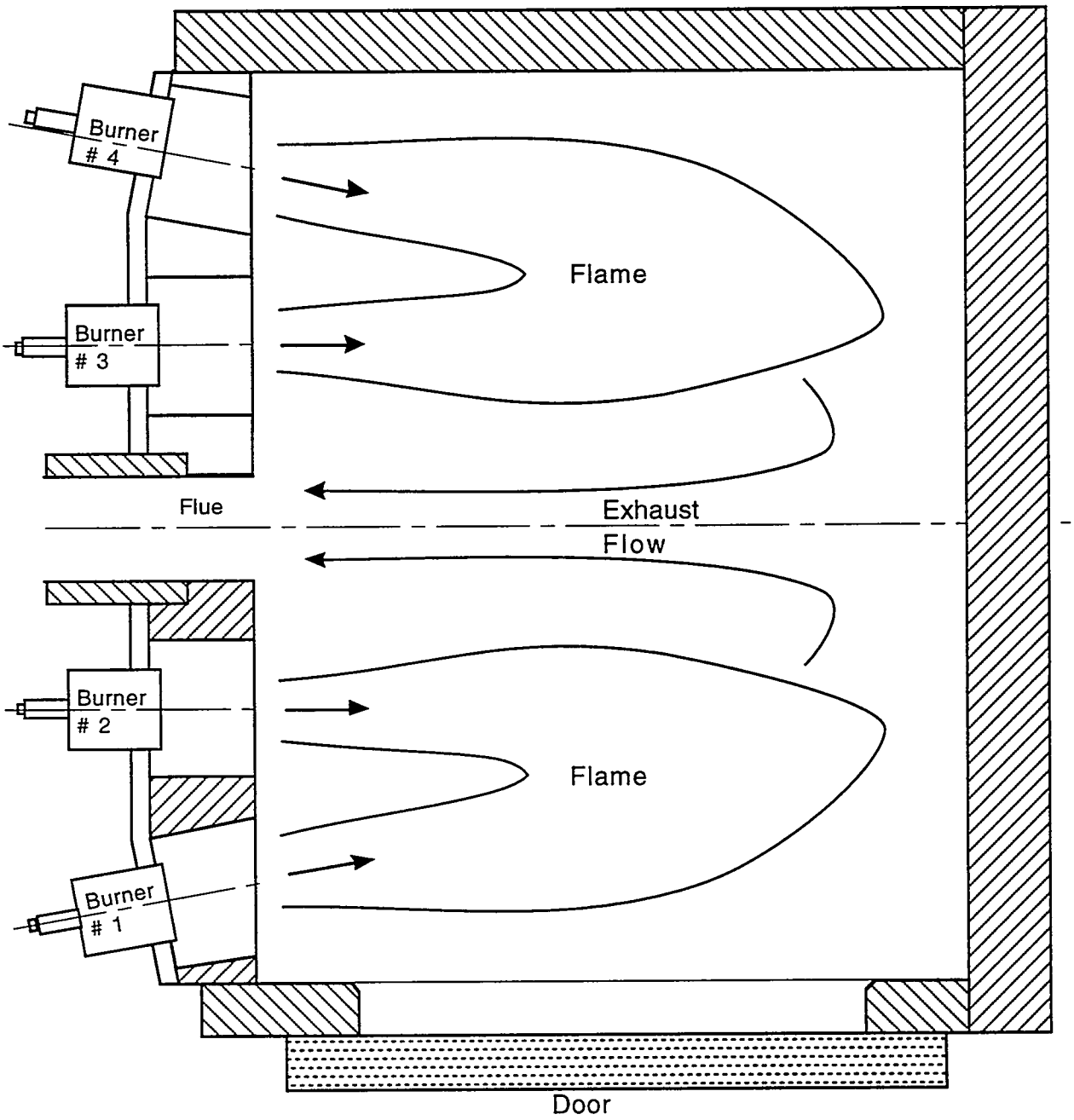

Figure 1. Top-view schematic drawing of the natural gas-fired aluminum melting furnace illustrating the complex reacting flow field including the four burners and exhaust port.

is approximately 49.5 in (1.26 m) high from the melt line (fully charged) to the roof, 12 ft (3.66 m) wide, and 17.5 ft (5.33 m) from front to back. Two Air Products oxygen enrichment burners of proprietary design are located on either side of the exhaust flue. The outer burners (1 and 4) are vectored toward the furnace symmetry line at a 7° angle, while the inner burners (2 and 3) are fired parallel to the symmetry line. All four burners are vectored downward at a 10° angle. The burners are comprised of a central core oxygen/fuel burner, surrounded by an annular air/fuel burner. During high-fire operation, both central and annular burners operate simultaneously in an overall oxygen-enriched combustion mode. When furnace temperatures exceed desired levels or while tapping of the molten aluminum occurs, the furnace is operated in low-fire mode, utilizing only the annular air/fuel burner. A large door, which can be opened for dross removal, forms the front wall of the furnace parallel to the furnace symmetry line.

A furnace wall insert was constructed by Roth Brothers personnel to provide access to the combustion space of Furnace 8 during operation. The insert was constructed of mild steel with five 4 in (10 cm) diameter pipes welded to the wall through which water-cooled probes could be inserted for furnace probing. The insert was centered in the front wall of the furnace, and the five access holes were spaced at 19.5 in (0.5 m) intervals. The flame-exposed face of the insert was wrapped in high-temperature insulation to prevent heat loss from the furnace while the insert was in place. The furnace door was lifted, the insert was placed on the furnace sill, and the door was lowered onto the insert until a relatively tight seal was achieved. The clearance gap between the wall insert and the furnace, as well as unused access holes were plugged with high temperature blanket insulation. Figure 2 shows the position of the wall insert and probe locations relative to the furnace geometry and burner vectoring. The figure is drawn to scale to illustrate the probing locations relative to the anticipated flame.

Effluent species concentration and gas temperature measurements were made during high-fire furnace operation. These measurements were made by inserting the water-cooled probes through an access hole in the refractory flue.

Fuel (natural gas) flow rates were measured for the oxygen/fuel and air/fuel central and annular segments, respectively, to each skid. The air and oxygen flow rates were metered by the plant.

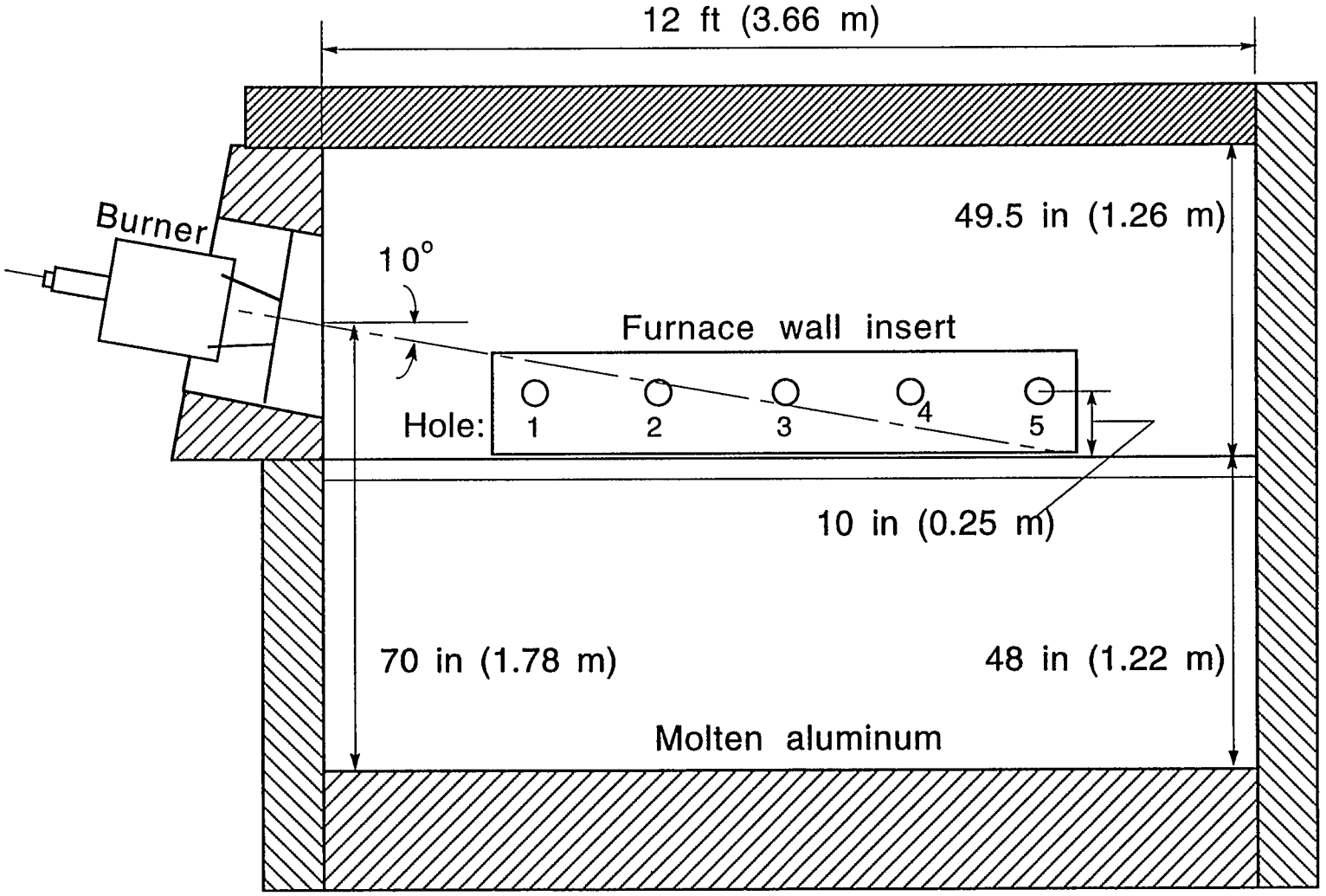
12 ft (3.66 m)
Burner
10°
49.5 in (1.26 m)
Furnace wall insert
Hole:
1
2
3
4
5
10 in (0.25 m)
70 in (1.78 m)
48 in (1.22 m)
Molten aluminum

These data enabled the calculation of the overall furnace stoichiometry and the level of oxygen enrichment. Stoichiometry is defined here as the total oxygen volume flow (from air and O_2 feed) through the burners divided by the total fuel flow through the burners. A ratio of 2.0 is nominally stoichiometric, while less than 2.0 is fuel-rich and greater than 2.0 is fuel-lean. Excess air is then calculated as (stoichiometry - 2)/2 × 100%. The overall oxygen enrichment is defined as the total oxygen volume flow through the burners divided by the total volume of air plus oxygen through the burners. An nominal oxygen enrichment of 21% is air/fuel combustion, while an enrichment of 100% is oxygen/fuel combustion. Intermediate values represent partial oxygen enrichment.

INSTRUMENTATION AND EXPERIMENTAL PROCEDURE

Gas Concentration

Combustion gases were sampled by drawing them through a water-cooled, stainless steel collection probe using a four-head suction pump. As illustrated in Fig. 3, the probe was made of a 0.875 in (22.2 mm) outside diameter, 9.8 ft (3 m) long annular tube with a 0.375 in (9.5 mm) suction tube on the inside. The gases were rapidly quenched upon being drawn into the tube due to the high water-cooling rate in the surrounding annulus. The combustion gases were drawn through the probe and passed through two in-line condenser coils with integral water trap immersed in an ice bath. The two condenser coils eliminated the water from the gases prior to species concentration measurement by the gas analyzers.

The sampled gases were analyzed in real-time with four on-line gas analyzers, yielding measurements in either volume percent (vol%) or parts per million on a dry basis (ppmvd): two Nova infrared analyzers for CO_2, Nova and Testo electrochemical analyzers for O_2, NO, and low (< 2000 ppmvd) and high (> 2000 ppmvd) CO, and a North American Enviromate electrochemical analyzer for duplicate O_2, NO, and low CO measurements. The measurement limits for the analyzers used are summarized in Table 1. The accuracy reported for the CO_2 measurement is ±0.3%. The manufacturer-specified accuracy for the electrochemical analyzers is ±0.05% for O_2, and ±4% and ±100 ppmvd for CO measurements greater than and less than 2000 ppmvd, respectively.

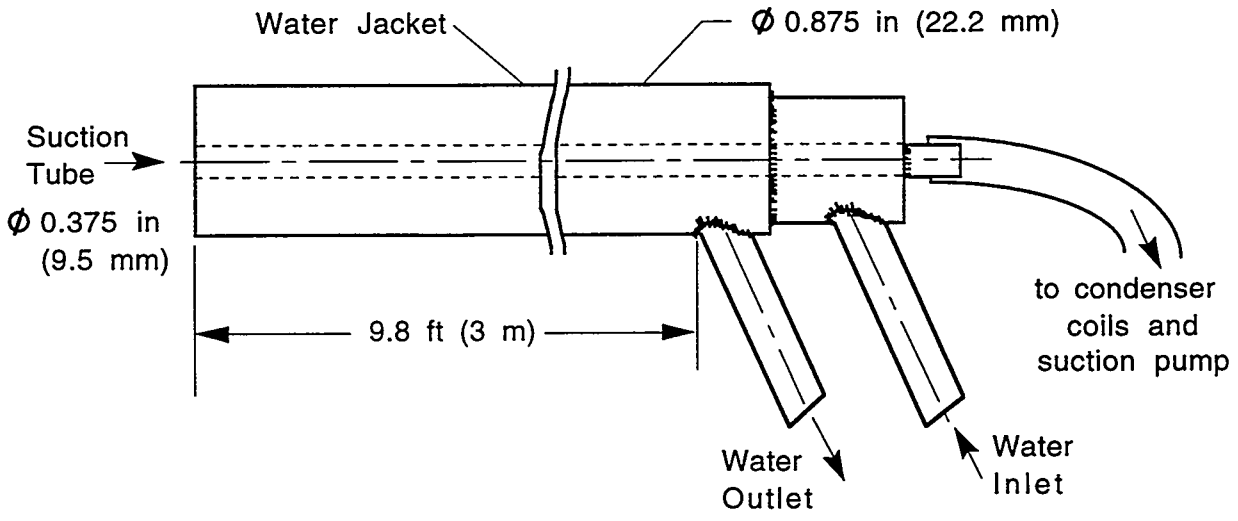

Figure 3. Schematic drawing of gas sampling probe.

Table 1. Measurement limits for the on-line gas analyzers used.

	CO_2	O_2	CO (low)	CO (high)	NO
Nova	50 vol%	-	-	-	-
Testo	-	21 vol%	2000 ppmvd	40,000 ppmvd	4000 ppmvd
Nova	20 vol%	21 vol%	2000 ppmvd	40,000 ppmvd	4000 ppmvd
North American	-	21 vol%	4000 ppmvd	-	4000 ppmvd

All units were carefully calibrated before and after each test case using research-grade calibration gas standards for O_2, CO_2, CO, and NO. The gas calibration standards were designed to provide instrument calibration over the range of values anticipated. Calibration gas concentrations were:

O_2	21 vol% (atmospheric)
CO:	900 ppmvd and 25,000 ppmvd (2.5 vol%)
CO_2:	10.0 vol%
NO:	900 ppmvd and 1800 ppmvd

Research grade pure nitrogen was also used to test for leakage in the gas sampling train.

Very good agreement was observed throughout the tests in the duplicate measurements for the different electrochemical analyzers. Response time for species measurements was estimated for the sample train used in the tests to be approximately 2 mins for all gas species.

A dilution system was used to make measurements possible where species concentrations exceeded the analyzer capabilities. Research grade pure nitrogen was mixed with the sampled combustion gases in known proportions prior to on-line gas concentration analysis. The measured results were then scaled by the appropriate scaling factor using the known combustion gas and dilution nitrogen flow rates.

Gas Temperature

Gas temperature was measured using a conventional, shielded, water-cooled suction pyrometer illustrated schematically in Fig. 4. The pyrometer was fabricated by the International Flame Research Foundation. A 1.7 in (43 mm) outside diameter, 4.25 ft (1.3 m) long, stainless steel water-cooled pyrometer with 4.7 in (12 cm) long double alumina radiation shields was used for the flue gas temperature measurements. Gas suction was provided by a venturi pump that was attached to a 1 in (2.54 cm) pressure line at 80 psi (550 kPa). The thermocouple voltage was measured with a type-S, cold-junction compensator and amplifier using a hand-held voltmeter. A ninth-order polynomial was used to describe the thermocouple temperature as a function of the voltage output. The accuracy of the pyrometer is reported by the manufacturer to be ±8K when operated at the recommended gas flow rate.

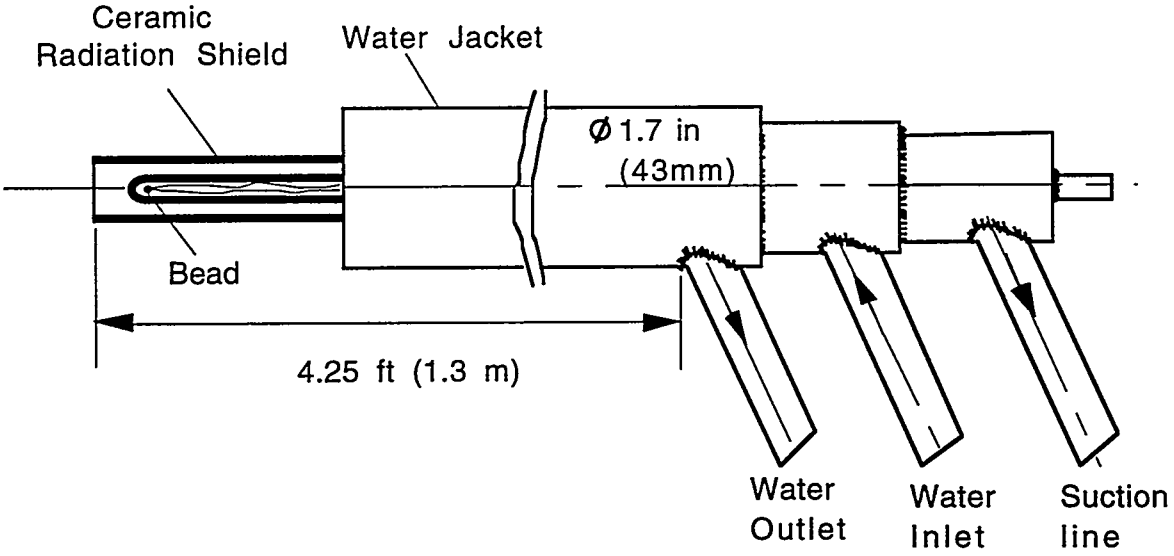

Figure 4. Schematic drawing of suction pyrometer.

RESULTS AND DISCUSSION

Exhaust Measurements

Exhaust measurements of average gas temperature and species concentrations were made for ten different furnace operating conditions, including oxygen enrichment values based on the furnace settings ranging from 32 to 41% and combustion stoichiometries based on the same variables ranging from 1.94 to 2.22. These ten furnace-operating conditions are identified in Table 2, where the following variables, obtained from the furnace control panel, are listed: furnace pressure, air side fuel and air flow rates, oxygen side fuel and oxygen flow rates for both sets of burners (T1 and T2), roof and bath temperature, and air damper pressure differential. The results for the exhaust measurements of species concentrations and gas temperature are shown in Table 3a, where a summary of the total furnace fuel and oxidizer flow rates, obtained from Table 2, are also included. Based on the total flow rates of fuel and oxidizer and accounting for the 90% oxygen purity of the VSA plant (with the exception of Case 1 as noted in that table) the overall stoichiometry and percent oxygen enrichment variables were calculated for each furnace operating condition using the equations included in the footnote to Table 3a. For comparison purposes, the same variables measured for the three high-fire operating conditions tested before the furnace rebuild are included in Table 3b.

With the measurements of O_2, CO_2, CO, and NO on a dry basis and the plant-measured total fuel flow rate to the furnace (shown in Tables 3a and 3b), it is possible to perform a mass balance for an overall reaction equation, allowing the amount of air supplied and infiltrated into the furnace as well as the amount of oxygen enrichment supplied to vary. This analysis would provide an estimate of the total airflow and oxygen flow rates as well as the overall stoichiometry in the furnace corresponding to the measured concentration of these four species. Such a reaction for one mole of fuel is of the form

$$CH_4 + \alpha(O_2 + 3.76N_2) + \beta O_2 + \frac{\beta}{9} N_2 \rightarrow \gamma CO_2 + \delta CO + \varepsilon H_2O + \kappa O_2 + \mu N_2 + \eta NO \qquad (1)$$

The eight unknowns in this equation are solved for using four equations that state the conservation of mass of oxygen, nitrogen, carbon, and hydrogen, and the four equations that represent the

measured average concentrations on a dry basis of oxygen, carbon dioxide, carbon monoxide, and nitric oxide as shown below.

$$[CO_2]_{dry} = \frac{\gamma}{\gamma+\delta+\kappa+\mu+\eta} \quad (2)$$

$$[CO]_{dry} = \frac{\delta}{\gamma+\delta+\kappa+\mu+\eta} \quad (3)$$

$$[NO]_{dry} = \frac{\eta}{\gamma+\delta+\kappa+\mu+\eta} \quad (4)$$

$$[O_2]_{dry} = \frac{\kappa}{\gamma+\delta+\kappa+\mu+\eta} \quad (5)$$

The results of this analysis after and before the furnace rebuild are shown in Tables 4a and 4b, respectively. Also shown in these two tables are the calculated results for the total air and oxygen flow rates as well as furnace stoichiometry and oxygen enrichment corresponding to the measured species concentrations in the exhaust and plant-measured fuel flow rates.

As shown in Table 3a, NO concentrations in the furnace exhaust after the rebuild ranged from 103 ppm (for *Stoich* = 1.98 and 33% O_2 enrichment) to 651 ppm (for *Stoich* = 2.11 and 41% O_2 enrichment). The lowest NO concentration before the rebuild (1390 ppm for *Stoich* = 2.01 and 35% O_2 enrichment) was higher than the highest NO concentration measured after the rebuild (651 ppm). The highest NO concentration measured before the rebuild was 3509 ppm (for *Stoich* = 2.22 and 36% O_2 enrichment). In general, NO concentrations before and after the furnace rebuild correlated well with furnace stoichiometry. The highest concentrations were found in lean conditions where the temperatures are still high and the availability of nitrogen is increased. The lowest NO concentrations were found for slightly fuel-rich conditions. The tests after the rebuild also show that NO concentration correlate well with percent oxygen enrichment, *i.e.*, the highest measured NO concentrations were from furnace settings with the highest oxygen enrichment levels. NO concentrations in the furnace exhaust did not necessarily correlate with exhaust gas temperature as shown in Table 3a. A comparison of the NO production data of Tables 3a and 3b reveal a significant drop in the NO production rate of 0.172 lb NO/MMBtu for the furnace design condition (Case 10) from the 2.448 lb NO/MMBtu seen in the standard operating condition prior to the rebuild.

CO concentration levels in the exhaust were generally negligible with the exception of the three test conditions very close to stoichiometric conditions, Cases 4, 7, and 9, where the concentrations of this species were 12,250, 892, and 1800 ppm, respectively.

Exhaust gas temperatures after the furnace rebuild varied between a low of 1918°F (for *Stoich* = 2.09 and 34% O_2 enrichment), and a high of 2056°F (for *Stoich* = 1.94 and 39% O_2 enrichment) for the near-stoichiometric combustion cases. Correspondingly, the highest exhaust gas temperature measured before the rebuild was 2281°F (for *Stoich* = 2.10 and 35% O_2 enrichment). Complete combustion was observed (absence of CO in the exhaust) for all fuel-lean conditions before and after the rebuild. A peak CO concentration of 12,250 ppm was measure after the rebuild for the furnace setting corresponding to *Stoich* = 1.98 and 33% O_2 enrichment.

The mass-balance analysis of the effluent species concentration data shown in Tables 4a and 4b also provided an estimate of the true air and oxygen flow rates into the furnace. Deviations between the air damper orifice plate measurements and estimated airflow rates after the furnace rebuild were as high as 17% and as low as 4% with the estimated values always larger than the measured values, indicating the constant presence of air infiltration in the furnace. That same average difference for the oxygen flow rates was -4%, suggesting that on average the indicated oxygen flow may be slightly overestimating the true amount fed to the furnace (although this may be within the uncertainty of the flow measurement device). Despite these differences, there was good agreement between the measured and calculated furnace overall stoichiometry and percent oxygen enrichment.

Table 2. Furnace operating conditions for the ten cases where exhaust measurements were made.

	Furnace pressure (in. H_2O)	Air side fuel flow (scfh)	Air flow (scfh)	T1 fuel flow (scfh)	T1 O_2 flow (scfh)	T2 fuel flow (scfh)	T2 O_2 flow (scfh)	Roof temp. (°F)	Bath temp. (°F)	Orifice Δp (in. H_2O)[a]
Case 1[b]	0.02	5515	68,700	5000	10,000	4998	10,000	2110	1367	0.8
Case 2	0.02	5537	77,500	4997	9000	4998	9000	2159	1364	1.0
Case 3	0.01	5513	87,500	5024	8000	4992	8000	2170	1444	1.2
Case 4	0.01	5525	78,500	5004	8000	5004	8000	2162	1504	1.0
Case 5	0.01	5525	57,500	4995	11,450	4998	11,600	2173	1527	-
Case 6	0.01	5537	74,000	4994	9500	5014	9700	2203	1457	-
Case 7	0.02	5530	68,000	4992	9500	5014	9500	2219	1481	-
Case 8	0.01	5558	59,000	5003	10,600	4990	10,500	2228	1463	-
Case 9	0.00	5546	58,000	5002	10,000	5000	10,000	2235	1455	-
Case 10	0.01	5549	71,000	5000	9100	5003	9000	2234	1445	-

[a] Manometer was not functioning properly for Cases 5 – 10.
[b] Flow rates shown include nominal 10% N_2 resulting from 90% O_2 purity in VSA plant output.

Table 3a. Summary of total furnace fuel and oxidizer flow rates, and exhaust species concentration and temperature measurements for the post-rebuild tests. The stoichiometry and oxygen enrichment values are calculated from the total flow rates shown.

	Total fuel flow (scfh)	Total VSA O_2 flow[a] (scfh)	Air flow[b] (scfh)	*Stoich*[c]	% O_2[d] enrich	$[O_2]_{dry}$ (vol%)	$[CO_2]_{dry}$ (vol%)	$[NO]_{dry}$ (ppm, lb/MMBtu)[e]	$[CO]_{dry}$ (ppm)	Temp. (°F)
Case 1[f]	15,513	20,020	68,700	2.22	39	5.93	19.7	518, 0.327	0.0	1963
Case 2	15,532	17,990	77,500	2.09	34	2.83	18.4	235, 0.159	0.0	1918
Case 3	15,529	15,955	87,500	2.10	32	1.67	17.2	145, 0.105	0.0	1961
Case 4	15,533	15,980	78,500	1.98	33	0.15	17.5	103, 0.073	12,250	2053
Case 5	15,518	23,030	57,500	2.11	41	5.37	21.1	651, 0.383	0.0	1939
Case 6	15,545	19,150	74,000	2.10	35	2.7	18.6	268, 0.179	0.0	1983
Case 7	15,536	19,000	68,000	2.02	36	1.03	20.0	251, 0.156	892	2037
Case 8	15,551	21,100	59,000	2.01	39	2.07	21.7	411, 0.235	0.0	1957
Case 9	15,548	20,050	58,000	1.94	39	0.6	21.6	308, 0.177	1800	2056
Case 10	15,552	18,050	71,000	2.00	35	0.9	19.3	267, 0.172	21	1983

[a] Flow rates shown include nominal 10% N_2 resulting from 90% O_2 purity in VSA plant output.
[b] For the purpose of the results presented here air is assumed to be 20.9% oxygen on a volume basis.

[c] $Stoich = \frac{O_2\ purity \times O_2\ flow + 0.209 \times Air\ flow}{CH_4\ flow}$. Oxygen purity was 100% for Case 1, 90% for Cases 2 – 10.

[d] $\%O_2\ enrich = \frac{O_2\ purity \times O_2\ flow + 0.209 \times Air\ flow}{O_2\ flow + Air\ flow}$. Oxygen purity was 100% for Case 1, 90% for Cases 2 – 10.

[e] NO concentration in lb/MMBtu calculated according to EPA Method 19: NO [lb/MMBtu] = NO [ppm] × 1.194×10^{-7} × 1040 × (100/%CO_2).
[f] VSA system was not operational at the time data were taken for Case 1 so (100% pure) liquid oxygen was used.

Table 3b. Summary of total furnace fuel and oxidizer flow rates, and exhaust species concentration and temperature measurements for the oxygen-enriched firing conditions of the pre-rebuild tests (see "Combustion Measurements in an Industrial Gas-Fired Aluminum Recycling Furnace: Pre-Rebuild Results," December 15, 1997). The stoichiometry and oxygen enrichment values are calculated from the total flow rates shown.

	Total fuel flow (scfh)	Total O_2 flow (scfh)	Air flow (scfh)	*Stoich*	% O_2 enrich	$[O_2]_{dry}$ (vol%)	$[CO_2]_{dry}$ (vol%)	$[NO]_{dry}$ (ppm, lb/MMBtu)[a]	$[CO]_{dry}$ (ppm)	Temp. (°F)
Case 1[b]	15,020	17,500	75,020	2.22	36	4.4	17.8	3509, 2.448	5	2153
Case 2[c]	16,970	17,500	79,020	2.01	35	0.1	19.5	1390, 0.885	10,820	2132
Case 3[d]	16,970	18,440	82,000	2.10	35	0.3	20.3	1775, 1.086	7700	2281

[a] NO concentration in lb/MMBtu calculated according to EPA Method 19: NO [lb/MMBtu] = NO [ppm] × 1.194×10^{-7} × 1040 × (100/%CO_2).
[b] Normal operation
[c] Low stoichiometry
[d] High O_2 enrichment

Table 4a. Results of mass balance analysis for the post-rebuild tests.

	Fuel flow (scfh)	α	β	γ	δ	ε	κ	μ	η	O_2[a] (scfh)	Air (scfh)	*Stoich*[c]	% O_2[c] enrich
Case 1[b]	15,513	1.0037	1.2987	1.0	0.0	2.0	0.30182	3.7725	0.002629	20,147	74,115	2.30	38
Case 2	15,532	1.1074	1.047	1.0	0.0	2.0	0.15380	4.2797	0.001277	18,069	81,873	2.15	33
Case 3	15,529	1.2323	0.8645	1.0	0.0	2.0	0.09738	4.7327	0.000846	14,916	91,163	2.10	31
Case 4	15,533	1.1271	0.8485	0.9346	0.0654	2.0	0.00801	4.3319	0.000550	14,644	83,334	1.98	31
Case 5	15,518	0.8859	1.3701	1.0	0.0	2.0	0.25450	3.4817	0.003085	23,624	65,439	2.26	39
Case 6	15,545	1.0940	1.0518	1.0	0.0	2.0	0.14516	4.2297	0.001440	18,167	80,950	2.15	34
Case 7	15,536	1.0135	1.0362	0.9956	0.0044	2.0	0.05127	3.9253	0.001249	17,887	74,950	2.05	34
Case 8	15,551	0.9015	1.1951	1.0	0.0	2.0	0.09561	3.5214	0.001898	20,650	66,761	2.10	37
Case 9	15,548	0.9149	1.1093	0.9917	0.0083	2.0	0.02755	3.5624	0.001414	19,164	67,707	2.02	36
Case 10	15,552	1.0705	0.9768	0.9999	0.0001	2.0	0.04663	4.1328	0.001383	16,879	79,246	2.05	33

[a] Oxygen flow rates for Cases 2 - 10 include nominal 10% N_2 resulting from 90% O_2 purity in VSA plant output: O_2 flow = β (1 + 1/9) × Fuel flow

[b] VSA system was not operational at the time data were taken for Case 1 so (100% pure) liquid oxygen was used.

[c] Calculated from the fuel flow metered, and the O_2 and air flows determined as part of the mass balance analysis.

Table 4b. Results of mass balance analysis for the pre-rebuild tests (see "Combustion Measurements in an Industrial Gas-Fired Aluminum Recycling Furnace: Pre-Rebuild Results," December 15, 1997).

	Fuel flow (scfh)	α	β	γ	δ	ε	κ	μ	η	O_2 (scfh)	Air (scfh)	*Stoich*	% O_2 enrich
Case 1[a]	15,020	1.1264	1.1307	0.9999	0.0000	2.0	0.24720	4.3509	0.019710	16,961	80,425	2.26	35
Case 2[b]	16,970	0.9949	0.9871	0.9474	0.0526	2.0	0.00486	3.8470	0.006754	16,751	80,363	1.98	35
Case 3[c]	16,970	0.9607	1.0395	0.9635	0.0365	2.0	0.01424	3.7234	0.008424	17,640	77,603	2.00	36

[a] Normal operation
[b] Low stoichiometry
[c] High O_2 enrichment

Combustion Space Measurements

Profiles of gas species concentration in the combustion space were measured for the design condition, Case 10. As explained before, these measurements were obtained through the access insert mounted in the furnace door as illustrated in Fig. 2. Figures 5 through 8 show the results for the profiles of gas temperature, O_2, NO, CO, and CO_2 concentrations, respectively. The numerical data are tabulated in Appendix A. Included in each of these five figures is a top-view schematic (drawn to scale) of one half of the furnace showing the relative position of the profiles with respect to important features in the combustion space.

As one would expect, the flow structure is very complex in this highly three-dimensional combustion configuration. Interpretation of these experimental results can certainly be enhanced if accompanied by numerical simulations of the flow field in this furnace. In an attempt to aid in the understanding of this complex flow structure, Fig. 2 illustrates the probe locations relative to burner vectoring. Not only are all burners vectored downward by 10°, but the two exterior burners (burners 1 and 4) are also vectored towards the furnace centerline by 7°. A side view of the orientation of the burners with respect to the access insert has been presented in Fig. 2.

For the most part, the profiles of oxygen concentration were quite uniform with the exception of holes 1 and 2, where indication of the flame jets may be seen. The flame location may be inferred from regions of oxygen depletion. Interestingly, the O_2 concentration seems to climb somewhat at the horizontal plane where measurements were made from holes 2 to 5. O_2 concentrations in the exhaust were measured to be 0.9% for this case. The concentrations seen in Fig. 5 are quite similar in magnitude to those observed prior to the rebuild.

NO profiles (Fig. 6) indicate relatively flat behavior over most of the furnace. It is interesting to contrast these data with those from the previous burner configurations prior to the rebuild. NO concentrations before the rebuild varied between 2000 and 3000 ppm with the exception of a peak in hole 2 which reached nearly 8000 ppm. Clearly, the new burners yield superior NO characteristics, with NO concentrations in the furnace never exceeding 350 ppm. Indeed, the NO concentration in the stack for the design condition (Case 10) was 267 ppm. This may be contrasted with an exhaust NO concentration of 3509 ppm at the conventional furnace operating condition prior to the rebuild.

CO concentrations (Fig. 7) were flat except near 4.5 feet of penetration for holes 1 and 2, suggesting the location of the flame core. This coincides with the region of oxygen depletion in Fig. 5. Exhaust stack measurements indicated complete combustion (CO concentration of 21 ppm) for this case. CO_2 concentration profiles were flat at approximately 16 – 17% throughout the furnace, as seen in Fig. 8.

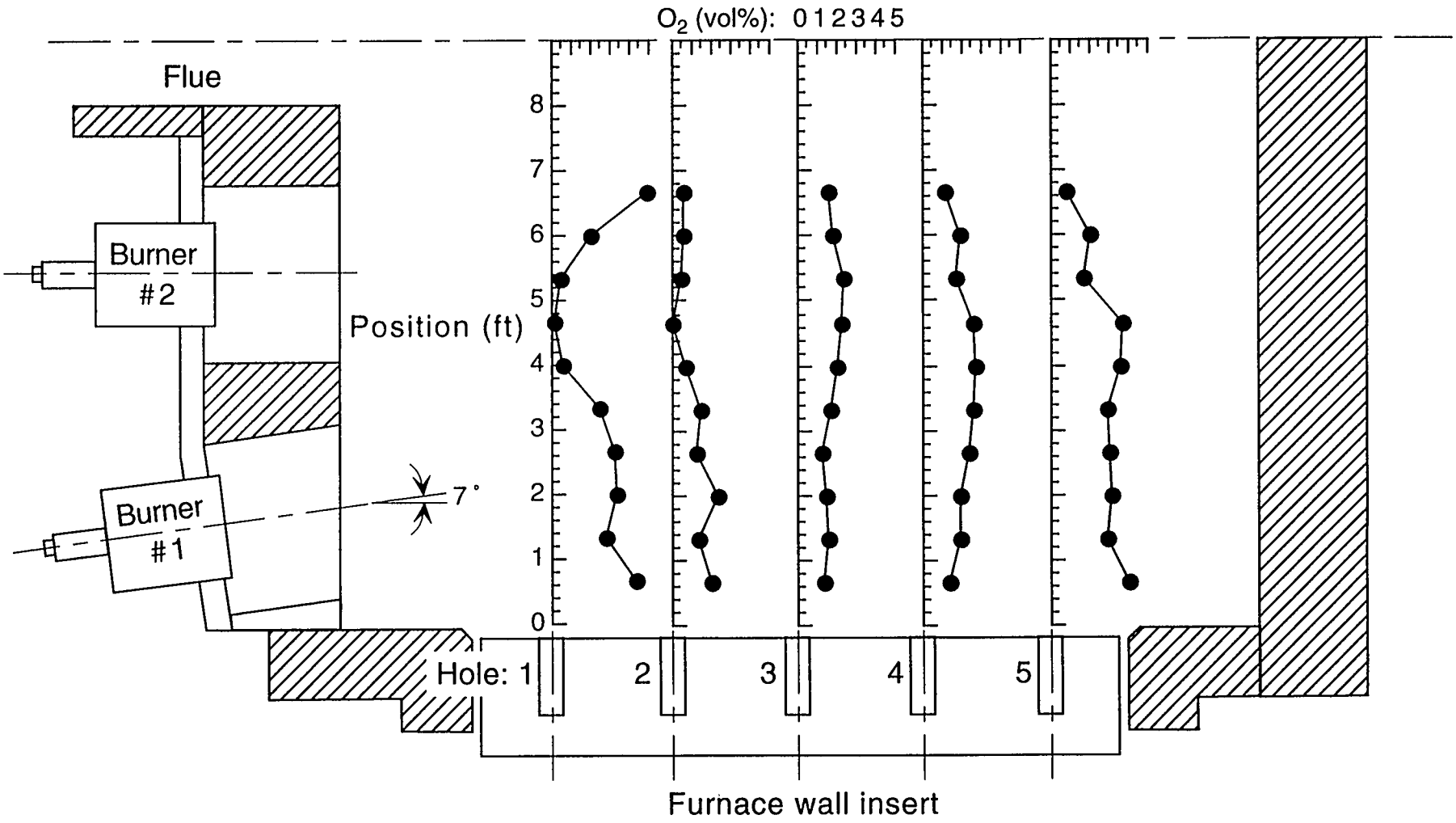

Figure 5. Profiles of the O_2 concentration in the furnace.

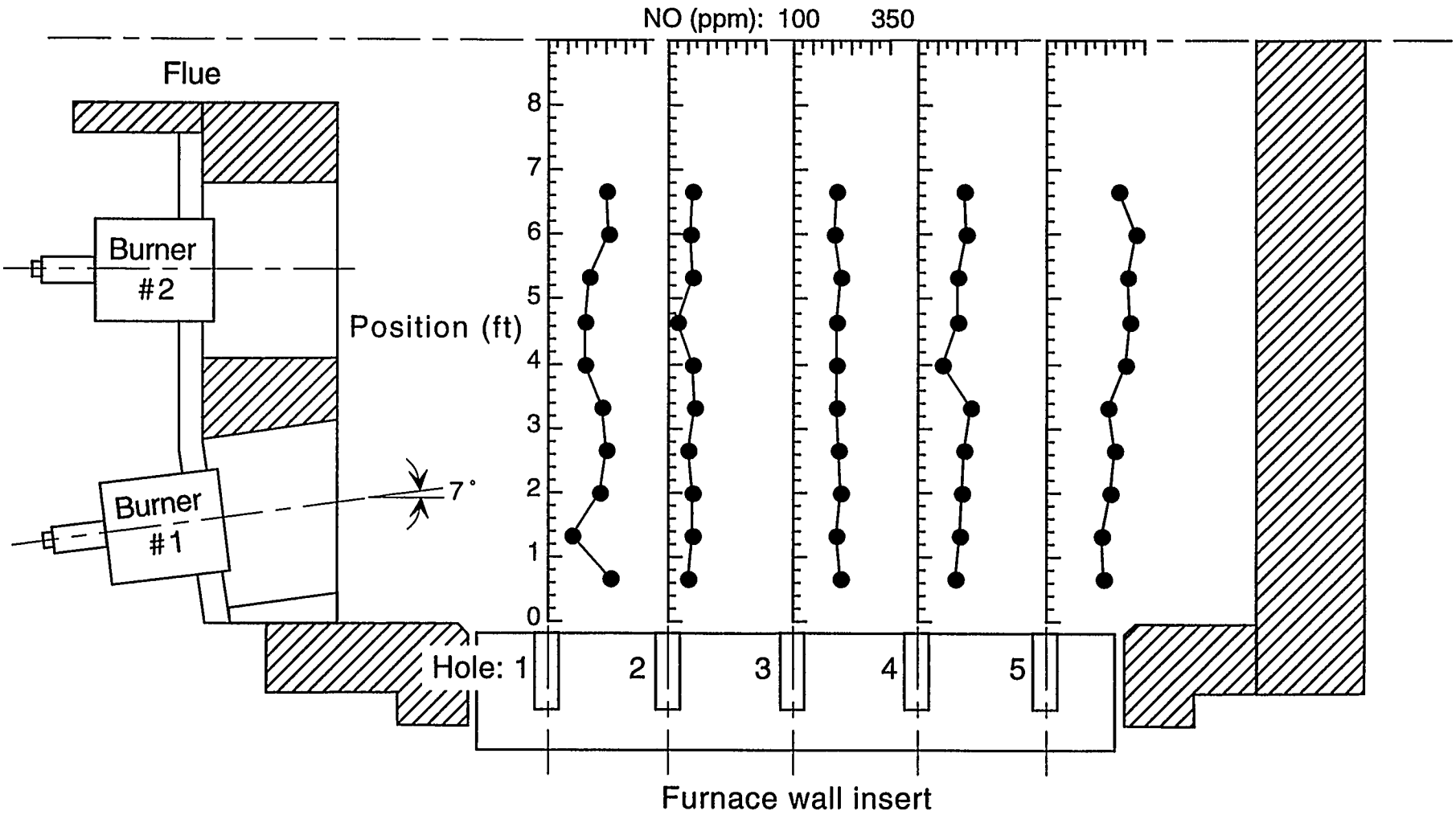

Figure 6. Profiles of the NO concentration in the furnace. (Data are uncorrected for varying O_2 concentration.)

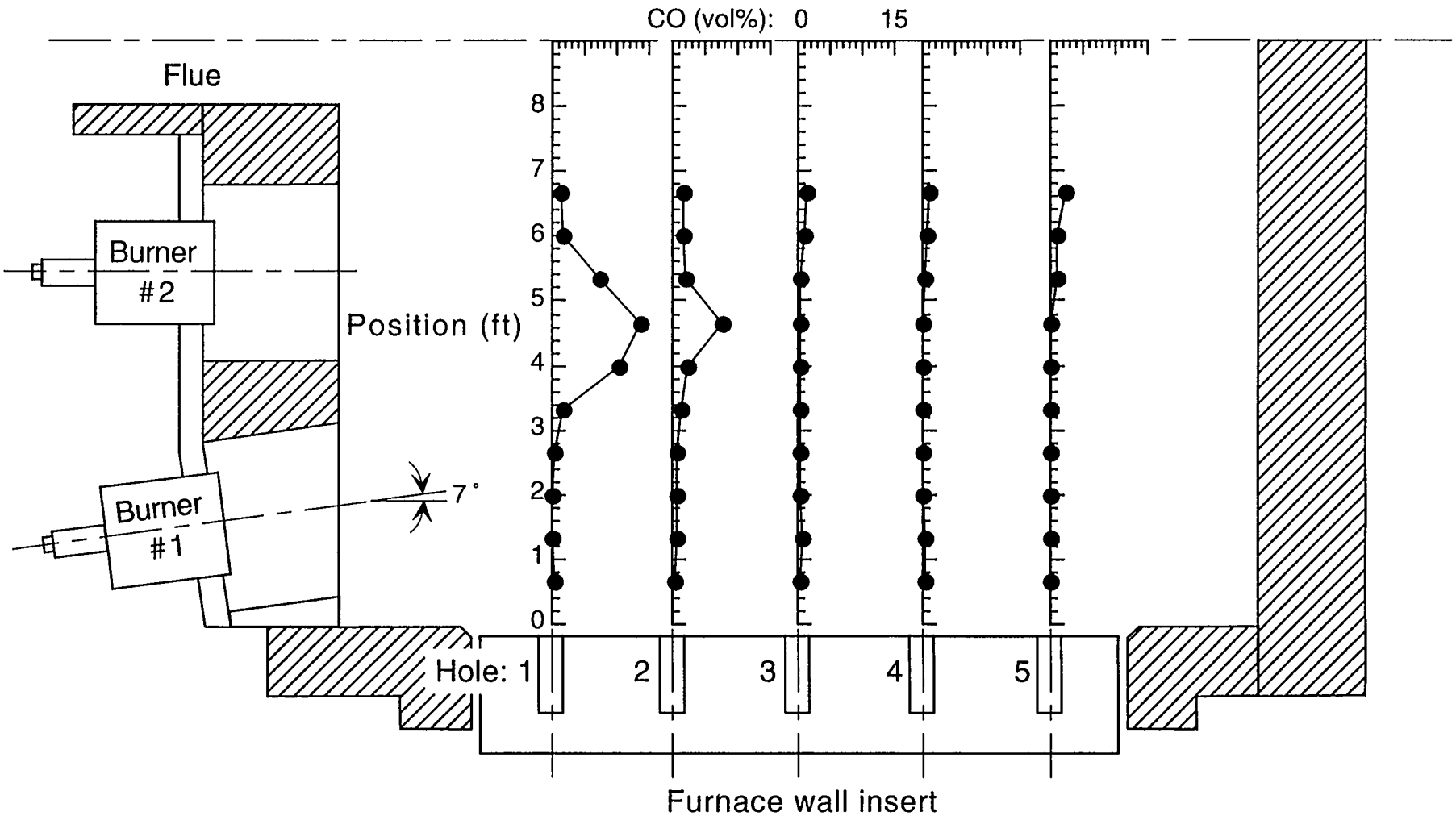

Figure 7. Profiles of the CO concentration in the furnace.

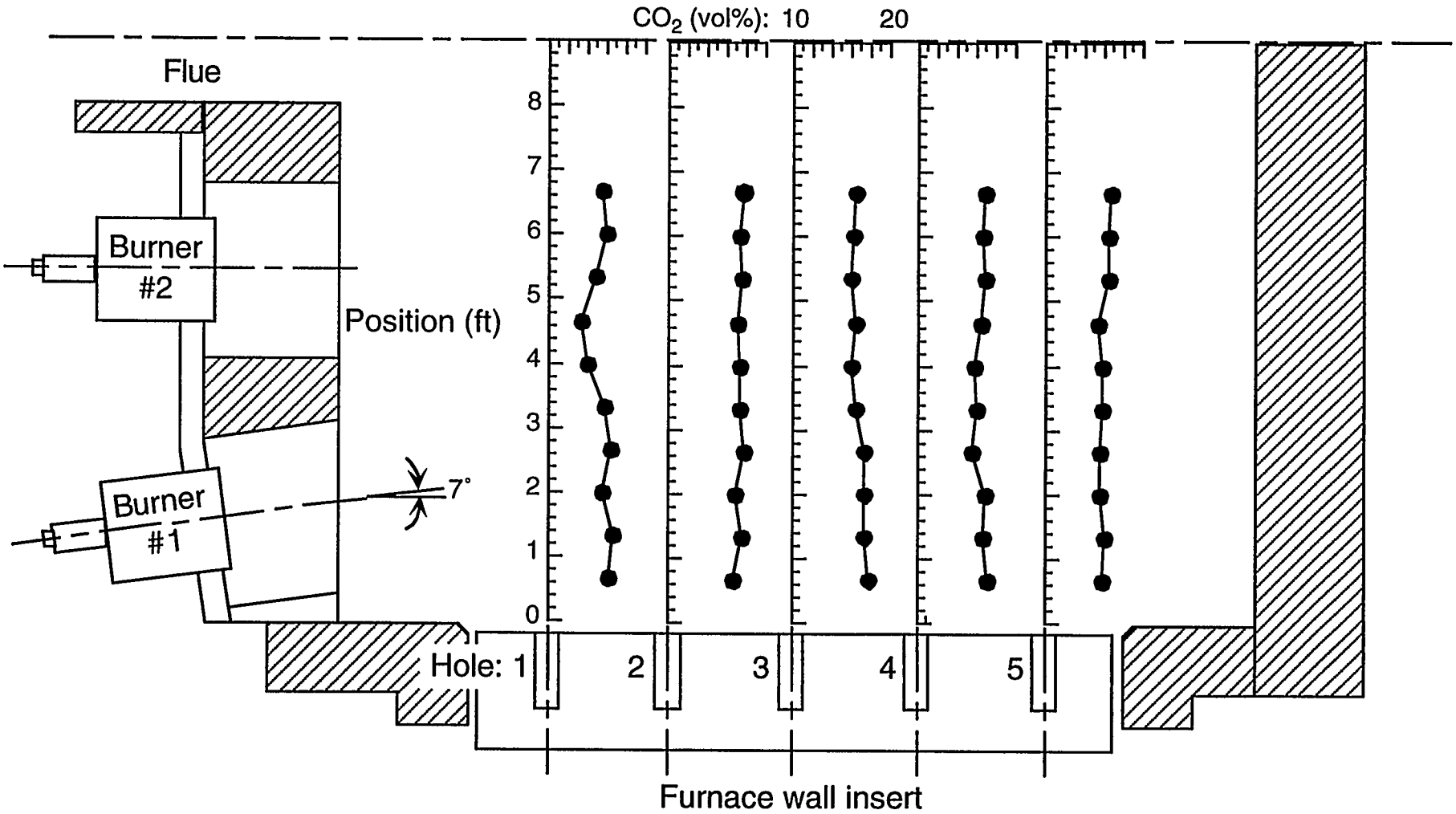

Figure 8. Profiles of the CO_2 concentration in the furnace.

CONCLUSIONS

The objective of the work reported here was to characterize the post-rebuild combustion performance in the natural-gas-fired, partially oxygen-enriched, aluminum recycling furnace (Furnace 8) operated by Roth Brothers Smelting Corporation (now Wabash Alloys) in Syracuse, New York. Measurements of gas temperature and species concentration (O_2, CO, NO, and CO_2) were made in the exhaust of the furnace. Local species concentration measurements were also made in the combustion space for the furnace/burner design condition: Stoichiometry at or near 2.0 with 35% oxygen enrichment.

The combustion space measurements showed clear evidence of the flame zone with oxygen depletion and high carbon monoxide (as high as 13% in the flame core). The new low-NO_x burner designs yielded NO concentrations below 350 ppm at all locations in the furnace. The corresponding stack NO concentration was 267 ppm. CO_2 concentrations showed little variation in the combustion space except in hole 1 of the insert, where some flame structure was observed.

The stack measurements were performed for a range of furnace operation conditions: Oxygen enrichment values ranging from 32 to 40% and combustion stoichiometries ranging from 1.94 to 2.22 (with 2.0 being stoichiometric combustion). NO concentrations ranged from 103 ppm (for *Stoich* = 1.98, 33% O_2 enrichment) to 651 ppm (for *Stoich* = 2.11, 41% O_2 enrichment). Exhaust temperatures were a maximum for the near-stoichiometric combustion cases, reaching a maximum of 2056°F for *Stoich* = 1.94, 39% oxygen enrichment. Complete combustion was observed (absence of CO in the exhaust) for all fuel-lean conditions. A peak CO concentration of 12,250 ppm was measured for *Stoich* = 1.98, 33% O_2 enrichment.

A mass-balance analysis of the effluent species concentration data is conducted to estimate the true air and oxygen flow rates into the furnace. Deviations from the differential pressure orifice air flow measurement may be due to error in the orifice plate measurement and/or infiltration into the furnace by leakage. The data analysis suggests that the actual air flow is, on average, 10% above the measured air flow rate. The same analysis shows that the metered oxygen flow is within 4% of the actual values.

ACKNOWLEDGMENTS

The support of the Roth Brothers Smelting Corporation personnel is gratefully acknowledged, with particular thanks to Neal Schwartz, Robert Hubbert, and John Sessler. Significant pre- and post-test support was provided by Mark D'Agostini from Air Products and Chemicals, Inc. Financial support of the project was provided by Air Products and Chemicals, Inc., and the U.S. Department of Energy. The help of student assistant Robert Hayes is also gratefully acknowledged.

APPENDIX A

Tabulation of Combustion Space Data

Furnace Operating Conditions for Combustion Space Measurements

Roof temperature (nominal)	2100°F
Bath temperature (nominal)	1463°F
Furnace pressure (nominal)	0.01" H_2O
Fuel flow, air side	5600 scfh
Air flow	72,000 scfh
T1 fuel flow	4980 scfh
T1 O_2 flow	8960 scfh
T2 fuel flow	4970 scfh
T2 O_2 flow	8980 scfh

COMBUSTION SPACE DATA

HOLE 1

Position (ft)	O2 (%)	CO2 (%)	NO (ppm)	CO (ppm)
0.67	4.32	16.24	259	618
1.33	2.81	16.65	159	376
2.00	3.36	15.63	234	1,730
2.67	3.22	16.35	248	2,969
3.33	2.47	15.83	236	16,495
4.00	0.55	14.08	194	104,860
4.67	0.14	13.36	192	136,620
5.33	0.41	14.80	207	73,553
6.00	2.06	16.04	257	15,317
6.67	4.93	15.52	252	11,896

HOLE 2

Position (ft)	O2 (%)	CO2 (%)	NO (ppm)	CO (ppm)
0.67	1.98	16.76	148	3,001
1.33	1.37	17.58	163	6,610
2.00	2.33	16.86	161	6,285
2.67	1.23	17.78	149	6,785
3.33	1.44	17.27	168	11,822
4.00	0.69	17.37	162	24,220
4.67	0.00	17.07	124	76,380
5.33	0.41	17.48	163	19,953
6.00	0.54	17.27	156	17,270
6.67	0.54	17.89	163	15,420

HOLE 3

Position (ft)	O2 (%)	CO2 (%)	NO (ppm)	CO (ppm)
0.67	1.37	17.68	221	3,516
1.33	1.51	17.27	210	5,397
2.00	1.44	17.37	225	3,618
2.67	1.23	17.37	217	2,994
3.33	1.72	16.55	214	3,055
4.00	1.98	16.04	213	3,033
4.67	2.26	16.45	211	3,444
5.33	2.33	15.93	222	4,760
6.00	1.78	16.14	205	10,177
6.67	1.57	16.45	209	13,775

HOLE 4

Position (ft)	O2 (%)	CO2 (%)	NO (ppm)	CO (ppm)
0.67	1.31	17.17	194	3,366
1.33	1.92	16.76	204	2,673
2.00	1.85	16.96	213	1,264
2.67	2.33	15.63	218	947
3.33	2.60	15.93	233	577
4.00	2.67	15.83	160	1,097
4.67	2.54	16.55	201	1,283
5.33	1.64	16.86	201	4,184
6.00	1.85	16.76	225	8,397
6.67	1.16	16.86	216	10,288

HOLE 5

Position (ft)	O2 (%)	CO2 (%)	NO (ppm)	CO (ppm)
0.67	3.98	15.73	244	196
1.33	2.88	16.04	242	229
2.00	3.08	15.52	260	235
2.67	3.01	15.63	272	328
3.33	2.88	15.83	258	688
4.00	3.57	15.83	301	737
4.67	3.63	15.32	311	1,597
5.33	1.64	16.55	307	11,514
6.00	1.98	16.55	326	11,246
6.67	0.75	16.65	282	22,924

APPENDIX 3

REPORT ON THE AIR PRODUCTS/ARGONNE VIRTUAL REALITY PROJECT

Project Background and Goals

The overall goal of this project is to develop a nozzle and fuel combination for industrial furnaces that achieves high efficiency and low nitrogen oxide (NO_x) emissions at a low cost to the furnace operator. To determine the best combination, computational experiments that coupled the combustion chamber to the molten smelt were used to examine the performance of various scenarios. These experiments result in a large number of data sets that must be compared to understand the differences in temperature distribution, O_2 levels in furnace, and mixing characteristics of each fuel type. Unfortunately, most visualization and analysis tools are limited to importing and displaying a single data set; multiple data sets must be loaded in successive order and displayed individually. To compare simulation results in this paradigm, the user must either remember the characteristics of interest from one data set to the next or initiate multiple visualization sessions and display the windows side by side. In both cases it is difficult, if not impossible, to isolate the differences among the data sets, particularly if the differences are significantly smaller than the physical features of the numerical simulation. To rectify this situation, we created a virtual reality analysis toolkit that allowed multiple data sets to be displayed simultaneously in a virtual furnace, and contained paradigms for interactively analyzing the differences between the data sets, both directly and through image differencing. To test the usefulness of our environment, a particular nozzle design was chosen for an aluminum smelting furnace and compared the data sets for three different fuel choices: air, pure oxygen (O_2), and air enriched with O_2.

Technical Progress and Results:

The Virtual Environment: The virtual reality toolkit was designed for the CAVE family of display devices developed at the Electronic Visualization Laboratory at the University of Illinois at Chicago (see Figure 1). Users are immersed in the virtual world by stepping into a ten foot cube that has stereo images projected onto three walls and the floor. One user is tracked using Ascension's Flock of Birds magnetic tracker, and the image orientation is calculated with respect to the head position of that user. Objects in the CAVE are manipulated by the user through the use of a passive wand device with three buttons and a joystick. To provide access to the simulation data sets and visualization toolkits, we developed a 3D control panel with button and slider widgets that are accessed with the wand (see the left image of Figure 2). Navigation through the virtual world is accomplished using the joystick functionality of the wand; users point the wand in the desired direction and use the up/down degrees of freedom to move forward or backward.

To provide a realistic frame of reference for engineers developing and analyzing computational results, we constructed a virtual aluminum smelting furnace using texture-mapped polygons. The texture images consist of digital pictures of an operating furnace and include, for example, the melt surface, the charging bins, and the exhaust stack. The right image in Figure 2 shows the virtual aluminum smelting furnace that corresponds to the computational domain used in the numerical simulations. To obtain an unimpeded view of the simulation data, the texture-mapped polygons are replaced with a wireframe

representation of the furnace where key reference points, such as the burners and exhaust stacks, are retained.

Data Visualization. To allow the engineers to quickly and intuitively make comparisons between data sets, we developed a visualization toolkit that provides three primary functionalities as shown in Figure 3: 1) the visualization of individual data sets, 2) the visualization of the differences between data sets via direct data comparison, and 3) the simultaneous visualization of two or more data sets via image comparison. For each functionality, one or more standard visualization techniques, such as vector field glyphs, animated streamlines and flow fields, cutting planes, and scalar field height profiles, are used to gain insight into the data. Additional insights are gained through the dynamic selection of the color maps and through data manipulation techniques such as magnification, culling, and exaggeration.

Visualization of Individual Data Sets. A static view of each data set can be obtained using tetrahedral dart vector glyphs to represent vector and scalar fields simultaneously; their direction and length correspond to the direction and magnitude of the vector field at that data point. The color, C, assigned to each vector glyph is determined by interpolating the field value of interest, s, over some range, $[m_r, M_r]$, which can be dynamically selected by the user. That is, $C = (M_r - s) / (M_r - m_r)$. If $s = m_r$, the color assigned to the vector glyph is blue; if $s = M_r$, the color assigned to the vector glyph is red. The extrema values, m_r and M_r, can be chosen in a number of different ways: by the individual data set extrema; by the global extrema over all the data sets, or by user-defined bounds. In addition, the user may manipulate the vector field glyphs by culling vectors whose corresponding scalar value falls outside the user-defined range or by uniformly magnifying them for easier viewing. The use of vector field glyphs to visualize the combustion velocity field and temperature in the air/O_2 data set is shown in Figure 4.

To facilitate the study of the flue gas flows, we developed an interactive system that allows the user to initiate a streamline from any position within the virtual furnace. The starting point of the streamline is given by the location of the wand at the time of initiation. The streamline is calculated using the forward Euler technique, colored by the scalar field of choice, and rendered in approximately .2 s. By requesting a number of streamlines initiated from a two-dimensional cross-section of the furnace and displaying them simultaneously as a flow field movie, large-scale structures in the flow can be easily identified and examined. For example, we show the use of this technique to examine the mixing characteristics of flows originating from a particular burner in Figure 4.

In addition to vector field glyphs and animated streamlines, the user may choose to visualize scalar fields in individual data sets by using interactively defined cutting planes. These interactively defined cutting planes have the most flexible color maps, and the user may choose the ranges corresponding to any of the bounds previously defined or the range defined by the cutting plane extrema. In addition, if the user-defined range is used, data culling is used to eliminate regions that fall outside the bounds (see Figure 5).

Data Comparison Techniques. To perform comparative analysis using the differences between data sets, the user interactively selects the two data sets to be compared, for example, data sets i and j. We currently assume that the computational grid is identical for all the data sets, thereby eliminating concern regarding the error associated with data interpolation to common coordinate locations. We compute pointwise differences between the two data sets as follows: pointwise scalar field differences are computed directly as $S_{diff} = |S_i - S_j|$, and pointwise differences in vector fields are computed by $\mathbf{u}_{diff} = [u_i-u_j, v_i-v_j, w_i-w_j]$. The primary visualization technique used to display the differenced data is the vector field glyphs. In this case the color map corresponds to the range of values in S_{diff} or to the range of magnitudes of $\mathbf{u}_{diff}$. In addition, the user may interactively select a subset range of values in S_{diff} to both determine the color map and cull the vector glyphs.

The differenced data set is more likely than the original data to contain small data values that are difficult to discern, and we therefore allow the user to manipulate the vector field glyphs in a variety of ways. The vectors may be culled to focus on regimes of interest, for example, the maximum or minimum values in S_{diff}, and/or magnified uniformly for easier viewing. In addition, the user may exaggerate the differences in the scalar field above a user-defined threshold by using the formula Scale Factor = $(s/f)_\alpha \times M$, where s is the scalar value at the current data point, f is the threshold value, α ranges from 0 to 5, and M is the magnification constant. The resulting Scale Factor value is multiplied by the vector glyph magnitude to determine the final size. As α increases, vectors whose corresponding scalar values are greater than f grow exponentially, whereas those with scalar values less than f decrease, resulting in an exaggeration of the differences above the threshold value. If α=0, changes in f result in no changes to the vector glyph appearance. Examples of the data comparison technique applied to the aluminum smelting furnace data are shown in Figure 6. The first two images in this series from left to right show the difference between the pure O_2 and air cases and the pure O_2 and air/O_2 cases. Each point's color gives the difference in temperature at that point: blue corresponds to the smallest difference and red to the largest difference. In this case, the maximum differences are seen between the pure O_2 and air cases, on average 1500° F difference, and the minimum differences are seen between the pure O_2 and air/O_2 mix, on average 180° F difference. Because the colors range from blue to red for each case, quantitative feedback regarding the values of S_{diff} must be provided in the form of a colorbar as illustrated in each image. Because the differences between O_2 and air/O_2 can be difficult to see, the third image shows the use of magnification for easier viewing.

Image Comparison Techniques. Comparative analysis using image techniques can be as simple as plotting simulation data from different experiments in the same one- or two-dimensional graphs and coordinate spaces. We provide the analogous mechanism for this type of analysis for scalar fields in three-dimensional data sets. The user may select any number of data sets and display the scalar fields from an interactively defined cutting plane using height profiles. Each data set is identified by a uniquely colored outline that corresponds to the control panel button color. Additional insights in this case are obtained through manipulation of the color map which can be determined by using any of the

ranges discussed above. In addition, the differences in the heights of the cutting plane are more clearly delineated if the user selects the option to color by data source. In this case each data set is assigned a unique color, and subtle differences between the height profiles are easier to discern.

In Figure 7 we show the use of the image comparison technique for the aluminum smelting furnace data. The cutting plane from which the data is displayed is shown by the flat, gray surface; the height of the data surfaces above the cutting plane corresponds to the temperature at that point. The colored markers and outline on the boundary of each data set indicate the source of the data: red markers indicate the air case, green markers indicate the air/O_2 mix, and blue markers indicate the pure O_2 case. In the three images we show different options for displaying the height profiles: in the left image, the color of the data surface corresponds to temperature; in the middle image, the color of the surface corresponds to data source and the height field is displayed with the computational grid; the rightmost view shows the advantage of immersive display to gain additional insight from within the data set.

Publications:

L. Freitag and T. Urness, "Comparative Visualization Techniques to Analyze Aluminum Smelting Furnace Efficiency in a Virtual Environment", (Editors P. Banerjee and T. Kesavadas). *In Industrial Virtual Reality: Manufacturing and Design Tool for the Next Millenium. Proceedings of the 1999 ASME International Mechniacial Engineering Congress and Exposition*, pages 191—199, 1999.

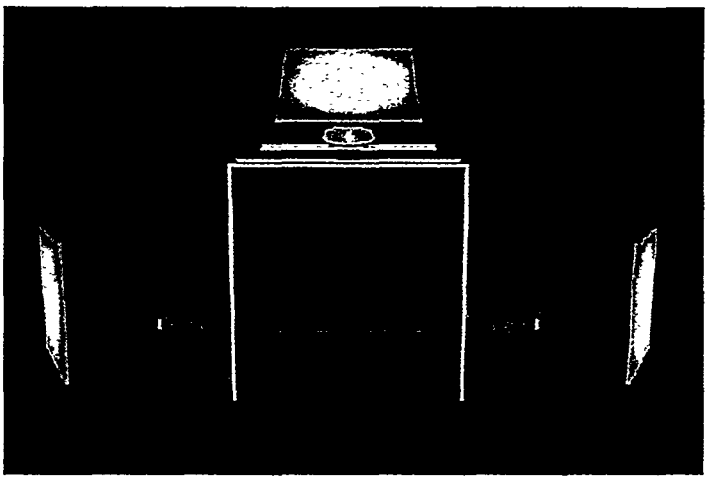

Figure 1: Schematic of the CAVE display device (image courtesy of the Electronic Visualization Laboratory, University of Illinois at Chicago)

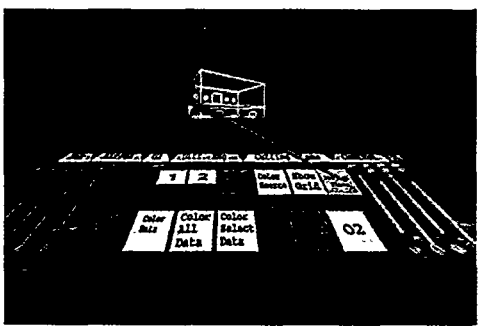

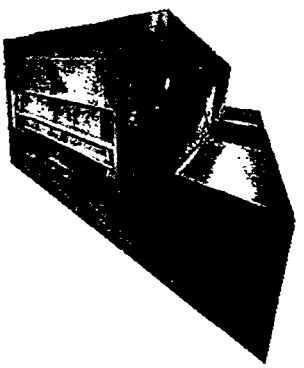

Figure 2: The control panel mechanism used for interacting with the virtual reality simulation and the exterior of the virtual aluminum smelting furnace

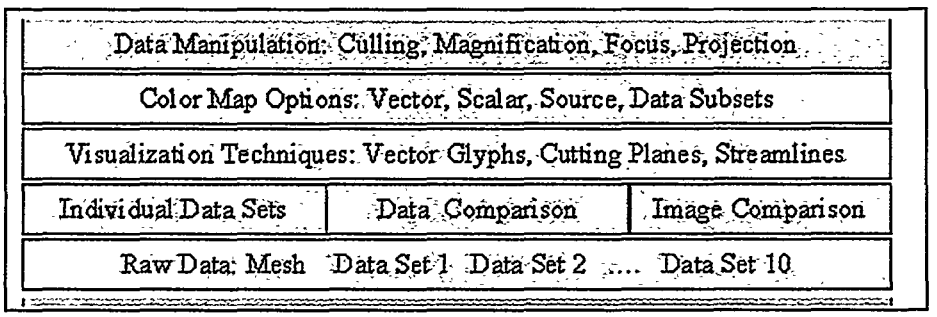

Figure 3: Overview of the toolkit for comparative analysis of multiple data sets

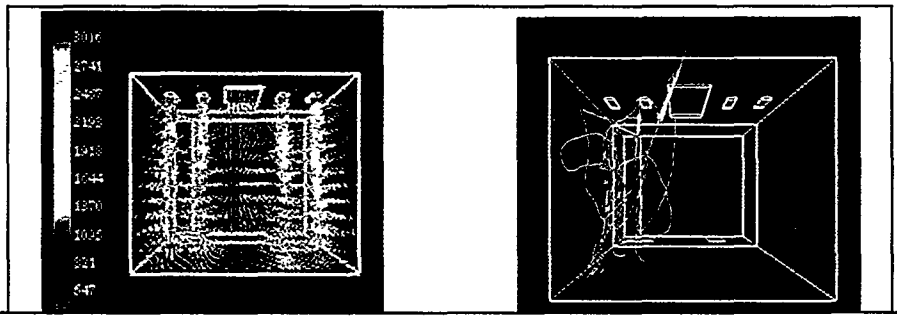

Figure 4: The use of vector field glyphs and animated streamlines to interactively explore the velocity fields and temperature distributions in the air/oxygen data set

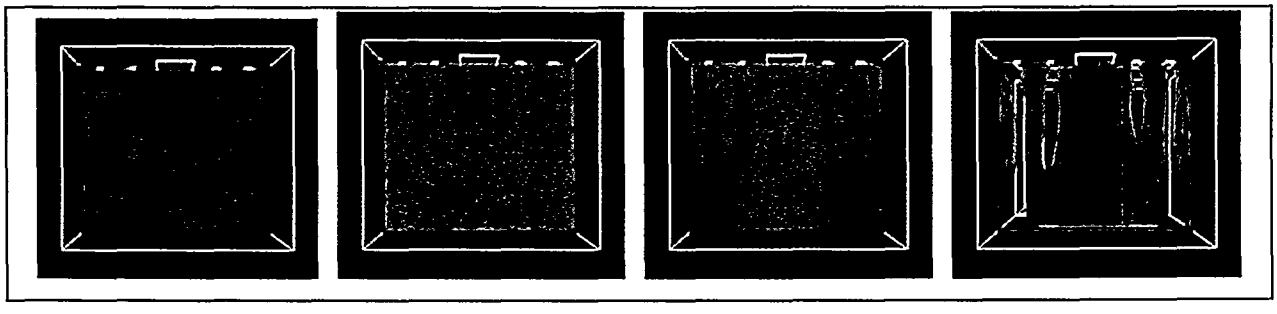

Figure 5: Four color maps using different ranges that show temperature at the level of the burners for the air fuel data set; the ranges from right to left: over all data sets, within the air data set, within the cutting plane, within a restricted, user-defined range

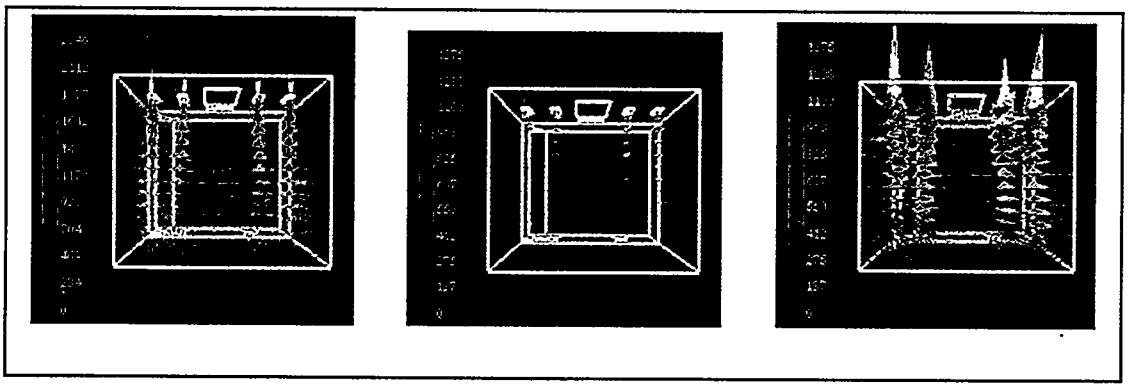

Figure 6: Example use of the data difference technique in the aluminum smelting furnace. The first two images from the left show the temperature difference between the O_2 and air fuels and the air/O_2 and O_2 fuels. The last image shows a magnified view of the second image

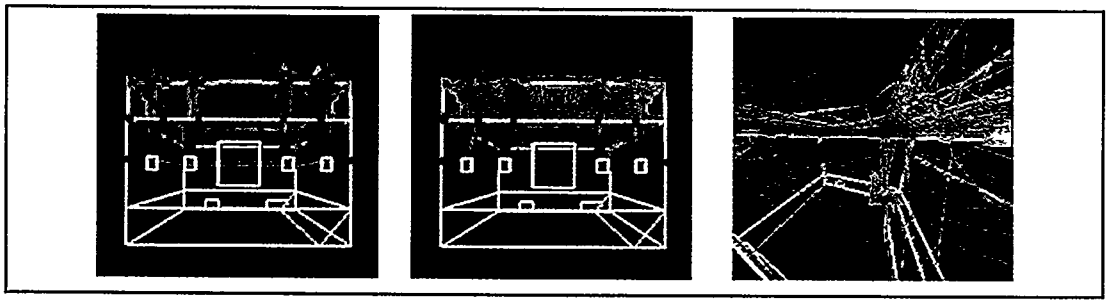

Figure C-7: Data displayed from a cross-sectional cutting plane in the aluminum furnace. The location of the cutting plane is given by the gray surface. Image comparison is accomplished by plotting height profiles of scalar fields of interest, in this case temperature. The colored markers outlining each data set indicate the source of the data: red markers indicate the air case, green markers indicate the air/O_2 mix, and blue markers indicate the O_2 case. The height profiles are colored by temperature in the leftmost image and by source in the middle and rightmost images.